Structure and Thermochronology of an E-W profile through the Mount Painter Province, Northern Flinders Ranges, South Australia: is this a southern example of deformation and exhumation driven by the Alice Springs Orogeny?

Vair Jennifer Pointon

Centre for Tectonics Resources and Exploration
Department of Geology and Geophysics
School of Earth and Environmental Sciences
University of Adelaide, South Australia
vair.pointon@student.adelaide.edu.au

31st of May, 2010

ABSTRACT

The Mount Painter Province in the Northern Flinders Ranges, South Australia is composed of Palaeoproterozoic to Mesoproterozoic basement overlain by 7-12 kilometres of Neoproterozoic to Cambrian sedimentary rocks and is associated with high lateral geothermal gradients. During the Early Paleozoic, deformation and metamorphism reached greenschist to amphibolite facies during the ~500 Ma Delamerian Orogeny. This study focuses on the subsequent thermal history of the area by studying an E-W profile through the Mount Painter Province using the widely used techniques of structural mapping, micro-structural analysis and $^{40}Ar/^{39}Ar$ thermochronology to characterise and date deformation and cooling (as a proxy for exhumation). The E-W trending profile, known as the Hamilton Fault, is south dipping oblique slip with a normal and dextral component overprinted by younger brittle structures and brecciation which is seen in the structural and micro-structural analysis.. It is proposed to have a very active past and there is evidence of movement in the Adelaidean due to an apparent formation offset of ~600 m. The regional context of the Hamilton Fault having a dextral and normal component suggests an ε_3 uplift, an ε_2 extension SW to NE and ε_1 NW-SE shortening. This is similar in character to the N-S shortening which is seen in the Alice Springs Orogeny (ASO). Results from the $^{40}Ar/^{39}Ar$ thermochronology show the basement metasedimentary rocks have cooling ages of around ~350 Ma between 300 to 400 °C and 312 Ma at 150 °C. Interestingly, the younger Adelaidean metasedimentary rocks have an older cooling age of 390 Ma between 300 to 400 °C. The thermochronology data suggests differential cooling has occurred. The observations suggest that exhumation is driven following the Delamerian folding event and forced the earlier cooling of shallower samples at a slower rate and later cooling of the deeper samples at a faster rate, a process caused by differential tilting. The cooling paths are well represented in this example as shown by converging cooling paths. Overall I attribute this subsequent thermal history and structural similarity to the ASO, a major widespread dramatic orogenic event which has not been widely recognized as a significant tectonic event in the Adelaide Fold Belt.

CONTENTS

1. INTRODUCTION

The Cambrian-Ordovician Delamerian Orogeny is the main event thought to have caused deformation and metamorphism of the Adelaide Fold Belt (AFB) (Jenkins & Sandiford 1992, Foden *et al.* 2006). Geochronological studies that have focused on synkinematic and postkinematic granites in the Mount Lofty Ranges, Fleurieu Peninsula and Kangaroo Island regions of the southern AFB (Fig. 1) have constrained the metamorphism (locally reaching upper amphibolite facies) and deformation in those areas to between 515 and 490 Ma (Jenkins & Sandiford 1992, Foden *et al.* 1999). In other areas of the AFB it has been proven more difficult to determine reliable ages for both metamorphism and deformation. In the central and northern AFB the metamorphic grades tend to generally be low (subgreenschist) such that the dominant sedimentary sequences don't contain minerals that are commonly used for dating the metamorphism or post-metamorphic cooling in higher grade rocks such as accessory minerals (e.g. Monazite, zircon) or k-bearing phases (e.g. hornblende, muscovite, biotite, k-feldspar). The exception is in the Mount Painter Province and areas in and around the NW Northern Flinders Ranges, where metamorphic grades in basement and immediately overlying metasedimentary rocks reach amphibolite facies at 3-4 Kb (Sandiford *et al.* 1998b). Preliminary U-pb, Sm-Nd and Rb-Sr geochronology conducted by Elburg *et al.* (2003) appears to support a Cambrian Delamerian metamorphic age in these rocks and ^{39}Ar/^{40}Ar thermochronology conducted by McLaren *et al.* (2002) indicates prolonged cooling between the late Ordovician and Carboniferous (440-320 Ma). The concentric folding of metamorphic zones by the large scale anticline (Fig. 2) which exposes the Mt Painter Inlier firstly implies that the original metamorphic zones were near horizontal, secondly implies the deformation post-dated metamorphism and finally that the cooling and inferred exhumation dated by McLaren *et al.* (2002) provided an Mid-Paleozoic and not Cambrian age for the deformation.

This study applies structural mapping, micro-structural analysis and ^{40}Ar/^{39}Ar thermochronology to characterise and date deformation and cooling (as a proxy for exhumation) along a long lived profile of the WNW trending, Hamilton Fault on the western margin of the Mount Painter Province (MPP) (Fig. 3). This is a region which is suggested to be affected by both the Delamerian and Alice Springs Orogeny. The Hamilton Fault is located in the central domain of the Geological Survey of South Australia, Department of Mines, Adelaide: Mount Painter Province 1:125,000 Sheet (Coats *et al.* 1969). It is situated at the northern part of the Flinders Ranges, south-east of central Australia (Fig. 1), the MPP is highly deformed, complex tectonic-thermal history with numerous deformational and intrusive events, involving basin formation and inversion ranging from Mesoproterozoic to the present (Teale 1993, 1995, Sandiford *et al.* 1998b, Paul *et al.* 1999). Extraordinary heat production resulting in high thermal gradients in the crust (McLaren *et al.* 2002) is recognised in this area with peak P-T conditions of amphibolite facies at 3 to 4kb (Sandiford *et al.* 1998a). It has been widely accepted that the MPP metamorphism and deformational history occurred during the Cambrian Delamerian Orogeny (Jenkins & Sandiford 1992, Teale 1993, Haines & Flottmann 1998, Sandiford *et al.* 1998b, Paul *et al.* 1999, Preiss 2000, Foden *et al.* 2006) but has been the subject of an intracontinental orogenesis evolution in relation to the Alice Springs Orogeny (400 to 300 Ma) by McLaren et al. (2002). Thus this study provides a more understanding in the timing of exhumation across the Hamilton Fault. This is significant as an active fault during this time would alter areas surrounding the fault and active folding during exhumation which would lead to younger exhumation ages for comparable minerals towards the core of the fault.

Thermochronology is widely used to constrain the thermal history of a mineral. One of the most prominent and precise dating methods to measure deformation and metamorphism is the ^{40}Ar/^{39}Ar dating method (Reiners *et al.* 2005). Originating from the K/Ar dating method (McDougall & Harrison 1999) the ^{40}Ar/^{39}Ar dating method has the advantage of heating the mineral samples at different temperatures in an step process (McDougall & Harrison 1999, McLaren *et al.* 2002, Reiners *et al.* 2005) compared with K/Ar one step fusion. The ^{40}Ar/^{39}Ar dating method has been very effective and is highly recommended for dating in the AFB.

2. GEOLOGICAL SETTINGS AND PREVIOUS WORK

The AFB is composed of Paleoproterozoic to Mesoproterozoic crystalline basement overlain by Neoproterozoic and Cambrian sedimentary rocks (Preiss 1987, Mildren & Sandiford 1995, Teale 1995, Sandiford *et al.* 1998b, McLaren *et al.* 2002, McLaren *et al.* 2006) and can be divided up into four sections (McLaren *et al.* 2002) being the southern Adelaide Fold Belt, the Northern Flinders Ranges, central Flinders Ranges and the Nackara Arc (Fig. 1).

The Mount Painter Province (MPP), found in the Northern Flinders, consists of the Mount Painter and Mount Babbage Inliers (Fig. 3). The crystalline basement found in the MPP encompasses Neoproterozoic to Mesoproterozoic metasedimentary rocks that have been intruded by Mesoproterozoic and Ordovician granites (Mildren & Sandiford 1995). McLaren *et al.* (2002) and Teale (1993) suggest that these metasedimentary rocks were deposited and then metamorphosed at high temperature and low pressure conditions during the Paleoproterozoic. These Paleoproterzoic units, are overlain by 7-12 km of Neoproterozoic to Cambrian sedimentary rocks (McLaren *et al.* 2002). This sequence consists of the Callanna, Burra and Umberatana Groups. The Callanna and Burra Groups contain minor volcanics from the Arkaroola Subgroup, (Mildren & Sandiford 1995) the Paralana Quartzite, Wooltana Volcanics and Wywyana Formation (Preiss 1987). The Umberatana incorporates clastic and carbonate lithologies including the Tapley Hill Formation and includes the sturtian glacial deposits of the Yudnamutana subgroup (Preiss 1987, Mildren & Sandiford 1995, McLaren *et al.* 2002).

In the Southern Flinders Ranges (Fig. 1) (Foden *et al.* 2006), dating techniques such as zircon and U-Pb, suggest that this area was deformed and metamorphosed during the Delamerian Orogeny, which occurred between 515 Ma and 490 Ma (Foden *et al.* 2006). The formation of the rest of the Adelaide Fold Belt, including the MPP, has been attributed to this same event on the basis of the similar structural style and depositional record which terminates at the Early Cambrian (McLaren *et al.* 2002). In the MPP, the only evidence that suggests deformation occurred after 550 Ma is the youngest sediments which were deposited in this area around Neoproterozoic to Cambrian time. McLaren *et al.* (2002), Mildren & Sandiford (1995) and Sandiford *et al.* (1998) describe the Palaeozoic deformation as typically thick skinned and with basement-cored upright folds which plunge southwest.

The metamorphic fabric in the MPP formed at high-temperature low-pressure conditions (Mildren & Sandiford 1995, McLaren *et al.* 2002). The region obtains an interesting ‘unconformity related contact metamorphism’ (Mildren & Sandiford 1995, p. 242) showing an unusual style of metamorphic zonation being near parallel with the basement unconformity (Fig. 2). Minerals, such as cordierite-anthophyllite and diopside, suggest that the peak metamorphic temperatures were on the order of 500 °C with pressures of ~3 kbars corresponding to depths of ~10 km. Also widespread scapolization evident in the area suggests metasomatism (Mildren & Sandiford 1995) which further suggests chemical alteration by a hydrothermal fluid from either an igneous or metamorphic source.

Mildren & Sandiford (1995) and McLaren *et al.* (2002) suggest that the timing of metamorphism was after 550 Ma but the cause of the metamorphism is less understood. Metamorphism could be related to either mafic intrusives or extraordinarily enriched heat producing elements in the basement. McLaren et al. (2002) suggests that mafic intrusives are not the reason for the metamorphism but could be the consequence rather than the cause. Another suggestion is the extraordinarily enriched heat producing elements in the Proterozoic basement contribute to the surface heat flow and increase the geothermal gradient (Sandiford *et al.* 1998a, Hand *et al.* 1999, McLaren *et al.* 2002) especially uranium which is common in this area.

Previous studies have attempted to constrain the timing of the metamorphism and deformation (Mildren & Sandiford 1995, Sandiford *et al.* 1998a, McLaren *et al.* 2006). McLaren et al. (2002) used 40Ar/39Ar and K/Ar dating technique to assess the thermal history of the Mt. Painter region. Her study included amphiboles, micas and K-feldspars from the southern margin of the MPP around the Arkaroola Wilderness Sanctuary. McLaren *et al.* (2002) preferred an interpretation of the data that suggests there were three cooling episodes around 430 Ma, 400 Ma and 330 Ma (Fig. 4). The deepest rocks were at about 500˚C until 430 Ma. At about 430 Ma and then again at 400 Ma the terrain underwent moderately fast cooling separated by isothermal residence. Following cooling at 400 Ma the terrain entered another isothermal residence until about 330 Ma. The thermal stability was then terminated by a further period of moderately fast cooling around 330 Ma to 320 Ma. McLaren et al. (2002) further inferred that these periods of cooling were a result of exhumation with a combined minimum denudation of 6 to 7 kilometres assuming geothermal gradient of ~50°C/km. The exhumation in the Northern Flinders Ranges suggested by McLaren et al. (2002) is attributed to the Alice Springs Orogeny , a major intraplate tectonothermal event known to have occurred throughout central Australia between 400 Ma and 320 Ma (Sandiford *et al.* 1998a, Hand *et al.* 1999, McLaren *et al.* 2002). In this paper we will follow the theme by attempting to determine whether exhumation was related to deformation as expressed by the large scale anticline which exposes the Mt. Painter Inlier and the prominent WNW trending fault that dissects it.

3. STRUCTURAL AND FIELD RELATIONSHIPS

Field work was undertaken along the Hamilton Fault which is situated in the central domain of the Geological Survey of South Australia, Department of Mines, Adelaide: Mount Painter Province 1:125,000 Sheet (Coats *et al.* 1969),. The Hamilton Fault is situated north-west of Arkaroola station on the western end of the Mount Painter Inlier (Fig. 2). An overall lithology is seen in Fig. 5 which highlights the stratigraphy situated at the Hamilton Fault. Detailed mapping was undertaken along the Hamilton Fault through the Proterozoic Adelaidean sedimentary rocks and the Mesoproterozoic metasedimentary rocks approximately six kilometres north of Mount Painter. A Geological map and cross-sections were constructed through these terrains and are seen in Fig. 6 and Fig. 7.

3.1 Lithology

The Mesoproterozoic metasedimentary rocks include the Radium Creek Metamorphics and Freeling Heights Quartzite. The Radium Creek Metamorphics contain medium to coarse-grained sericitic feldspathic quartzite with schist interbedding (Coats *et al.* 1969, Coats & Blissett 1971). These metasedimentary rocks are commonly overprinted by intense hematite alteration and brecciation. The metasedimentary rocks are intruded by the Mount Neil Granite (Fig. 8d). The Mount Neil Granite is a massive red weathering granite porphyry with minor adamellite (Coats & Blissett 1971, Ambrose 1978). A distinguishing feature is ~5mm diameter rounded quartz phenocrysts.

The Paralana Quartzite is unconformably situated above the Mesoproterozoic basement and is deposited in the Lower Callanna Beds during the Proterozoic Adelaidean Wilouran. It is a medium grained grey orthoquartzite and grey-green argillceous quartzite with minor actinolitic quartzite and massive amphiboles (Coats *et al.* 1969, Preiss 1987, Teale 1993). At the Hamilton fault the unit occupies a poorly vegetated strike ridge with large quartz veins (Fig. 8a). The unit is a poorly sorted, pale grey, pink weathering quartzite. Locally it contains fine conglomerate with well rounded quartz pebbles which grades to a massive quartzite with sandy siltstone and well sorted quartzite. It is estimated by Priess (1987) that on the margins of the southern Mt Painter Inlier the average thickness of the Paralana Quartzite is two hundred metres. Sample VP09013 was taken from this area and shows large feldspathic influenced quartzite with fine grained alteration which is partly sericitised.

The Wywyana Formation, deposited in the Lower Callanna during the same time as the Parlana Quartzite, is a thin dominantly calcareous metasedimentary unit (Coats & Blissett 1971, Preiss 1987). It runs parallel to the Hamilton Fault and changes to a dark-green colour as it moves closer to the Hamilton Fault. It consists of soft, white, actinolitic calcite marble overlain by 85m of interbedded massive and laminated actinolitic amphibole (Preiss 1987). Blisset (1964) and Priess (1987) suggested that when the Wywyana Formation is metamorphosed it forms a hornblende-andesine and hornblende-microcline hornfels, actinolite or tremolite marble and hornblende-scapolite rock. Evidence of this is seen at the Hamilton Fault as the Wywyana Formation has large amount of scapolite and tremolite alteration. There is also evidence of siliceous fluids suggesting it is a hydrothermally altered dolomite (seen in sample VP09009). It is structurally situated next to the Paralana Quartzite on the southern and north western side of the Hamilton Fault and unconformably overlies the Mesoproterozoic basement on the north eastern side of the Hamilton Fault.

The Sturtian Bolla Bollana Formation lies unconformably over the Wywyana Formation to the south of the Hamilton Fault but is absent to the north. Sedimentary rocks of the Burra Group (including the Skillogalee Dolomite) are also absent from the field area. The Bolla Bollana Formation occurs at the bottom of the Umberatana Group within the Yudamutana sub-group. It is a massive blue-green greywacke tillite with interbeds of siltstone and quartzite. Two types were seen on the Hamilton Fault. These were greywacke tillite beds overlain by dark carbonaceous shale and dark blue massive irregular dolomite with interbeds of yellow, silty and boulder dolomite. Wide spread haematitic alteration is also seen.

The Tapley Hill Formation lies above the Bolla Bollana Formation south of the Hamilton Fault and lies directly above Paralana Formation to the north. The Tapley Hill Formation is a finely laminated blue-grey silty shale with thin alternating siltstones. Seen in sample VP09002, minerals such as quartz, biotite, orthoclase and muscovite are evident suggesting greenschist facies. Fluid precipitation supports two types of quartz growth and quartz veins. Grain size and carbonate content tend to increase in the unit to a well sorted, dark bluish grey calcareous texture. Ambrose (1978) describes the Wywyana as yellow-brown weathered blue-grey dolomites with brown gritty limestone, and these are present and seen in the field closer to the Hamilton Fault zone. On the northern side of the Hamilton Fault it unconformably overlies the Paralana Quartzite.

The Yankaninna Siltstone Member overlies the Tapley Hill Formation and is deposited in the centre of the Umberatana Group. It varies in thickness across the fault from ~700m on the north side to less than 200m on the south side. It is a thinly bedded highly weathered shale-like blue-grey calcareous siltstone (Coats & Blissett 1971) with well bedded weathered grey limestone at base. Oxidation of the pink quartz is present in smaller veins and can be related to the high weathering in this area. Larger scale oxidation is seen in the Yankannina Siltstone Member on the northern side of the Hamilton Fault appearing as an intensely weathered black rock due to this oxidation. Closer to the Hamilton Fault the Yankaninna Siltstone Member displays highly folded veins suggesting both hydrothermal fluid and deformational influence (Fig. 8e). There is also evidence of a breccia which is a large red-weathered unit on the northern side of the Hamilton Fault (Fig. 8d). It is suggested to be a breccia as it is in proximity of the fault. The breccia contains large clasts of granite (Mount Neil Granite) and the main minerals seen are muscovite and potassium feldspar. Sample VP09008 and VP09012 are taken from the breccia and show a highly weathered matrix with a large amount of quartz crystals.

The Amberoona Formation is situated in the centre of the Umberatana Group and is comprised of finely laminated green and green-grey siltstone with minor well bedded sandy limestone (Coats & Blissett 1971). The Tapley Hill Formation is shale-like and is distinctively different from the Amberoona Formation suggesting that it could be formed during a different depositional environment. Pink quartz is present is both small veins and larger surface areas. Scapolization (Fig. 8g) occurs in outcropping seen at the western end of the Hamilton Fault and as the geological unit moves closer to the fault area the fine laminated layers of the Amberoona Formation become a highly folded rock (Fig. 8f). Amphibole and tremolite are also seen and it is suggested that the rock metamorphosed under low metamorphic facies conditions.

The Pegmatoidal Granite is thought to have intruded the Mesoproterozoic basement metasedimentary rocks after the fault formed. The Pegmatitc granite is seen intruding the Mesoproterozoic metasedimentary rocks on the south eastern end of the Hamilton Fault. The intruding granite has k-feldspar and quartz fibres intergowing the pegmatitc fabric (Fig. 8h).

3.2 Structure

On the western domain of the Hamilton Fault the Adelaide sedimentary rocks show macroscopic folds. The metasedimentary sequences and basement unconformity dip toward the WNW and are folded by a macroscopic scale syncline with a moderate WNW plunge (Fig. 9a, Fig. 9b and Fig. 6). The axial trace of the fold parallels the trace of the Hamilton Fault and the axial plane cleavage in the low grade sedimentary rocks are near parallel to shear fabric along fault in central and eastern parts of the field area.

On the northern side of the Hamilton Fault the Bolla Bollana Formation and the Wywyana Formation are not present while they are present on the southern side. Both the Bolla Bollana Formation and the Wywyana Formation unconformably overlie the Paralana Quartzite. The missing stratigraphy suggest that during the Sturtian (rifting phase) the Hamilton Fault was active and the southern side dropped, sedimentary rocks were eroded and Adelaidean sedimentary rocks were deposited over the top. On the northern side of the Hamilton Fault, within the Paralana Quartzite and Mount Neil Granite, there is macroscopic folding of the Paralana Quartzite over the Mount

Neil Granite which is dipping north. This was also observed by Coats *et al.* (1969). This is not directly related to the Hamilton Fault but suggests there is more complex deformation in the area.

The Hamilton Fault is the dominant feature in this area and is a large shear zone that runs from NW to SE (Fig. 2). It is a south dipping structure with moderate to shallow west plunging lineations (Fig. 9c). The kinematic indicators (Fig. 8b, Fig. 8i and Fig. 10g to 10i) show that the fault underwent oblique-slip western domain as maximum apparent dextral offset is ~600m at the contact between the Yankaninna Siltstone Formation and the Amberoona Formation on the southern side and ~200 m on the northern side. Towards the central domain of the fault the offset decreases significantly suggesting a normal and dextral component for at least some part of its history.

The Hamilton Fault is not a continuous planar fault zone but is made of splays ranging from 1 km to 3 km long in size (Fig. 6). Working from the western domain to the eastern domain of the mapping area (Fig. 6) the foliation varies. In the western domain of the mapping area the shear zone through the Adelaidean sedimentary rocks is thin and discrete fault zone with veins and brecciation zone ~1 m wide. As the Hamilton Fault moves from the western domain to the central domain the shear foliation intensity increases. Referring to Fig. 6 in the central domain the shear zone is thick and becomes more widespread through the Paralana Quartzite, Mount Neil Granite and the Mesoproterozoic metasedimentary rocks. This is where shear schists feature with strong structural fabrics (see section 3.1). On the eastern domain of the mapping area the Hamilton Fault decreases in size and appears thin but the shear intensity is still high and forms schist. These schists are highly flaky foliated rocks and the elongated biotite and muscovite in these schists define the lineation boundaries which dominantly plunge towards the west (Fig. 9a).

Structural evidence indicating the movement of the Hamilton Fault is seen in shear sense kinematic indicators, deformation of veins. Shear sense indicators are evident in both internal kinematics (micro-analysis) (Fig. 10g to 10i) and hand specimen scale kinematics (Fig. 8b and Fig. 8i). Internal kinematics consistently show dextral movement, south side down, examples include VP09015, VP09017 and VP09018. Sample VP09015 shows phenocrysts of muscovite, σ-clasts rotating in a dextral movement (Fig. 10g). Sample VP09017 shows a phenocryst of muscovite rotating in a dextral movement which suggests the fault moved south side down (Fig. 10h). Sample VP09018 shows a phenocryst of orthoclase again rotating at a dextral movement suggesting south side down (Fig. 10i). Hand specimen scale kinematics seen in the central domain of the mapping area are seen in Fig. 8b and Fig. 8i and sample VP09015 (Fig. 10g). Lineations of these rocks are consistently plunging towards the west suggesting a dextral movement, south side down.

Other shear sense indicators include deformed quartz veins seen in Fig. 8c and Fig. 10g and a more complex deformed quartz vein in Fig. 8j. The first three samples shows passive marking stretching due to simple shear and these markers have moved in a dextral motion. The quartz vein has been offset and a secondary crystallisation occurred. This has occurred pre or syn-shearing because the bedding of the shear zone plane has overprinted the deformed quartz vein and exhibits a more complex history and possible reactivation along the Hamilton Fault. Another example of shear sense is a brecciated rock situated in the western domain of the mapping zone (Fig. 8d). Sample VP09008 taken from this rock shows a fine matrix rock with angular clasts that originated from the Mount Neil Granite.

4. MICRO-STRUCTURE

The Hamilton Fault is manifested by structural features which describe the orientation of the fault movement. Seventeen orientated thin sections were made by Pontifex & Associates. The following descriptions below are allocated into different categories; these are Mesoproterozoic metasedimentary rocks, Adelaidean samples, Pegmatites intruding the basement and Fabric developed within the Hamilton Fault. Multiple rock samples were analysed within the shear zone because the Hamilton Fault cross cuts different units. Sample locations are shown in Fig. 11 and the microstructural observations are presented below.

4.1 Mesoproterozoic metasedimentary rocks

4.1.1 VP09024 – Biotite-Andalusite Schist

This sample is taken from interbedded psammitic and pelitc metasedimentary rocks of the Radium Creek Metamorphics south of the Hamilton Fault near the Commonwealth mine workings (Fig. 6). The khaki brown biotite and quartz are fine grained (<0.5mm) and define the dominant schistosity (Fig. 10c). Large andalusite poikiloblasts (~10-15mm) have the shape of rounded rectangular prisms are aligned with the fabric. Multi-domain quartz porphyroblasts (~1 to 3mm) occur at the margins of the andalusite grains and have a shape preferred orientation aligned with the matrix fabric (Fig. 10d). Minor sericitic alteration of andalusite and biotite occurs along narrow zones within, and at the margins of, the andalusite poikiloblasts. Inclusions of biotite, quartz and opaques (0.1 to 0.2 mm) are aligned with the matrix fabric.

4.1.2 VP09022- Biotite-Muscovite-Andalusite Schist

This sample is taken from a similar area to VP09024, an interbedded psammitic and pelitic metasedimentary rock. The biotite and andalusite are very fine grained (~0.5 mm) and defines the schistosity (Fig. 10b). There is a dominant chlorite alteration throughout the sample and shows an intense green alteration. Chlorite also occurs within a very discrete zone (~1 mm) wide which coincides with an asymmetric crenulated band. The biotite has been kept in pristine condition and there is no evidence to show alteration or intergrowing along the biotite boundary by the chlorite alteration

4.1.3 VP09021- Muscovite- Quartz Schist

This sample is taken from a similar area as VP09024 and 022 and is a Mesoproterozoic sedimentary rock of the Radium Creek Metamorphics. Quartz and andalusite are fine grained (~0.5 mm) and are the dominant minerals that define the fabric (Fig. 10a). The quartz shows recrystallised boundaries and the andalusite has two stages of growth, defining the fabric and overprinting the fabric with muscovite. Large grained muscovites (~1 mm) are pristine rectangular shaped prisms are overprinting the fabric and andalusite grains (~0.5-1 mm) are intergrowing these muscovites.

4.2 Adelaidean Samples

4.2.1 VP09008- Breccia

Sample VP09008 is taken from breccias situated on the northern side of the Hamilton Fault in the central domain of the mapping area and has diapric characteristics. The sample is highly weathered (brown colour) and there is no distinctive boundary between crystals. Predominantly quartz is the most noticeable and is a large grained porphyroblast (~1 mm) with an altered boundary. Smaller orthoclase, biotite and opaque minerals are exposed with tabular shape (~0.1-0.25 mm) with a fine grained matrix surrounding these minerals.

4.2.2 VP09012- Breccia

VP09012 is taken from the same area as VP09008 and shows very similar characteristics. VP09012 is a highly weathered sample with no distinct boundary between the smaller clasts. Predominantly quartz is the most noticeable crystal as is a large grained (~ 1 mm) tabular shaped crystals.

4.2.3 VP09009- Adelaidean marble

VP09009 (Fig. 10j) is a non-sheared carbonate marble rock showing metasomatic alteration and was taken from the upper Adelaidean sequence. Metasomatic alteration is evident because there are hydrous minerals dominantly muscovite (~ 1mm). The two prominent minerals are carbonate and actinolite. Carbonates are light grey small grained mineral (~0.5 m) and are aligned with the minimal fabric. Actinolite has high birefringence and is a large grained splay shaped mineral (~2 mm) which grows with carbonate.

4.2.4 VP09010- Sheared Adelaidean marble

VP09010 (Fig. 10k) is a sheared version of VP09009 as it was taken from the same area. The dominant minerals are the muscovite (~1 mm) and carbonate (~0.5 mm) which are aligned with the medium strength fabric. The carbonates have the same characteristics as VP09009, small grained and light grey colour. Muscovite has a porphyroblastic texture with pristine boundaries with no alteration present. Other minerals include large grained amphiboles (~2 mm) which overprint the fabric.

4.3 Pegmatite intruded in basement

4.3.1 VP09020- Pegmatoidal Granite

VP09020 (Fig. 10e) predominant minerals are quartz, k-feldspars, hornblendes and muscovite. This samples includes both large (~1-3 mm) and small (~0.2-0.5 mm) grained minerals. The small grained minerals are characterised as small veins surrounding the boundary of the large grained minerals. The small grained minerals predominantly quartz and k-feldspars (plagioclase) are suggested to be part of metasomatism. The large grained minerals consist of quartz, orthoclase, hornblende and muscovite.

4.3.2 VP09023- Pegmatoidal Granite

VP09023 (Fig. 10f) predominant minerals are quartz, k-feldspar and muscovite. The sample has a pegmatodial characteristic as the minerals are large grained (~1-3 mm). Quartz is the predominant mineral it is small grained (~0.5 mm) compared with the other minerals and has recrystallised boundaries. The muscovite is a large grain (~1 mm) tabular shape with pristine boundaries. There is a relationship between k-feldspar and quartz and Fig. 10f shows a quartz vein protruding a large grained (~1.5 mm) k-feldspar mineral.

4.4 Fabrics developed within the Hamilton Fault

4.4.1 VP0915- Sheared marble in the Wywyana Formation

VP09015 is a shear marble extracted from the shear zone in the central domain of the mapping area. It has marble characteristics of the Wywyana Formation. This sample is highly deformed and shows evidence of metasomatism. Fig. 10g shows a large (~6 mm) σ-clast poikilobastic kinematic indicator as there are inclusion of other small grained minerals (<0.5 mm) such as biotite, muscovite and opaque minerals. The poiklioblast has a dextral movement, south side down.

4.4.2 VP09017- Muscovite schist in the Mt. Neil Granite

VP09017 is a muscovite rich sample (~60%) and has a strong shear fabric which both muscovite (~0.5- 2 mm) and quartz (~0.5 mm) are aligned. The original magmatic mineralogy has been replaced and overprinted. The main focus in Fig. 10h is the σ-clast kinematic indicator which a muscovite phenocryst (~2-3 mm) has been rotated in a dextral movement, south side down. The σ-clast has similar initial development of a δ-clast (Fig. 10.1) but the bow-tie shaped tails show a more surface area around the phenocryst which matches Fig. 10h. Another thing to note is the rootless folds opaque bands (~ 2 mm) suggesting the opaque orginially formed pre or syn- deformation.

4.4.3 VP09018- Biotite-Muscovite Schist in the Mt. Neil Granite

The sample shows strained induced recrystallisation which is starting to make a shear zone as has two stages of crystal growth. The main characteristic of this sample is the large grained (~2 mm) kinematic indicators. In Fig. 10i this large grained (~2 mm) quartz phenocryst kinematic indicator and shows dextral movement, south side down. Interestingly there is no k-feldspar present which is found in the non-shear samples of the Mt. Neil Granite.

4.4.4 VP09019- Biotite Schist in the Mesoproterozoic metasedimentary rocks

VP09019 has two fabrics in the rock with the dominant mineral, of biotite which defining the schistosity of this sample. The main characteristic in this sample is the differential crenulated biotite (Fig. 10l) which has eventually recrystallised and new biotite grown and starting to crenulate again. Comparing this with Fig. 10.2, a prime example of differential crenulation the characteristics of the biotite in VP09019 are the same. This evidence could suggest the biotite grew pre and syn-deformation as it was crenulated during higher temperatures.

5. ^{40}ARGON- ^{39}ARGON GEOCHRONOLOGY OF THE HAMILTON FAULT

Geochronological analysis using the $^{40}Ar/^{39}Ar$ method was conducted to determine the thermal history and absolute age of deformation of the Hamilton Fault and apply its significance to crustal orogenic events. Studies (McLaren *et al.* 2002) have used the Argon method as a preferred choice for constraining ages in the AFB, as it is the most precise low-temperature thermochronology dating deformation (McDougall & Harrison 1999, Reiners *et al.* 2005). The Argon method has become increasingly popular for constraining ages as it has a number of advantages over other methods. The advantage is a greater precision and accuracy compared to other methods due to the high degree of analytical sensitivity with a further advantage due to the degassing the sample so both parent and daughter isotopes are the same (McDougall & Harrison 1999, Giles 2000). The Argon method can also be progressively degassed by a process of incremental heating which can provide further detailed information (Giles 2000) including a higher accuracy of degassed parent to daughter ratio. Argon ages in this study were achieved using the method of McDougall & Harrison 1999; Reiners *et al.* 2005. This method uses a 110 W Spectron Laser System associated with an Nd-YAG (IR;1064nm) laser for data acquisition. Argon age estimates were conducted on seven samples (VP09010, VP09019, VP09020, VP09021, VP09022, VP0923 and VP09024) and are presented in the following section.

5.1 Sample Preparation

Seven fresh samples were selected for $^{40}Ar/^{39}Ar$ dating and from which unaltered, optically transparent, <425 µm-size, muscovite, biotite and potassium feldspars were separated. The fresh samples were cut into smaller pieces using a diamond saw and then crushed into smaller pieces using a stainless steel jaw crusher. The samples were then sieved to attain a grain size <425 µm. The minerals for dating were separated using a Frantz magnetic separator, and then carefully hand-picked under a binocular microscope. The selected muscovite, biotite and potassium feldspar minerals were further leached in diluted Hydrofluoric acid for one minute and then thoroughly rinsed with distilled water in an ultrasonic cleaner.

These mineral samples were then loaded into seven large wells, 1.9 cm diameter and 0.3 cm depth, of one aluminum disc. These wells were bracketed by small wells that included Fish Canyon sanidine (FCs) used as a neutron fluence monitor for which an age of 28.03 ± 0.08 Ma was adopted (Reiners *et al.* 2005, Jourdan & Renne 2007). The discs were Cd-shielded (to minimize undesirable nuclear interference reactions) and irradiated for 25 hours in the Hamilton McMaster University nuclear reactor (Canada). The mean J-values computed from standard grains within the small pits range from 0.0096090 ± 0.0000183 determined as the average and standard deviation of J-values of the small wells for each irradiation disc. Mass discrimination was monitored using an automated air pipette and provided a mean value of 1.00134 ± 0.00033 per dalton (atomic mass unit). The correction factors for interfering isotopes were $(^{39}Ar/^{37}Ar)_{Ca}$ = 7.30x10^{-4} (± 11%), $(^{36}Ar/^{37}Ar)_{Ca}$ = 2.82x10^{-4} (± 1%) and $(^{40}Ar/^{39}Ar)_{K}$ = 6.76x10^{-4} (± 32%).

The $^{40}Ar/^{39}Ar$ analyses were performed at the Western Australian Argon Isotope Facility at Curtin University, operated by a consortium consisting of Curtin University and the University of Western Australia.

In these 40Ar/39Ar analyses the aim was to reach a plateau. A plateau suggest that the information produced from the data is relatively stable. The criteria for the determination of a plateau are:

- Plateaus must include at least 70% of ^{39}Ar.
- The plateau should be distributed over a minimum of 3 consecutive increments agreeing at 95% confidence level and satisfying a probability of fit (P) of at least 0.05.

Plateau ages (Table 8) are given at the 2σ level and are calculated using the mean of all the plateau steps, each weighted by the inverse variance of their individual analytical error. Mini-plateaus are defined similarly except that they include between 50% and 70% of ^{39}Ar.

The uncertainties on the $^{40}Ar^{*}/^{39}Ar$ ratios of the monitors are included in the calculation of the integrated and plateau age uncertainties, but not the errors on the age of the monitor, and on the decay constant (internal errors only, see discussion in (Min *et al.* 2000).

5.2 $^{40}Ar/^{39}Ar$ Data Acquisition

The samples were step-heated using a 110 W Spectron Laser Systems, with a continuous Nd-YAG (IR; 1064 nm) laser rastered over the sample to ensure a homogenously distributed temperature. The gas was purified in a stainless steel extraction line using a GP50 and two AP10 SAES getters and a liquid nitrogen condensation trap. Argon isotopes were measured in static mode using a MAP 215-50 mass spectrometer (resolution of ~600; sensitivity of 2x10^{-14} mol/V) with a Balzers SEV 217 electron multiplier mostly using 9 to 10 cycles of peak-hopping. Blanks were monitored every 3 to 4 steps to ensure the machine accuracy. A typical ^{40}Ar blank ranged from 1 x 10^{-16} to 2 x 10^{-16} mol.

5.3 Results

Data reduction and processing for the micas and potassium feldspars (Sample VP09010 and VP09019 to 024) deformation ages and ratio estimates was achieved using an Argus program written by M.O. McWilliams and run under a labview environment. The raw data was processed using the ArArCalc software (Koppers 2002) and determined the ^{40}Ar/^{39}Ar concordance for the corrected ages and ratios. The ArArCalc software used the decay constants recommended by Stager & Jager (1977). Plateaus showing the corrected ages and ratios should agree with 95% confidence level (2σ) and satisfy a probability of at least 0.05. Ages quoted in this study are quoted with errors at 95% confidence (2σ). The age quoted in this study are presented in Fig. 11.

5.3.1 Sample VP09010

VP09010 is a sheared Adelaidean marble (Fig. 6). VP09010 shows medium structural fabrics (Fig. 10k) and the muscovite which was anaylsed defines a plateau age of 390.37 ± 1.95 Ma and this age was obtained using 16 consecutive steps using 81% of ^{39}Ar (Table 2 and Fig. 12). The appearance shows no excess or Argon loss and therefore meets the initial requirement of a plateau age. Chi-statistics have been applied producing a MSWD of 0.42 and a p-value of 0.79. This indicates that 390.37 ± 1.95 Ma reflects the time at which muscovite cooled through the closure temperature of ~350 °C. The corresponding normal isochron is equal to 390.97 ± 3.14 Ma.

5.3.2 Sample VP09019

Sample VP09019 is a Biotite schist in the Mesoproterozoic metasedimentary rocks. Originally a Radium Creek Metamorphic it has been overprinted by the shear zone. Sample VP09019 analysed biotite and suggests that it is associated with the plateau age ≥344 Ma (Fig. 13). This age was obtained using 10 consecutive steps, using 17.3% of ^{39}Ar (Table 3). The age spectra expresses an inverse saddle-shape age spectra (Fig. 13) compared with the horizontal plateau age obtained for VP09010 and VP09020 to VP09024 (Fig. 14 to Fig. 18). This infers that there was probably a loss of Argon in the biotite crystals for sample VP09019 (McDougall & Harrison 1999).

5.3.3 Sample VP09020

Sample VP09020 is a feldspar, hornblende and muscovite bearing pegmatoidal granite (Fig. 10e). Muscovite was analysed in this sample and defines a plateau age of 359.44 ± 1.68 Ma and this age was obtained using 17 consecutive steps, using 100% of ^{39}Ar (Table 4 and Fig. 14). Sample VP09020 does not show characteristics of excess or Argon loss, as seen in VP09019 (Fig. 10) therefore meets the initial requirement of a plateau age. Chi-statistics have been applied producing a MSWD of 0.73 and a p-value of 0.76, as p-value is > 0.05 it is therefore acceptable. This indicates that 358.44 ± 1.68 Ma reflects the time at which muscovite cooled through the closure temperature of ~350 ˚C. The corresponding normal isochron is equal to 359.79 ± 2.59 Ma.

5.3.4 Sample VP09021

VP09021 is a Muscovite-Quartz Schist in the Mesoproterozoic metasedimentary rocks (Fig. 7a). Muscovite was analysed in this sample which defines a plateau age of 346.77 ± 1.53 Ma and this age was obtained using 20 consecutive steps, using 100% of ^{39}Ar (Table 5 and Fig. 15). Again the appearance shows no excess or Argon loss (Fig. 15) and therefore meets the initial requirement of a plateau age. Chi-statistics have been applied producing a MSWD of 1.3 and a p-value of 0.16, as the p value is >0.05 it is therefore acceptable. This indicates that 346.77 ± 1.53 Ma reflects the time at which muscovite cooled through the closure temperature of ~350 °C. The corresponding normal isochron is equal to 346.49 ± 1.82 Ma.

5.3.5 Sample VP09022

VP09022 is a Biotite- Muscovite- Andalusite Schist in the Mesoproterozoic metasedimentary rocks. The protolith is a Radium Creek Metamorphic rock which has been overprinted by the shear zone. The biotite analysed in sample VP09022 defines a plateau age of 357.39 ± 2.88 Ma and this age was obtained using 9 consecutive steps, using 80.44% of ^{39}Ar (Table 6 and Fig. 16). The appearance of the sample meets the initial requirement of a plateau age as it shows no excess or Argon loss (Fig. 16). Chi-statistics have been applied producing a MSWD of 0.63 and a p-value of 0.71, as the p value is >0.05 it is therefore acceptable. This indicates that 357.39 ± 2.88 Ma reflects the time at which biotite cooled through the closure temperature of ~300 °C. The corresponding normal isochron is equal to 359.21 ± 7.28 Ma.

5.3.6 Sample VP09023

Sample VP09023 is a muscovite and k-felspar bearing pegmatitic rock and with the shear zone overprinting it. The potassium feldspar analysed in this sample defines a plateau age of 312.77 ± 1.34 Ma and this age was obtained using 26 consecutive steps, using 75.52% of ^{39}Ar (Table 7 and Fig. 17). The appearance of the sample meets the initial requirement of a plateau age as it shows no excess or Argon loss (Fig. 17). Chi-statistics have been applied producing a MSWD of 1.02 and a p-value of 0.44, as the p value is >0.05 it is therefore acceptable. This indicates that 312.77 ± 1.34 Ma reflects the time at which potassium feldspar cooled through the closure temperature of ~125 to 350 °C. The corresponding normal isochron is equal to 313.05 ± 1.87 Ma.

5.3.7 Sample VP09024

Sample VP09024 is a Biotite- Andalusite Schist in the Mesoproterozoic metasedimentary rocks. The biotite analysed defines a plateau age of 351.75 ± 1.76 Ma and this age was obtained using 16 consecutive steps, using 86.74% of ^{39}Ar (Table 8 and Fig. 18). The appearance of the sample meets the initial requirement of a plateau age as it shows no excess or Argon loss (Fig. 18). Chi-statistics have been applied producing a MSWD of 0.38 and a p-value of 0.93, as the p value is >0.05 it is therefore acceptable. This indicates that 351.75 ± 1.76 Ma reflects the time at which biotite cooled through the closure temperature of ~300 °C. The corresponding normal isochron is equal to 353.77 ± 4.46 Ma.

6. DISCUSSION

6.1 Interpretation of structure

The Hamilton Fault has a long and complex history, the interpretation of the structures suggests it was originally Delamerian or older with a low pressure amphibolite facies in the basement and sub-greenschist higher in the stratigraphy, which is consistent with the metamorphic zoning described by Mildren & Sandiford 1995 and Sandiford *et al.* 1998. This 'unconformity-related contact metamorphism' (Mildren & Sandiford p. 242) suggests zones are parallel to the basement contact and increase towards the core of the MPP. Intrusions of pegmatite in this region are interpreted from McLaren *et al.* (2006) to have a crystallization age of ~440 to 450 Ma. All these rocks are variably overprinted by the Hamilton Fault (refer to section 2.1). Examples are seen in samples VP09015, 017 and 018 which show overprinting by the shear fabric, biotites in sample VP09019 inferring differential crenulations, sample VP09024 showing down temperature alteration and the pegmatoidal samples VP09020 and VP09023 original textures being recrystallised. This shear fabric that overprints the original rock is interpreted to be post-Delamerian.

The latest kinematics from the Hamilton Fault are dextral and normal oblique but these are overprinted by younger brittle structures and brecciation (see section 2.1). Changes in stratigraphy are also evident and differential unit thickness indicates that the structure was active during the deposition of the lower Adelaidean sequence. These events indicate that the Hamilton Fault has a long complex history of reactivation.

6.2 Hamilton Fault through time

The Hamilton fault is a south dipping oblique slip fault with a normal and dextral component and is suggested to have a very active past. There is evidence to show that it has brittle characteristics. Examples are found in the Mt. Neil Granites which show a broad shear zone with ductile textures overprinting it including breccia zones. Breccia fault rocks are also seen in the lower grade rocks suggesting quartz veins.

During the Adelaidean there was growth in the fault during deposition of the overlying sediments (Tapley Hill Formation etc.) and was active during the Delamerian, as evidence by fabrics in the basement rocks parallel to the fault. The post-Delamerian movement was oblique slip with normal and dextral components with apparent offset of ~600m. Overall, this amount and style of offset is unlikely to have significantly perturbed isotherms and thus it is unlikely to have influenced the cooling history. Rather than controlling the exhumation, the Hamilton Fault was exhumed with the surrounding rocks.

6.3 Interpretation of the ages

The Ar ages presented here are interpreted as cooling ages, combined with and in comparison to previous thermochronology in and around the MPP they constraint on cooling along the transect of the Hamilton fault. This is inferred as a proxy for exhumation.

Past studies have shown metamorphism occurred during the Delamerian as a result of anomalous thermal gradients in the Upper Proterozoic metasedimentary and magmatic sequence (Mildren & Sandiford 1995). Metamorphism in the MPP ranges from low temperature, medium pressure greenschist facies to medium temperature amphibolite facies (Mildren & Sandiford 1995, Sandiford *et al.* 1998b, McLaren *et al.* 2002) which have similar conditions to those experienced in the southern Adelaide Fold Belt (Dymoke & Sandiford 1992, Foden *et al.* 2006). Magmatic activity, including intrusion of the British Empire Granite at ~440 to 450 Ma (McLaren *et al.* 2006) is consistent with melting of the local metasedimentary pile with minor additions from the mantle (Elburg *et al.* 2003). McLaren *et al.* (2002) inferred that the British Empire Granite was emplaced at ~14km consistent with zero exhumation up until that time. Palaeomagnetic measurements indicate that uraniferous Radium Ridge Breccias in the MPP were magnetized twice during the Permo-Carboniferous period indicating a major hydrothermal event during this time (Idnurm & Heinrich 1993). Textures and temperatures suggest that the hydrothermal system was near surface moving from higher temperature to low temperature (Brugger *et al.* 2005). These observations are consistent with existing Ar data (McLaren *et al.* 2002) which shows cooling from ~500-150°C between the late Ordovician and early Permian. Deformation has been dated through various dating analyses which show cooling after the Delamerian. McLaren et al. (2002) shows three cooling episodes using ^{40}Ar/^{39}Ar during 430 Ma, 390 Ma and 300 Ma. Apatite fission track results all indicate cooling below ~100°C between 280 Ma and 180 Ma (Foster *et al.* 1994, Mitchell *et al.* 2002). Folding of the contact metamorphism which is regionally extensive and unconformity-related (Fig. 2) (Mildren & Sandiford 1995) is an expected outcome of this interpreted sequence of events, metamorphism 500 Ma, little or no exhumation until 440 and exhumation controlled by deformation between 440-290 Ma.

My ^{40}Ar/ ^{39}Ar results presented in this study agree with results from Mitchell et al. (2002), McLaren et al. (2002), Elburg et al. (2003) and Indurm & Heinrich (1993). The Mesoproterozoic sedimentary rocks from the Radium Creek Metamorphic basement (VP09022 and VP09024) have identical biotite argon ages (Fig. 16 and Fig. 18). Both samples have Delamerian fabrics suggesting the biotites grew in the Late Cambrian during the metamorphism of the Delamerian Orogeny. The ages 351.75 ± 1.76 Ma and 357.39 ± 2.88 Ma presented for both these samples are late Devonian to early Carboniferous corresponding to the cooling age through closure temperatures of 300°C to

350°C (McDougall & Harrison 1999). Two muscovite samples (VP09021 and VP09020) were taken from the same basement Mesoproterozoic sediments as the biotite samples above. VP09020 originated from partial melts within the basement. It is suggested that this rock is unrelated to the British Empire Granite as it displays different characteristics but originates from a different location. VP09021 is related to partial melts in the sediments and shows pristine muscovite (Fig. 10a). These samples show similar muscovite ages of 359.44 ± 1.68 Ma and 346.77 ± 1.53 Ma and suggests a similar cooling history to the biotite samples and shows the cooling of the mineral through closure temperatures of 350°C to 400°C (McDougall & Harrison 1999).

The potassium-feldspar thermal argon data dates the granite suite from the pegmatitic dyke British Empire Granite at 440 Ma. A micro-analysis suggests that the k-feldspars dated in this sample were affected by deformation as the grain boundary is altered and there is differential colouring internally (Fig. 10f). The age produced (312.77 ± 1.34 Ma) is consistent with the monotonic cooling at similar rates to the muscovite and biotite from the Mesoproterozoic sediments in the basement. This sample is interpreted as cooling through a closure temperature of 150°C to 300°C (McDougall & Harrison 1999).

The argon data presented for VP09019 does not show a plateau age but a saddle-shaped curve (Fig. 13) and it is proposed that it is ≥344 Ma. This is a consistent age with the other biotite dated, but cannot be accepted as a valid date as there is evidence of excess argon and the relevance to cooling and exhumation is distorted. Excess argon is the result of high temperatures damaging the rock allowing the argon to move easily from one crystal lattice to another.

VP09010 is the lowest grade sample in the argon set and it is located within the Adelaidean. It is 4 kilometres west of the nearest sample which is equivalent to 3.5 km in stratigraphic height. It has a medium fabric with strung out carbonates and includes muscovite porphyroblasts that incorporate inclusions. The sample, when compared with its protolith partner VP09009, suggests that the actinolite aligned to the fabric is metasomatic. Therefore because the muscovite is overprinting in this sample, the argon date presented at 390.37 ± 1.95 Ma implies that deformation continues after metasomatism during the late Ordovician (Elburg *et al.* 2003). Interestingly the sample has an argon age 40 Ma older than the other biotite and muscovite sample, suggesting three possible interpretations of this date. One interpretation is that the metasomatism reset the argon producing data at a younger age than the Delamerian; this suggestion may not be the case as shown by the data presented in this study and previous studies (McLaren *et al.* 2002, McLaren *et al.* 2006). Another interpretation is that the rock never reached 300 degrees therefore it would only date muscovite growth. The final interpretation is there was differential cooling through the closure temperature which could account for different argon ages. Reasons for favouring the final interpretation is that muscovite appears to be a metamorphic mineral in the unstrained rock

(VP09009) that is overprinted in the strained rock (VP09010). Metasomatised version (VP09009) of the Wywyana Formation contain large unaligned splays of actinolite and relatively less muscovite and doesn't appear to be a likely protolith to the dated sample (VP09010).

6.4 Differential cooling

Sample VP09010, from the Adelaidean sediments, has an interestingly older argon cooling age of 390 Ma than those samples from the basement rocks with 350Ma. Sample VP09010 is currently 4 km from the other argon data but assuming the stratigraphy was originally flat the Adelaidean samples were located 3.5 km above the other samples in the basement rocks (Fig. 19). During the Delamerian the MPP was metamorphosed (McLaren *et al.* 2002) and the isograds equilibrated between 500 and 390 Ma. After the Delamerian, folding occurred throughout the region but, as evident in McLaren et al. (2002), Mildren & Sandiford (1995) and Sandiford *et al.* (1998), the metamorphic zones are in line with the folding boundary (Fig. 2). Also interestingly there is a trend developing in McLaren *et al*. 2002 which shows a correlation of metasedimentary Ar samples displaying cooling ages older than basement rock cooling ages (Table 9).

In this study we discuss three possible options to explain the older cooling age of the Adelaidean sample. Option one (Fig. 19) suggests a model where Delamerian folding occurred followed by relaxation of isotherms to horizontal and subsequent exhumation. Prediction for argon data if this were the case would be all Ar data of the same minerals would give the same cooling age across the profile. In this study Ar data does not allow for this as the cooling ages are different across the profile. For example muscovite analysed in the older cooling age of the Adelaidean sample compared with the basement. Option two (Fig. 19) suggests Delamerian folding occurred without relaxation of isotherms because the cooling temperature is totally dependent on basement heat flow. The prediction of results through this option is that the samples higher in the stratigraphy cool through closure temperature than those samples that are deeper. All the samples cool at the same rate, assuming there is a linear or near linear geotherm from surface (Sandiford *et al.* 1998b). Since the surface isotherms should be the same across the profile the lower starting temperature samples (in this case VP09010 from the Adelaidean) must cool slower. The predicted cooling paths would show paths that were parallel to each other following in the same direction (Fig. 19). Finally option three (Fig. 19) suggests that exhumation is driven subsequent to the Delamerian folding. The prediction of the argon samples would show earlier cooling of shallower sample but at a slower rate and later cooling of deeper samples at a faster cooling rate suggesting differential tilting. The cooling paths of the Ar data would merge when the folding is finished (Fig. 19).

The preferred model is option three as it best represents the cooling paths in Fig. 4 which infer converging cooling paths however the reality could be between option two and three if the ASO aged folding produced doming of the isotherms as the heat producing basement was folding. More thermochronology would be needed to constrain the different options however that is outside the scope of this present study.

6.5 Regional and Relationship to other orogenic events

Exhumation is driven by tectonic processes and nearly always has a structural signature. In the case of the MPP, since most of the rocks that were originally of the highest grade have been exhumed. These basement rocks appear in the core of the anticline and the hanging-wall of thrusts and dating the exhumation will allow us to date these structures.

Prior to this study there was an extensive amount of thermochronology in relation to both the ASO (Dunlap & Teyssier 1995, Flottmann & Hand 1999, Hand *et al.* 1999, Haines *et al.* 2001) and the Delamerian Orogeny (Foden *et al.* 1999, Foden *et al.* 2006) but this thermochronology had not extended to the MPP in the Northern Flinders Ranges and therefore the Delamerian Orogeny was ascribed to the MPP due to the similar tectonism. McLaren et al. (2002) used the $^{40}Ar/^{39}Ar$ analyses to date hornblendes, k-feldspars, biotite and muscovite at selected sites throughout the Mount Painter Inlier and suggested that this area had been influenced by the ASO. The new argon ages presented in this study suggest post-Delamerian cooling along the Hamilton Fault profile between 390 to 312 Ma (Fig. 4). This correlates with the theory proposed by McLaren et al. (2002) that the MPP was exhumed during the ASO between 400 and 300 Ma. Further we raise the possibility that this period of exhumation produced a significant proportion of the folding (which defines the MPP) and the faulting which bounds and dissects it. This extends on McLaren *et al.* (2002)'s notion that deformation was essentially Delamerian and was followed by exhumation without significant folding (Fig. 20 and see McLaren *et al.* (2002) Fig. 7).

The regional context of the Hamilton Fault having a dextral and normal component suggests a ε_3 uplift, an ε_2 extension SW to NE and ε_1 NW-SE shortening which is similar in character to the N-S shortening which is seen in the ASO. The sediments derived from erosion of this shortening could have been deposited in the different basin surrounding the Northern Flinders (Fig. 21 and Fig. 22) such as the Warburton basin in the north or the Arkaringa basin in the west.

The ASO is a compressional orogenic zone which is dramatic and is suggested to occur mainly in the central region of Australia. There are indications that the ASO is widespread throughout Australia, contributing to the occurrence of the Fitzroy Trough (Willcox 1996), Mount Isa Inlier (Spikings *et al.* 1997), Broken Hill region (Hartley *et al.* 1998) and the Darling River lineament (O'Sullivan *et al.* 1998). There has also been suggestions that other events such as the Kanimblan Orogen (400 to 300 Ma) (Foster *et al.* 1999) and Queensland tectonism (300-325 Ma) (Little *et al.* 1995) may be linked to the deformation of the MPP as the dates correlate with the argon age data presented in this study. If this is the case, much of the tectonism recorded within the Australian plate is connected (Foster *et al.* 1994, McLaren *et al.* 2002).

6.6 Future Research

The MPP history is poorly constrained, to further constrain this area more investigation into metamorphism, hydrothermal events, deformation and exhumation would allow more of an insight into this area which is outside the scope of this project. Possible ways of confining metamorphism and hydrothermal events could be to calculate the average pressure or temperature evolution using titanium quartz vein thermochronology or thermobarometry. Exhumation and deformation are also poorly constrained in the MPP, more studies including thermochronology over a wider geographical area, in younger formations and different minerals in the same lithology could provide more of an insight into the area. From this information various scenarios could be modeled to further constrain the different options discussed.

7. CONCLUSION

The main findings in this study are:

- The micro-tectonic analysis and structural features of the Hamilton Fault are dextral, south side down, and normal oblique overprinted by younger brittle structures. The Hamilton Fault is a south dipping slip fault with normal and dextral components.

- Post-Delamerian movement shows apparent offset of ~600 m in the Adelaidean sedimentary rocks, suggesting it is a south dipping oblique slip with normal and dextral components. The large offset of the Hamilton Fault throughout the stratigraphy indicates that it is unlikely to have significantly perturbed the isotherms and thus didn't influence the cooling history but rather was exhumed with the surrounding rocks.

- The ^{39}Ar/^{40}Ar results presented in this study show a cooling age during the late Devonian to early Carboniferous. The new argon ages presented in this study suggest post-Delamerian cooling along the Hamilton Fault profile between 390 to 312 Ma (Fig. 16). This correlates with the theory proposed by McLaren et al. (2002) that the MPP was exhumed during the ASO between 400 and 300 Ma.

- The regional context of the Hamilton Fault having a dextral and normal component suggests a ε_3 uplift, an ε_2 extension SW to NE and ε_1 NW-SE shortening which is similar in character to the N-S shortening which is seen in the ASO.

- Therefore micro-tectonic analysis, structural features and thermochronology appears to correlate with the timing of the ASO indicating that both exhumation and deformation may have been the result of the widespread orogeny.

- Further we raise the possibility that this period of exhumation produced a significant proportion of the folding (which defines the MPP) and the faulting which bounds and dissects it. This extends on McLaren *et al.* (2002)'s notion that deformation was essentially Delamerian and was followed by exhumation without significant folding (see McLaren *et al.* (2002) Fig. 7).

- The MPP is still poorly constrained and future research, which is outside of this projects scope, would contribute to the insight of the complex history of this region.

8. ACKNOWLEDGEMENTS

I would like to thank my supervisors David Giles, Alan Collins and Guillaume Backe for their support and guidance throughout the year. I would like to especially thank David Giles for his fantastic effort throughout this year especially during my first sole expedition as an honours student. A special thanks goes to the lovely Stephen Hore of PIRSA for an insight into his passion and wisdom on the geology of Arkaroola. I would like to thank the Sprigg Family at Arkaroola Sanctuary for having me in rain, wind and shine, Fred Jourdan of Curtin University for his week of argon experience and an insight into postgraduate geological and geochronogical study. I would like to thank Honours class of 2009 and 2010 especially David Segui for just being Sog Dog, David Nettle, David Haddow and Pete Coleman for helping me during the year and introducing me to new concepts of doing all nighters and Thursday afternoon schnitzels. I would like to thank my friends, special thanks goes to Rebecca and Thi. Tom, thank you, words cannot describe what you have put up with. To my family; Mum, Dad and Jack for the good and the bad, for the financial and emotional support without you guys I wouldn't be who I am and for that I thank you. And finally this thesis is dedicated to both sets of Grandparents especially to the late Peter and Jenny James, the most inspiring people I have known.

9. REFERENCES

AMBROSE G. J. 1978. The Geology and Geochemistry of Adelaidean Sediments, Mount Painter Province, South Australia, with emphasis on the upper Umberatana Group. Bachelor of Science (Hons) thesis, Geology and Geophysics, The University of Adelaide, Adelaide (unpubl.).

BRUGGER J., LONG N., MCPHAIL D. C. & PLIMER I. 2005. An active amagmatic hydrothermal system: The Paralana hot springs, Northern Flinders Ranges, South Australia. *Chemical Geology* 222, 35-64.

COATS R. P. & BLISSETT A. H. 1971. Regional and Economic Geology of the Mount Painter Province.

COATS R. P., HORWITZ R. C., CRAWFORD A. R., CAMPANA B. & THATCHER D. 1969. *Mount Painter Province, S.A Sheet Geological Survery of South Australia, 1:125000*, Adelaide.

DUNLAP W. J. & TEYSSIER C. 1995. Paleozoic Deformation and Isotopic Disturbance in the Southeastern Arunta Block, Central Australia. *Precambrian Research* 71, 229-250.

DYMOKE P. & SANDIFORD M. 1992. Phase relationships in Buchan facies series pelitic assemblages: calculations with application to andalusite- staurolite parageneses in the Mount Lofty Ranges, South Australia. *Contributions to Mineralogy and Petrology* 110, 121-132.

ELBURG M. A., BONS P. A., FODEN J. & BRUGGER J. 2003. A newly defined Late Ordovician magmatic-thermal event in the Mount Painter Province, northern Flinders Ranges, South Australia. *Australian Journal of Earth Sciences* 50, 611-631.

FLOTTMANN T. & HAND M. 1999. Folded basement-cored tectonic wedges along the northern edge of the Amadeus Basin, Central Australia: evaluation of orogenic shortening. *Journal of Structural Geology* 21, 399-412.

FODEN J., ELBURG M. A., DOUGHERTY-PAGE J. & BURTT A. 2006. The timing and duration of the Delamerian orogeny: Correlation with the Ross Orogen and implications for Gondwana assembly. *Journal of Geology* 114, 189-210.

FODEN J., SANDIFORD M., DOUGHERTY-PAGE J. & WILLIAMS I. 1999. Geochemistry and geochronology of the Rathjen gneiss: Implications for the early tectonic evolution of the Delamerian Orogen. *Australian Journal of Earth Sciences*, 377-389.

FOSTER D., MURPHY J. M. & GLEADOW A. J. W. 1999. Chronology of deformation within the turbidite-dominated Lachlan orogeny: Implications for the tectonic evolution of eastern Australia and Gondwana. *Tectonics* 18, 452-485.

FOSTER D. A., MURPHY J. M. & GLEADOW A. J. W. 1994. Middle Tertiary Hydrothermal Activity and Uplift of the Northern Flinders Ranges, South Australia- Insights from Apatite Fission-Track Thermochronology. *Australian Journal of Earth Sciences* 41, 11-17.

GILES D. 2000. Tectonic Setting of Broken Hill-type Mineralisation the Cannington Perspective. Doctor of Philosophy thesis, Earth Sciences, Monash University, Melbourne (unpubl.).

HAINES P. W. & FLOTTMANN T. 1998. Delamerian Orogeny and potential foreland sedimentation: a review of age and stratigraphic constraints. *Australian Journal of Earth Sciences* 45, 559-570.

HAINES P. W., HAND M. & SANDIFORD M. 2001. Palaeozoic synorogenic sedimentation in central and northern Australia: a review of distribution and timing with implications for the evolution of intracontinental orogens. *Australian Journal of Earth Sciences* 48, 911-928.

HAND M., MAWBY J., KINNY P. & FODEN J. 1999. U-Pb ages from the Harts Range, central Australia: evidence for early Ordovician extension and constraints on Carboniferous metamorphism. *Journal of the Geological Society* 156, 715-730.

HARTLEY M. J., FOSTER D. & GRAY D. R. 1998. The significance of younger thermal events in the Willyama Inliers: Using 40Ar/39Ar thermochronology. *Geological Society of Australia Abstract*, 19-20.

IDNURM M. & HEINRICH C. A. 1993. A Paleomagnetic Study of Hydothermal Activity and Uranium Mineralization at Mt Painter, South Australia. *Australian Journal of Earth Sciences* 40, 87-101.

JENKINS R. J. F. & SANDIFORD M. 1992. Observations on the Tectonic Evolution of the Southern Adelaide Fold Belt. *Tectonophysics*, 27-36.

JOURDAN F. & RENNE P. R. 2007. Age calibration of the Fish Canyon sanidine Ar-40/Ar-39 dating standard using primary K-Ar standards. *Geochimica Et Cosmochimica Acta* 71, 387-402.

KOPPERS A. A. P. 2002. ArArCALC - software for Ar-40/Ar-39 age calculations. *Computers & Geosciences* 28, 605-619.

LITTLE T. A., MCWILLIAMS M. O. & HOLCOMBE R. J. 1995. 40Ar/ 39Ar thermochronology of epidote blueschists from the North D'Aguilar Block, Queensland, Australia; timing and kinematics of subduction complex unroofing. *Geological Society of Australia Bulletin* 107.

MCDOUGALL I. & HARRISON M. T. 1999. *Geochronology and Thermochronology by the 40-Argon/ 39-Argon Method* (Second edition). Oxford University Press.

MCLAREN S., DUNLAP W. J., SANDIFORD M. & MCDOUGALL I. 2002. Thermochronology of high heat-producing crust at Mount Painter, South Australia: Implications for tectonic reactivation of continental interiors. *Tectonics* 21.

MCLAREN S., SANDIFORD M., POWELL R., NEUMANN N. & WOODHEAD J. 2006. Palaeozoic intraplate crustal anatexis in the Mount Painter Province, South Australia: Timing, thermal budgets and the role of crustal heat production. *Journal of Petrology* 47, 2281-2302.

MILDREN S. D. & SANDIFORD M. 1995. Heat Refraction and low-pressure metamorphism in the northern Flinders Ranges, South Australia. *Australian Journal of Earth Sciences* 42, 241-247.

MIN K. W., MUNDIL R., RENNE P. R. & LUDWIG K. R. 2000. A test for systematic errors in Ar-40/Ar-39 geochronology through comparison with U/Pb analysis of a 1.1-Ga rhyolite. *Geochimica Et Cosmochimica Acta* 64, 73-98.

MITCHELL M. M., KOHN B. P., O'SULLIVAN P. B., HARTLEY M. J. & FOSTER D. A. 2002. Low-temperature thermochronology of the Mt Painter Province, South Australia. *Australian Journal of Earth Sciences* 49, 551-563.

O'SULLIVAN P. B., KOHN B. P. & MITCHELL M. M. 1998. Phanerozoic reactivation along a fundamental Proterozoic crustal fault, the Darling River Lineament Australia: Constraints from apatite fission track thermochronology. *Earth Planet Science Letters* 164, 451-465.

PAUL E., FLOTTMANN T. & SANDIFORD M. 1999. Structural geometry and controls on basement-involved deformation in the northern Flinders Ranges, Adelaide Fold Belt, South Australia. *Australian Journal of Earth Sciences* 46, 343-354.

PREISS W. V. 1987. The Adelaide Geosyncline Late Proterozoic Stratigraphy, Sedimentation Palaeontology and Tectonics.

PREISS W. V. 2000. The Adelaide Geosyncline of South Australia and its significance in Neoproterozoic continental reconstruction. *Precambrian Research* 100, 21-63.

REINERS P. W., EHLERS T. A. & ZEITLER P. K. 2005. Past, Present, and the Future of Thermochronology *Reviews in Mineralogy and Geochemistry* 58, 1-18.

SANDIFORD M., HAND M. & MCLAREN S. 1998a. High geothermal gradient metamorphism during thermal subsidence. *Earth and Planetary Science Letters* 163, 149-165.

SANDIFORD M., PAUL E. & FLOTTMANN T. 1998b. Sedimentary thickness variations and deformation intensity during basin inversion in the Flinders Ranges, South Australia. *Journal of Structural Geology* 20, 1721-1731.

SPIKINGS R. A., FOSTER D. & KOHN B. P. 1997. Phanerozoic denudation history of Mount Isa Inlier, Northern Australia: A record of the response of a Proterozoic mobile belt to intraplate tectonics. *Int. Geological Review* 39, 100-124.

TEALE G. S. 1993. *The Geology of South Australia. Vol 1. The Precambrian* (Geology of the Mount Painter and Mount Babbage Inliers). South Australia. Geological Survey. Bulletin, 54.

TEALE G. S. 1995. Highly deformed alkaline granites from the southern Mount Painter Inlier, northern Flinders Ranges. *Quarterly Geological Notes Geological Survey of South Australia* 127, 19-28.

WILLCOX J. B. 1996. Critical tectonic events in the development of the North West Shelf. *Geological Society of Australia Abstract* 41, 473.

10. FIGURE CAPTIONS

Figure 1: Map of Australia showing the location of the AFB (light green). AFB located in South Australia also includes inferred sections of the Copper Basin, Curnamona Craton, Stuart Shelf and Gawler Craton. The AFB is divided up into four main areas these are the South Australia Fold Belt, Nackara Arc, Northern Flinders Ranges and Central Flinders Ranges. The Northern Flinders Ranges shows the location of the Mount Painter Province (modified after McLaren et al. 2002).

Figure 2: Unconformity related contact metamorphism. Section from the southern area of the Mount Painter Inlier illustrating the concordance of metamorphic isotherms (cordierite, tremolite and scapolite) with the basement cover unconformity (Modified after McLaren et al. 2006).

Figure 3: Regional geology of the Mount Painter Province showing the Mount Painter and Mount Babbage Inlier. Geological features include Paralana Fault on the eastern side and Hamilton Fault on the western side. The Hamilton Fault is indicated by a square (modified after McLaren et al. 2006).

Figure 4: Temperature-time path for the post-Delamerian history of the Mount Painter rocks. Our ^{39}Ar/^{40}Ar ages is compared with McLaren *et al.* (2002) hornblende, muscovite, biotite Ar/Ar and k-feldspar multiple-diffusion-domain thermal modeling, Elburg *et al.* (2003) various thermal dating (U/Pb, Rb/Sr, Sm/Nd, Monazite and Apatite Fission) and Indnurm & Heinrich (1993) Palaeomagnetic data. The duration of the Alice Springs Orogeny, Lachlan Orogeny, Queensland Tectonism and Delamerian Orogeny are also shown (McLaren *et al.* 2002).

Figure 5: Generalised tectono- stratigraphy of the Mount Painter Province showing major magmatic, sedimentary and deformational events. All Adelaidean cover sequence is summarized in Preiss (2000) including the depth of the Adelaidean sequence between 12 and 15 km. Other dates throughout the Mesoproterozoic basement and the major events are taken from McLaren *et al.* (2006).

Figure 6: Detailed 1: 20 000 Geological map of the WNW trending Hamilton Fault showing structural data and interpreted trend of lithological contacts (refer to attached .png document)

Figure 7: Structural N to S schematic cross section constructed through the Hamilton Fault. (Location of A to B and C to D is displayed on Fig. 22).

Figure 8: Outcrop photos taken at various locations throughout the Hamilton Fault area. (a) Large quartz vein taken in the Paralana Quartzite. The vein in situated on the Hamilton Fault in the central domain of the mapping zone about 500 metres from the boundary between the Wywyana Formation and the Paralana Quartzite. (b) Quartz kinematic clasts with dextral movement, south side down. Found in the same location as Fig. 5a, in the Paralana Quartzite. (c) Deformed quartz vein with a dextral passive strain, situated in the same area as Fig. 5 a & b. This suggests a hydrothermal event occurred pre-deformation. (d) Breccia caused by brittle friction of the Hamilton Fault. The breccia is matrix supporting with clasts of Mount Neil Granite. (e) Highly folded veins suggesting both hydrothermal and deformational influence, situated in the Yananinna Siltstone Member. (f) Deformation of quartz veining suggesting a hydrothermal event occurred pre-deformation. Situated in the Amberoona Formation and shows a different depositional environment than the Yankaninna Siltstone Member. (g) Outcrop of scapolisation in the Amberoona Formation. (h) Quartz fibres intergrown in pegmatitic fabric, situated in the pegmatoidal unit which is on the eastern side of the Hamilton Fault near the Commonwealth Mine. (i) Quartz kinematic indicator with dextral movement, south side down. This kinematic indicator is situated in the Paralana Quartzite in the central domain of the mapping area. (j) Quartz vein offset found in the Paralana Quartzite close to the shear zone, it is suggesting a pre or syn-deformation as the fabric has overprinted the offset.

Figure 9: Stereonets and associated contour plots of all the structural data attained from the Hamilton Fault and the surrounding area.

Figure 10: Photomicrographs of kinematic indicators and petrological relationships. (a) Sample VP09021 showing a muscovite mineral growing in with quartz. The muscovite shows pristine boundaries and its importance is that its cooling history was measured by the ^{40}Ar/^{39}Ar dating method. (Field of view is 3 mm) (b) Sample VP09022 showing crenulation with very fine grained biotite and andalusite (~0.5 mm) defining the schistosity, there is also a dominant chlorite alteration throughout the sample which shows and intense green alteration. (Field of view is 2 mm) (c) Sample VP09024 is photographed in plane polar showing the biotite (khaki colour) growing in with the fabric. (Field of view is 7 mm) (d) Sample VP09024 is photographed in cross polar showing the large porphyroblasts with biotite defining the outline. (Field of view is 7 mm) (e) Sample VP09020 (Field of view is 6 mm) pegmatoidal granite which has intruded pre-deformation. Larger grained (~1-3 mm) and small grained minerals (~0.2-0.5 mm), the predominate minerals are quartz and plagioclase. (f) Sample VP09023 (Field of view is 6 mm) shows pegmatoidal granite influenced by hydrothermal event as quartz veins have recrystallised on the boundary of muscovite grains. (g) VP09015 is a sheared marble and shows a large (~6 mm) σ-clast poikilobastic kinematic indicator as there are inclusion of other small grained minerals (<0.5 mm) such as biotite, muscovite and opaque minerals. The poiklioblast has a dextral movement, south side down. (h) VP09017 shows a σ-clast kinematic

indicator which a muscovite phenocryst (~2-3 mm) has been rotated in a dextral movement, south side down. (i) VP09017 shows a large grained (~2 mm) quartz phenocryst kinematic indicator and shows dextral movement, south side down. (l) VP09009 , a dolomitic marble rock showing carbonates, muscovite and actinolite, this sample is used in comparing to VP09010 which is the sheared version of this. (Field of view is 7 mm) (k) Sample VP09010, a sheared dolomitic marble rock showing carbonate minerals aligned with the fabric and overprinting by amphiboles. (Field of view is 2 mm) (l) VP09019 shows differential crenulated biotite (Fig. 7l) which has eventually recrystallised and new biotite grown and starting to crenulate again.

Figure 10.1 (INSET 1): Idealised development of mantled porphyroblasts around spherical core objects which don’t shrink during progressive deformation. Bow-tie shaped, note that δ-type and σ-type have a similar initial development. (Modified after Passchier & Trouw 2005)

Figure 10.2 (INSET 2): Inferred range of stages in crenulation cleavage development with increasing deformation. 1. Crenulations have formed in original foliation. 2. Crenulations are somewhat tighter and discrete cleavage is visible. 3. New cleavage has developed and recrystallised microfolds known as polyarcs may be visible. 4. New grains grow along dominate fabric. 5. The minerals are completely transposed and not recognisable. An example of the final stage is seen in the picture (1 mm width of view) (Modified after Passchier & Trouw 2005)

Figure 11: Detailed 1:25 000 Geological map of the Hamilton Fault showing the location of each sample and highlighting the locality of those samples used in ^{39}Ar/^{40}Ar thermochronology.

Figure 12 to 18: Summary of the 40Ar/39Ar age spectra for muscovite, biotite and k-feldspar. A spectrum arranged in order according to numerical position.

Figure 19: Tectonic Model of the three options discussed. Option one suggests a model where Delamerian folding occurred followed by relaxation of isotherms to horizontal and subsequent exhumation. Option two suggests Delamerian folding occurred without relaxation of isotherms because the cooling temperature is totally dependent on basement heat flow. Option three suggests that exhumation is driven subsequent to the Delamerian folding.

Figure 20: NE-SW and NW-SE schematic cross sections showing the Neoproterozoic to Carboniferous evolution of the MPP and adjacent crustal blocks. The first is McLaren et al. (2002) tectonic model showing (a) Deposition of the Adelaidean sedimentary cover during dominantly rift and sag phase subsidence. (b) Uplift of the MPP during the Delamerian orogeny was gradual and largely driven by isostatic rebound. (c) Very slow post-Delamerian isostatic rebound. Changing tectonic stresses, potentially related to the earliest ASO, and probably caused accelerated cooling at 430 Ma. (d) Exhumation of the MPP during the ASO at 400 Ma; possible intrusion of the British Empire

granite and locally derived pegmatites into the middle crust. The MPP was inferred to have been exhumed by at least 3 km from 430 Ma until this time, and the Warburton Basin was deformed under strong compression with folding and thrusting seen throughout the Cambrian and Ordovician sediments. (e) Post-ASO isostatic rebound of the MPP. (f) Final exhumation of the MPP by a further 3 km. The second is my interpretation from the new Argon data incorporating options two and three suggesting exhumation is driven subsequent of Delamerian folding. During (b) and (c) there was no exhumation but metamorphism and folding from the Delamerian Orogeny. (d) Exhumation occurs during the ASO at 400 Ma and throughout till 325 Ma (f) showing uplift of the Delamerian folding and sediments being deposited in various basin surrounding the MPP.

Figure 21: Overall Copley region (Coats *et al.* 1969) showing the locality of the MPP, the Paralana Fault and the Norwest Fault. The regional context of the Hamilton Fault having a dextral and normal component suggests a ε_3 uplift, an ε_2 extension SW to NE and ε_1 NW-SE shortening which is similar in character to the N-S shortening which is seen in the ASO.

Figure 22: Locality map showing basins and basement inliers associated with the former Centralian Superbasin. The Centralian Superbasin is suggested to be related to the Alice Springs Orogeny. The Northern Flinders Ranges with the Adelaide Fold Belt has been added showing the locality compared to basins of possible erosion deposits (e.g. the Warburton Basin).

11. TABLES

Table 1: Summary of $^{40}Ar/^{39}Ar$ thermochronology data

Sample	Lithology	Mineral	MSWD	Probability	Integrated Total Fusion 40Ar/39Ar Age, Ma ± 2σ	Plateau Age, Ma ± 1σ
VP09010	Adelaidean Marble	Muscovite	0.42	0.79	388.08 ± 1.95	390.31 ± 1.95
VP09019	Mesoproterozoic metasedimentary rock	Biotite	N/A	N/A	291.01 ± 1.83	344.26 ± 4.14
VP09020	Pegmatodial granite	Muscovite	0.73	0.76	359.47 ± 1.73	359.44 ± 1.68
VP09021	Mesoproterozoic metasedimentary rock	Muscovite	1.3	0.16	346.66 ± 1.52	346.77 ± 1.53
VP09022	Mesoproterozoic metasedimentary rock	Biotite	0.63	0.71	352.15 ± 3.03	357.39 ± 2.88
VP09023	Pegmatodial granite	K-Feldspar	1.02	0.44	314.03 ±1.4	312.77 ± 1.34
VP09024	Mesoproterozoic metasedimentary rock	Biotite	0.38	0.93	348.43 ± 1.79	351.75 ± 1.76

Table 2: ^{40}Ar/^{39}Ar data acquisition for sample VP09010

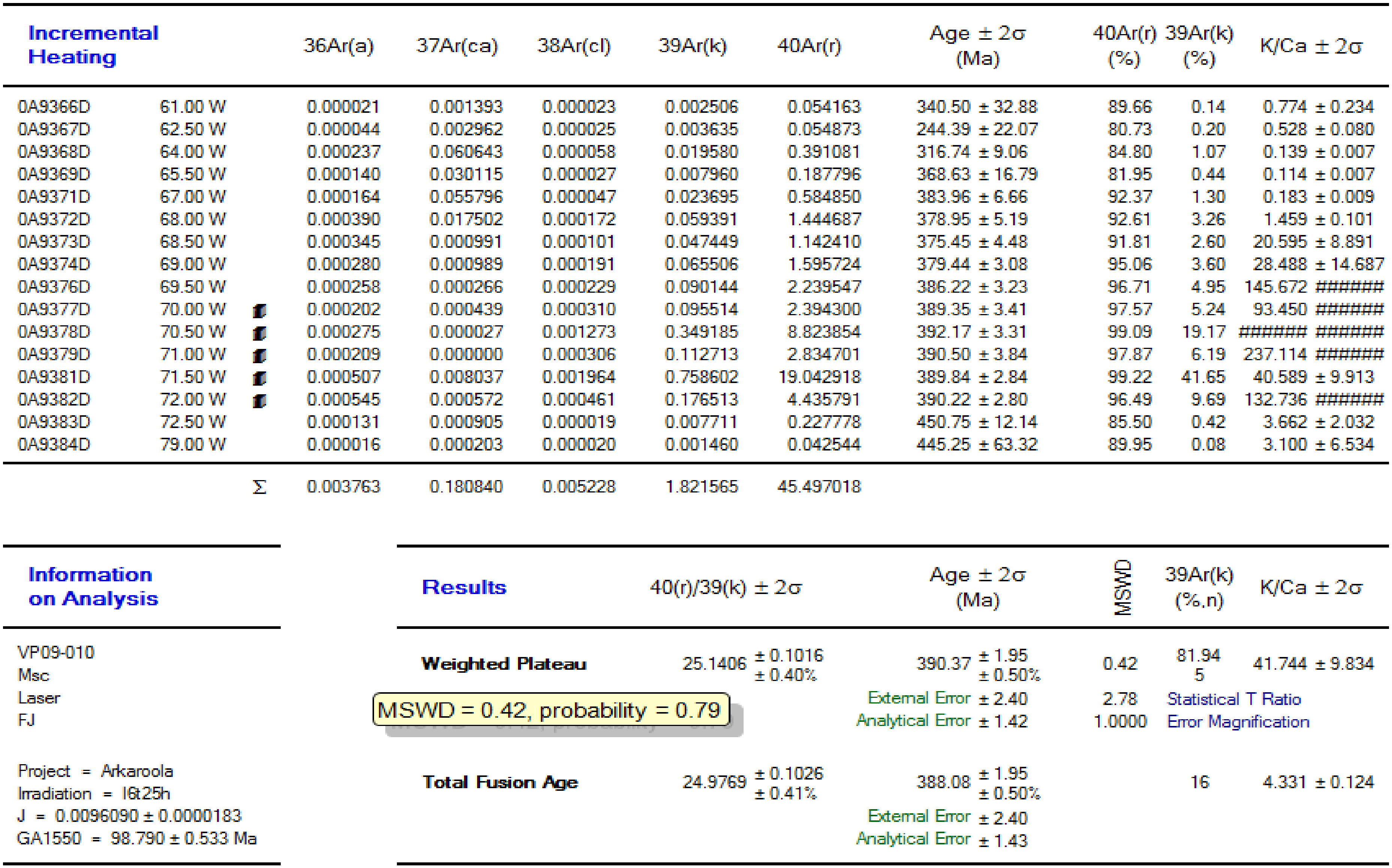

Incremental Heating			36Ar(a)	37Ar(ca)	38Ar(cl)	39Ar(k)	40Ar(r)	Age ± 2σ (Ma)	40Ar(r) (%)	39Ar(k) (%)	K/Ca ± 2σ
0A9366D	61.00 W		0.000021	0.001393	0.000023	0.002506	0.054163	340.50 ± 32.88	89.66	0.14	0.774 ± 0.234
0A9367D	62.50 W		0.000044	0.002962	0.000025	0.003635	0.054873	244.39 ± 22.07	80.73	0.20	0.528 ± 0.080
0A9368D	64.00 W		0.000237	0.060643	0.000058	0.019580	0.391081	316.74 ± 9.06	84.80	1.07	0.139 ± 0.007
0A9369D	65.50 W		0.000140	0.030115	0.000027	0.007960	0.187796	368.63 ± 16.79	81.95	0.44	0.114 ± 0.007
0A9371D	67.00 W		0.000164	0.055796	0.000047	0.023695	0.584850	383.96 ± 6.66	92.37	1.30	0.183 ± 0.009
0A9372D	68.00 W		0.000390	0.017502	0.000172	0.059391	1.444687	378.95 ± 5.19	92.61	3.26	1.459 ± 0.101
0A9373D	68.50 W		0.000345	0.000991	0.000101	0.047449	1.142410	375.45 ± 4.48	91.81	2.60	20.595 ± 8.891
0A9374D	69.00 W		0.000280	0.000989	0.000191	0.065506	1.595724	379.44 ± 3.08	95.06	3.60	28.488 ± 14.687
0A9376D	69.50 W		0.000258	0.000266	0.000229	0.090144	2.239547	386.22 ± 3.23	96.71	4.95	145.672 #######
0A9377D	70.00 W	■	0.000202	0.000439	0.000310	0.095514	2.394300	389.35 ± 3.41	97.57	5.24	93.450 #######
0A9378D	70.50 W	■	0.000275	0.000027	0.001273	0.349185	8.823854	392.17 ± 3.31	99.09	19.17	####### #######
0A9379D	71.00 W	■	0.000209	0.000000	0.000306	0.112713	2.834701	390.50 ± 3.84	97.87	6.19	237.114 #######
0A9381D	71.50 W	■	0.000507	0.008037	0.001964	0.758602	19.042918	389.84 ± 2.84	99.22	41.65	40.589 ± 9.913
0A9382D	72.00 W	■	0.000545	0.000572	0.000461	0.176513	4.435791	390.22 ± 2.80	96.49	9.69	132.736 #######
0A9383D	72.50 W		0.000131	0.000905	0.000019	0.007711	0.227778	450.75 ± 12.14	85.50	0.42	3.662 ± 2.032
0A9384D	79.00 W		0.000016	0.000203	0.000020	0.001460	0.042544	445.25 ± 63.32	89.95	0.08	3.100 ± 6.534
		Σ	0.003763	0.180840	0.005228	1.821565	45.497018				

Information on Analysis

VP09-010
Msc
Laser
FJ

Project = Arkaroola
Irradiation = I6t25h
J = 0.0096090 ± 0.0000183
GA1550 = 98.790 ± 0.533 Ma

Results	40(r)/39(k) ± 2σ	Age ± 2σ (Ma)	MSWD	39Ar(k) (%,n)	K/Ca ± 2σ
Weighted Plateau	25.1406 ± 0.1016 ± 0.40%	390.37 ± 1.95 ± 0.50%	0.42	81.94 5	41.744 ± 9.834
		External Error ± 2.40	2.78	Statistical T Ratio	
		Analytical Error ± 1.42	1.0000	Error Magnification	
Total Fusion Age	24.9769 ± 0.1026 ± 0.41%	388.08 ± 1.95 ± 0.50%		16	4.331 ± 0.124
		External Error ± 2.40			
		Analytical Error ± 1.43			

MSWD = 0.42, probability = 0.79

Table 3: ^{40}Ar/^{39}Ar data acquisition for sample VP09019

Incremental Heating			36Ar(a)	37Ar(ca)	38Ar(cl)	39Ar(k)	40Ar(r)	Age ± 2σ (Ma)	40Ar(r) (%)	39Ar(k) (%)	K/Ca ± 2σ
0A9179D	56.00 W		0.000381	0.001189	0.000615	0.076810	1.101903	232.98 ± 2.09	90.72	43.10	27.785 ± 22.657
0A9180D	56.10 W		0.000107	0.000561	0.000209	0.020458	0.409967	317.70 ± 4.11	92.83	11.48	15.684 ± 26.107
0A9181D	56.20 W		0.000046	0.000112	0.000079	0.010521	0.211281	318.32 ± 5.76	94.01	5.90	40.265 #######
0A9182D	56.30 W		0.000083	0.000478	0.000146	0.018089	0.389291	339.11 ± 4.32	94.04	10.15	16.270 ± 33.392
0A9184D	56.40 W	■	0.000101	0.000056	0.000213	0.024501	0.535482	343.91 ± 4.26	94.74	13.75	188.906 #######
0A9185D	56.50 W	■	0.000024	0.000000	0.000058	0.005018	0.111108	348.00 ± 11.54	93.97	2.82	27.484 #######
0A9186D	56.60 W	■	0.000008	0.000000	0.000017	0.001319	0.027963	334.42 ± 33.46	92.48	0.74	27.484 #######
0A9187D	56.90 W		0.000070	0.000000	0.000085	0.013859	0.297170	337.99 ± 6.08	93.49	7.78	27.484 #######
0A9189D	57.20 W		0.000046	0.000000	0.000060	0.007360	0.154471	331.45 ± 7.48	91.97	4.13	27.484 #######
0A9190D	57.40 W		0.000000	0.000000	0.000000	0.000295	0.008077	420.87 ± 34.45	100.00	0.17	27.484 #######
		Σ	0.000865	0.002396	0.001481	0.178229	3.246714				

Information on Analysis

VP09-019
Bio
Laser
AF

Project = Arkaroola
Irradiation = I6t25h
J = 0.0096090 ± 0.0000183
GA1550 = 98.790 ± 0.533 Ma

Results	40(r)/39(k) ± 2σ	Age ± 2σ (Ma)	MSWD	39Ar(k) (%,n)	K/Ca ± 2σ
Weighted Plateau	21.8799 ± 0.2772 ± 1.27%	344.26 ± 4.14 ± 1.20%	0.40	17.30 3	27.594 ± 82.992
		External Error ± 4.33	4.30	Statistical T Ratio	
		Analytical Error ± 3.97	1.0000	Error Magnification	
Total Fusion Age	18.2165 ± 0.1028 ± 0.56%	291.01 ± 1.83 ± 0.63%		10	31.989 ± 40.531
		External Error ± 2.11			
		Analytical Error ± 1.52			

Table 4: ^{40}Ar/^{39}Ar data acquisition for sample VP09020

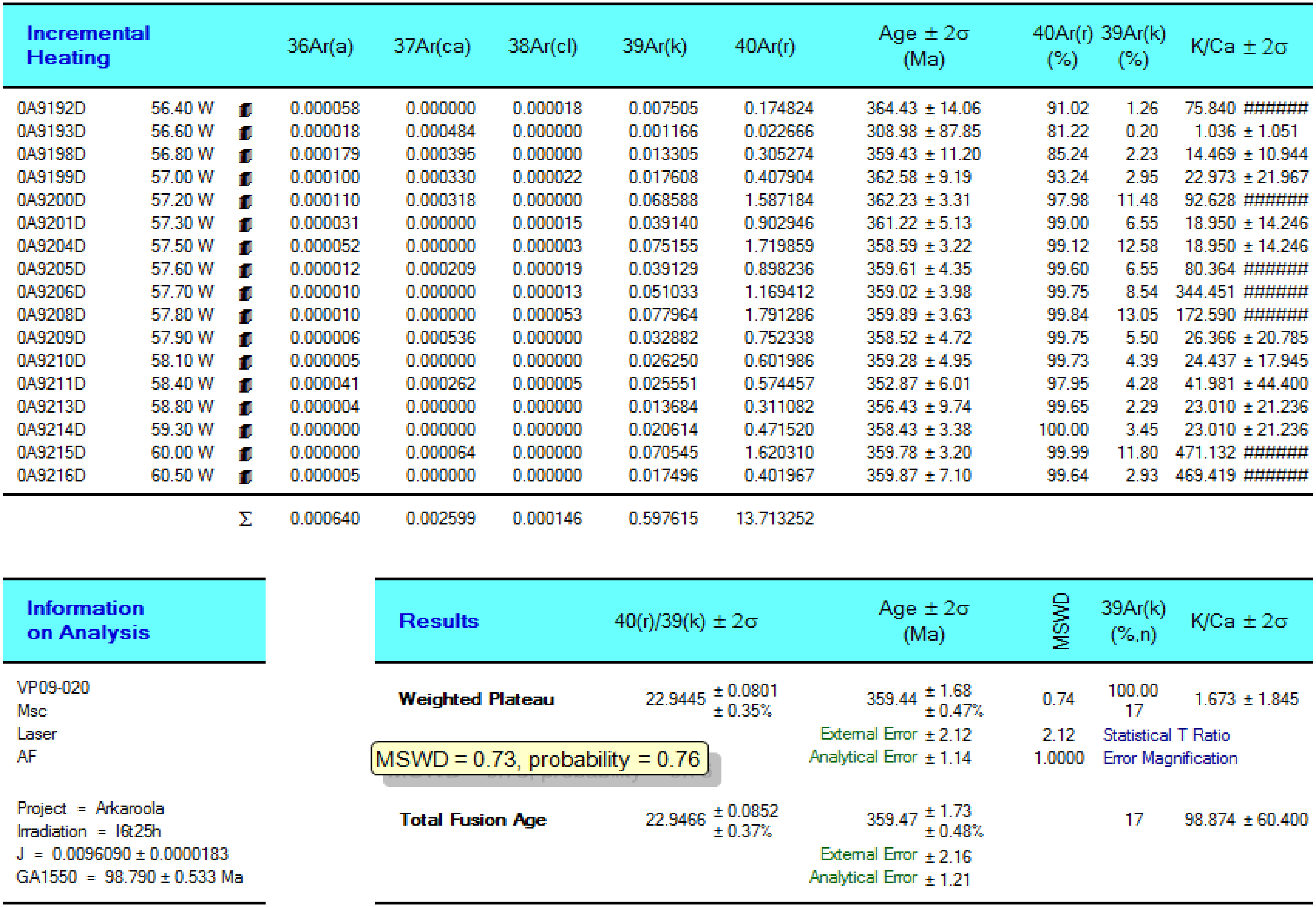

Incremental Heating			36Ar(a)	37Ar(ca)	38Ar(cl)	39Ar(k)	40Ar(r)	Age ± 2σ (Ma)	40Ar(r) (%)	39Ar(k) (%)	K/Ca ± 2σ
0A9192D	56.40 W	▮	0.000058	0.000000	0.000018	0.007505	0.174824	364.43 ± 14.06	91.02	1.26	75.840 ######
0A9193D	56.60 W	▮	0.000018	0.000484	0.000000	0.001166	0.022666	308.98 ± 87.85	81.22	0.20	1.036 ± 1.051
0A9198D	56.80 W	▮	0.000179	0.000395	0.000000	0.013305	0.305274	359.43 ± 11.20	85.24	2.23	14.469 ± 10.944
0A9199D	57.00 W	▮	0.000100	0.000330	0.000022	0.017608	0.407904	362.58 ± 9.19	93.24	2.95	22.973 ± 21.967
0A9200D	57.20 W	▮	0.000110	0.000318	0.000000	0.068588	1.587184	362.23 ± 3.31	97.98	11.48	92.628 ######
0A9201D	57.30 W	▮	0.000031	0.000000	0.000015	0.039140	0.902946	361.22 ± 5.13	99.00	6.55	18.950 ± 14.246
0A9204D	57.50 W	▮	0.000052	0.000000	0.000003	0.075155	1.719859	358.59 ± 3.22	99.12	12.58	18.950 ± 14.246
0A9205D	57.60 W	▮	0.000012	0.000209	0.000019	0.039129	0.898236	359.61 ± 4.35	99.60	6.55	80.364 ######
0A9206D	57.70 W	▮	0.000010	0.000000	0.000013	0.051033	1.169412	359.02 ± 3.98	99.75	8.54	344.451 ######
0A9208D	57.80 W	▮	0.000010	0.000000	0.000053	0.077964	1.791286	359.89 ± 3.63	99.84	13.05	172.590 ######
0A9209D	57.90 W	▮	0.000006	0.000536	0.000000	0.032882	0.752338	358.52 ± 4.72	99.75	5.50	26.366 ± 20.785
0A9210D	58.10 W	▮	0.000005	0.000000	0.000000	0.026250	0.601986	359.28 ± 4.95	99.73	4.39	24.437 ± 17.945
0A9211D	58.40 W	▮	0.000041	0.000262	0.000005	0.025551	0.574457	352.87 ± 6.01	97.95	4.28	41.981 ± 44.400
0A9213D	58.80 W	▮	0.000004	0.000000	0.000000	0.013684	0.311082	356.43 ± 9.74	99.65	2.29	23.010 ± 21.236
0A9214D	59.30 W	▮	0.000000	0.000000	0.000000	0.020614	0.471520	358.43 ± 3.38	100.00	3.45	23.010 ± 21.236
0A9215D	60.00 W	▮	0.000000	0.000064	0.000000	0.070545	1.620310	359.78 ± 3.20	99.99	11.80	471.132 ######
0A9216D	60.50 W	▮	0.000005	0.000000	0.000000	0.017496	0.401967	359.87 ± 7.10	99.64	2.93	469.419 ######
		Σ	0.000640	0.002599	0.000146	0.597615	13.713252				

Information on Analysis

VP09-020
Msc
Laser
AF

Project = Arkaroola
Irradiation = I6t25h
J = 0.0096090 ± 0.0000183
GA1550 = 98.790 ± 0.533 Ma

Results	40(r)/39(k) ± 2σ		Age ± 2σ (Ma)		MSWD	39Ar(k) (%,n)	K/Ca ± 2σ
Weighted Plateau	22.9445	± 0.0801 ± 0.35%	359.44	± 1.68 ± 0.47%	0.74	100.00 17	1.673 ± 1.845
			External Error	± 2.12	2.12	Statistical T Ratio	
			Analytical Error	± 1.14	1.0000	Error Magnification	
Total Fusion Age	22.9466	± 0.0852 ± 0.37%	359.47	± 1.73 ± 0.48%		17	98.874 ± 60.400
			External Error	± 2.16			
			Analytical Error	± 1.21			

MSWD = 0.73, probability = 0.76

Table 5: ^{40}Ar/^{39}Ar data acquisition for sample VP09021

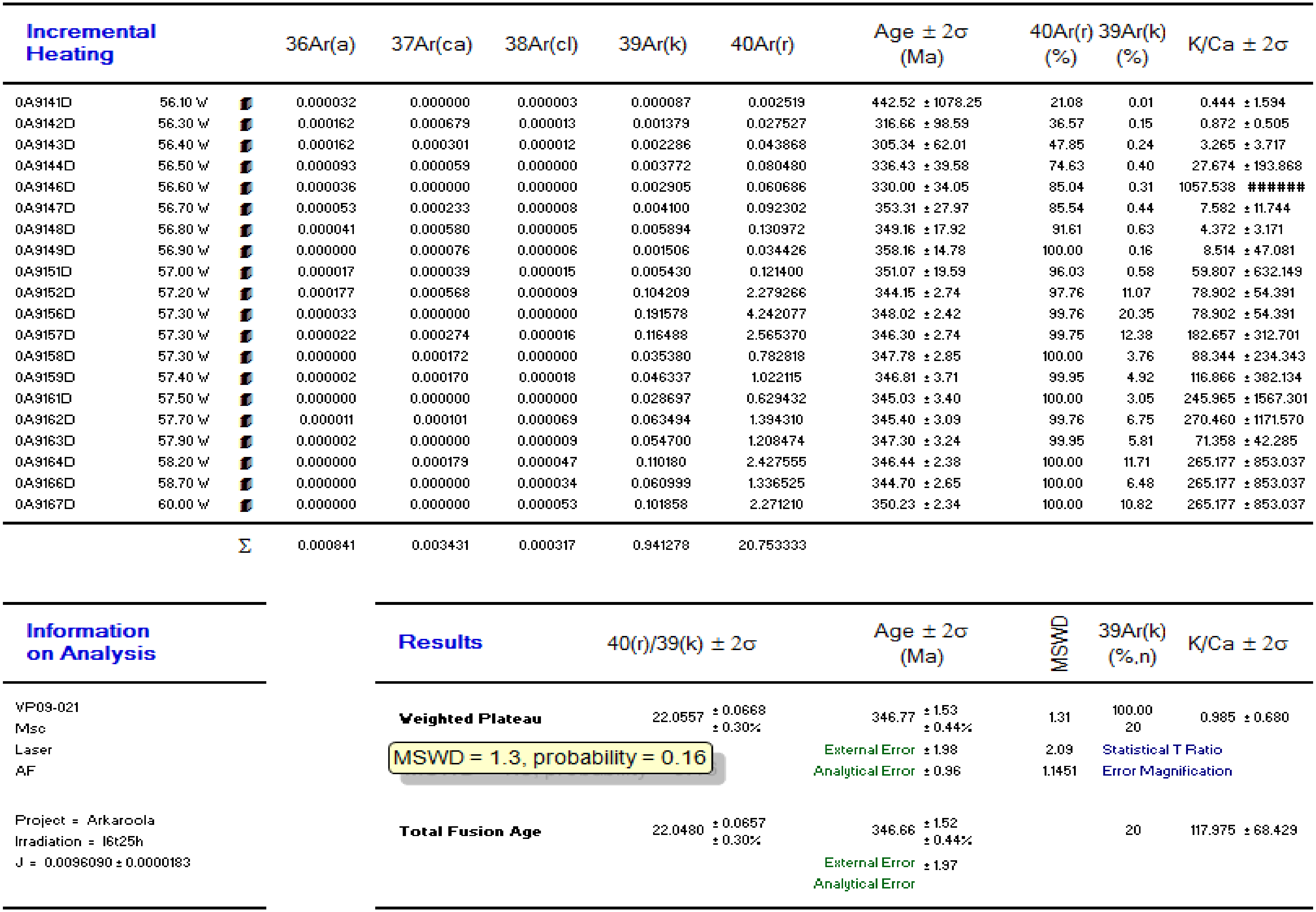

Incremental Heating			36Ar(a)	37Ar(ca)	38Ar(cl)	39Ar(k)	40Ar(r)	Age ± 2σ (Ma)		40Ar(r) (%)	39Ar(k) (%)	K/Ca ± 2σ	
0A9141D	56.10 W		0.000032	0.000000	0.000003	0.000087	0.002519	442.52	± 1078.25	21.08	0.01	0.444	± 1.594
0A9142D	56.30 W		0.000162	0.000679	0.000013	0.001379	0.027527	316.66	± 98.59	36.57	0.15	0.872	± 0.505
0A9143D	56.40 W		0.000162	0.000301	0.000012	0.002286	0.043868	305.34	± 62.01	47.85	0.24	3.265	± 3.717
0A9144D	56.50 W		0.000093	0.000059	0.000000	0.003772	0.080480	336.43	± 39.58	74.63	0.40	27.674	± 193.868
0A9146D	56.60 W		0.000036	0.000000	0.000000	0.002905	0.060686	330.00	± 34.05	85.04	0.31	1057.538	######
0A9147D	56.70 W		0.000053	0.000233	0.000008	0.004100	0.092302	353.31	± 27.97	85.54	0.44	7.582	± 11.744
0A9148D	56.80 W		0.000041	0.000580	0.000005	0.005894	0.130972	349.16	± 17.92	91.61	0.63	4.372	± 3.171
0A9149D	56.90 W		0.000000	0.000076	0.000006	0.001506	0.034426	358.16	± 14.78	100.00	0.16	8.514	± 47.081
0A9151D	57.00 W		0.000017	0.000039	0.000015	0.005430	0.121400	351.07	± 19.59	96.03	0.58	59.807	± 632.149
0A9152D	57.20 W		0.000177	0.000568	0.000009	0.104209	2.279266	344.15	± 2.74	97.76	11.07	78.902	± 54.391
0A9156D	57.30 W		0.000033	0.000000	0.000000	0.191578	4.242077	348.02	± 2.42	99.76	20.35	78.902	± 54.391
0A9157D	57.30 W		0.000022	0.000274	0.000016	0.116488	2.565370	346.30	± 2.74	99.75	12.38	182.657	± 312.701
0A9158D	57.30 W		0.000000	0.000172	0.000000	0.035380	0.782818	347.78	± 2.85	100.00	3.76	88.344	± 234.343
0A9159D	57.40 W		0.000002	0.000170	0.000018	0.046337	1.022115	346.81	± 3.71	99.95	4.92	116.866	± 382.134
0A9161D	57.50 W		0.000000	0.000000	0.000000	0.028697	0.629432	345.03	± 3.40	100.00	3.05	245.965	± 1567.301
0A9162D	57.70 W		0.000011	0.000101	0.000069	0.063494	1.394310	345.40	± 3.09	99.76	6.75	270.460	± 1171.570
0A9163D	57.90 W		0.000002	0.000000	0.000009	0.054700	1.208474	347.30	± 3.24	99.95	5.81	71.358	± 42.285
0A9164D	58.20 W		0.000000	0.000179	0.000047	0.110180	2.427555	346.44	± 2.38	100.00	11.71	265.177	± 853.037
0A9166D	58.70 W		0.000000	0.000000	0.000034	0.060999	1.336525	344.70	± 2.65	100.00	6.48	265.177	± 853.037
0A9167D	60.00 W		0.000000	0.000000	0.000053	0.101858	2.271210	350.23	± 2.34	100.00	10.82	265.177	± 853.037
		Σ	0.000841	0.003431	0.000317	0.941278	20.753333						

Information on Analysis

VP09-021
Msc
Laser
AF

Project = Arkaroola
Irradiation = I6t25h
J = 0.0096090 ± 0.0000183

Results	40(r)/39(k) ± 2σ		Age ± 2σ (Ma)		MSWD	39Ar(k) (%,n)	K/Ca ± 2σ	
Weighted Plateau	22.0557	± 0.0668 ± 0.30%	346.77	± 1.53 ± 0.44%	1.31	100.00 20	0.985	± 0.680
MSWD = 1.3, probability = 0.16			External Error	± 1.98	2.09	Statistical T Ratio		
			Analytical Error	± 0.96	1.1451	Error Magnification		
Total Fusion Age	22.0480	± 0.0657 ± 0.30%	346.66	± 1.52 ± 0.44%		20	117.975	± 68.429
			External Error	± 1.97				
			Analytical Error					

Table 6: ^{40}Ar/^{39}Ar data acquisition for sample VP09022

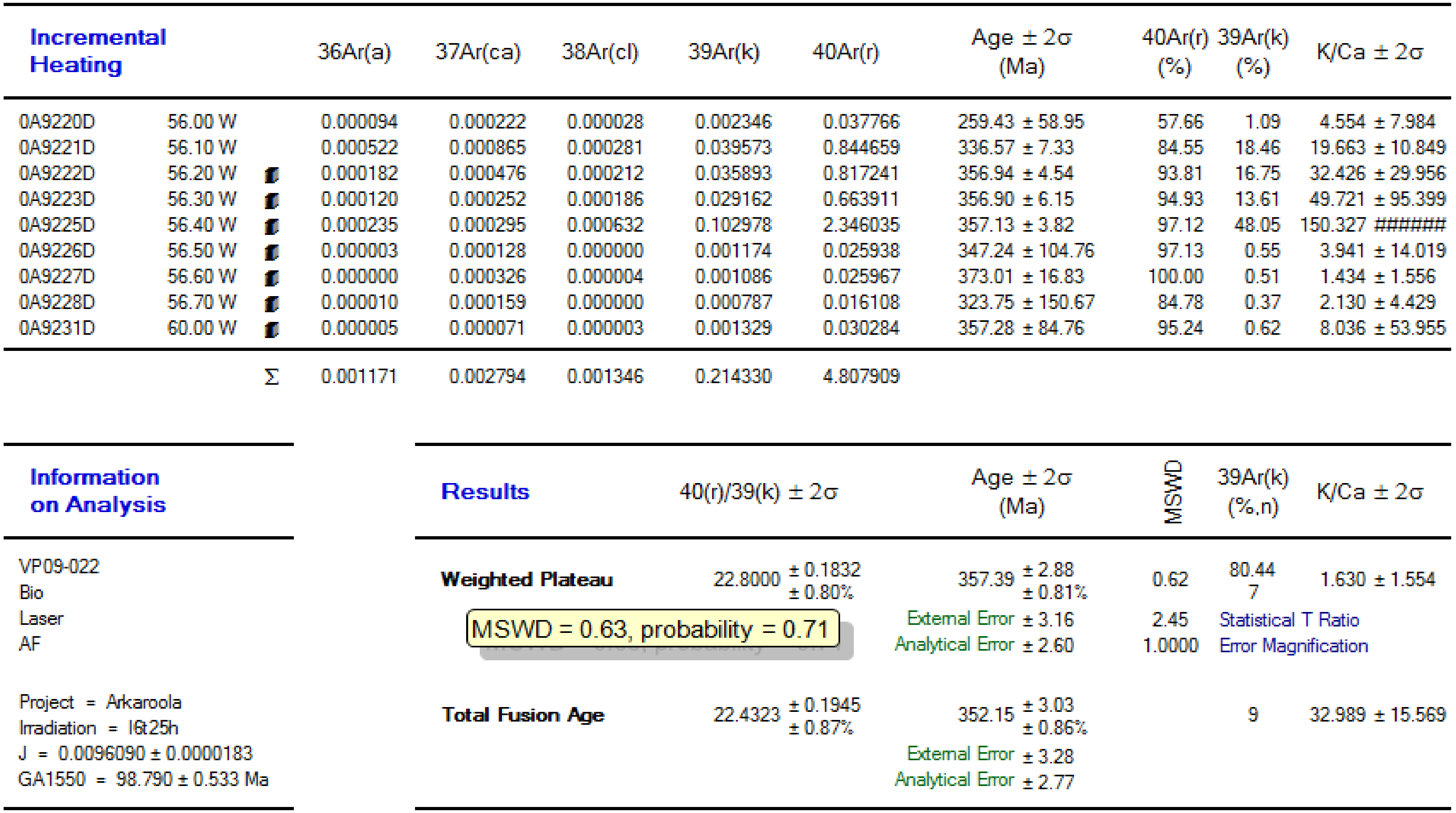

Incremental Heating			36Ar(a)	37Ar(ca)	38Ar(cl)	39Ar(k)	40Ar(r)	Age ± 2σ (Ma)	40Ar(r) (%)	39Ar(k) (%)	K/Ca ± 2σ
0A9220D	56.00 W		0.000094	0.000222	0.000028	0.002346	0.037766	259.43 ± 58.95	57.66	1.09	4.554 ± 7.984
0A9221D	56.10 W		0.000522	0.000865	0.000281	0.039573	0.844659	336.57 ± 7.33	84.55	18.46	19.663 ± 10.849
0A9222D	56.20 W	■	0.000182	0.000476	0.000212	0.035893	0.817241	356.94 ± 4.54	93.81	16.75	32.426 ± 29.956
0A9223D	56.30 W	■	0.000120	0.000252	0.000186	0.029162	0.663911	356.90 ± 6.15	94.93	13.61	49.721 ± 95.399
0A9225D	56.40 W	■	0.000235	0.000295	0.000632	0.102978	2.346035	357.13 ± 3.82	97.12	48.05	150.327 ######
0A9226D	56.50 W	■	0.000003	0.000128	0.000000	0.001174	0.025938	347.24 ± 104.76	97.13	0.55	3.941 ± 14.019
0A9227D	56.60 W	■	0.000000	0.000326	0.000004	0.001086	0.025967	373.01 ± 16.83	100.00	0.51	1.434 ± 1.556
0A9228D	56.70 W	■	0.000010	0.000159	0.000000	0.000787	0.016108	323.75 ± 150.67	84.78	0.37	2.130 ± 4.429
0A9231D	60.00 W	■	0.000005	0.000071	0.000003	0.001329	0.030284	357.28 ± 84.76	95.24	0.62	8.036 ± 53.955
		Σ	0.001171	0.002794	0.001346	0.214330	4.807909				

Information on Analysis

VP09-022
Bio
Laser
AF

Project = Arkaroola
Irradiation = I6t25h
J = 0.0096090 ± 0.0000183
GA1550 = 98.790 ± 0.533 Ma

Results	40(r)/39(k) ± 2σ			Age ± 2σ (Ma)	MSWD	39Ar(k) (%,n)	K/Ca ± 2σ
Weighted Plateau	22.8000	± 0.1832 ± 0.80%	357.39	± 2.88 ± 0.81%	0.62	80.44 7	1.630 ± 1.554
MSWD = 0.63, probability = 0.71			External Error	± 3.16	2.45	Statistical T Ratio	
			Analytical Error	± 2.60	1.0000	Error Magnification	
Total Fusion Age	22.4323	± 0.1945 ± 0.87%	352.15	± 3.03 ± 0.86%		9	32.989 ± 15.569
			External Error	± 3.28			
			Analytical Error	± 2.77			

Table 7: ^{40}Ar/^{39}Ar data acquisition for sample VP09023

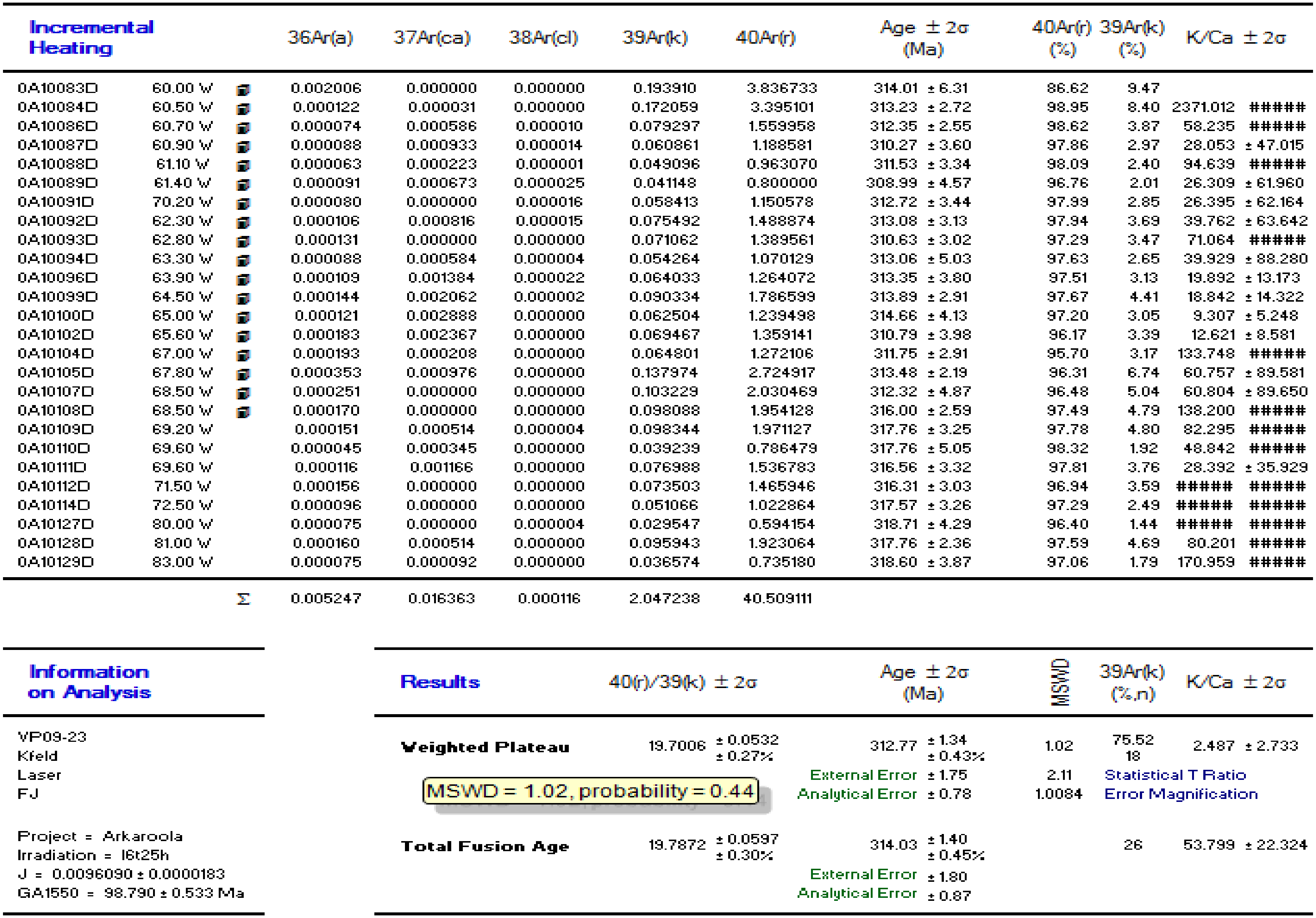

Incremental Heating			36Ar(a)	37Ar(ca)	38Ar(cl)	39Ar(k)	40Ar(r)	Age (Ma)	± 2σ	40Ar(r) (%)	39Ar(k) (%)	K/Ca	± 2σ
0A10083D	60.00 W	■	0.002006	0.000000	0.000000	0.193910	3.836733	314.01	± 6.31	86.62	9.47		
0A10084D	60.50 W	■	0.000122	0.000031	0.000000	0.172059	3.395101	313.23	± 2.72	98.95	8.40	2371.012	#####
0A10086D	60.70 W	■	0.000074	0.000586	0.000010	0.079297	1.559958	312.35	± 2.55	98.62	3.87	58.235	#####
0A10087D	60.90 W	■	0.000088	0.000933	0.000014	0.060861	1.188581	310.27	± 3.60	97.86	2.97	28.053	± 47.015
0A10088D	61.10 W	■	0.000063	0.000223	0.000001	0.049096	0.963070	311.53	± 3.34	98.09	2.40	94.639	#####
0A10089D	61.40 W	■	0.000091	0.000673	0.000025	0.041148	0.800000	308.99	± 4.57	96.76	2.01	26.309	± 61.960
0A10091D	70.20 W	■	0.000080	0.000000	0.000016	0.058413	1.150578	312.72	± 3.44	97.99	2.85	26.395	± 62.164
0A10092D	62.30 W	■	0.000106	0.000816	0.000015	0.075492	1.488874	313.08	± 3.13	97.94	3.69	39.762	± 63.642
0A10093D	62.80 W	■	0.000131	0.000000	0.000000	0.071062	1.389561	310.63	± 3.02	97.29	3.47	71.064	#####
0A10094D	63.30 W	■	0.000088	0.000584	0.000004	0.054264	1.070129	313.06	± 5.03	97.63	2.65	39.929	± 88.280
0A10096D	63.90 W	■	0.000109	0.001384	0.000022	0.064033	1.264072	313.35	± 3.80	97.51	3.13	19.892	± 13.173
0A10099D	64.50 W	■	0.000144	0.002062	0.000002	0.090334	1.786599	313.89	± 2.91	97.67	4.41	18.842	± 14.322
0A10100D	65.00 W	■	0.000121	0.002888	0.000000	0.062504	1.239498	314.66	± 4.13	97.20	3.05	9.307	± 5.248
0A10102D	65.60 W	■	0.000183	0.002367	0.000000	0.069467	1.359141	310.79	± 3.98	96.17	3.39	12.621	± 8.581
0A10104D	67.00 W	■	0.000193	0.000208	0.000000	0.064801	1.272106	311.75	± 2.91	95.70	3.17	133.748	#####
0A10105D	67.80 W	■	0.000353	0.000976	0.000000	0.137974	2.724917	313.48	± 2.19	96.31	6.74	60.757	± 89.581
0A10107D	68.50 W	■	0.000251	0.000000	0.000000	0.103229	2.030469	312.32	± 4.87	96.48	5.04	60.804	± 89.650
0A10108D	68.50 W	■	0.000170	0.000000	0.000000	0.098088	1.954128	316.00	± 2.59	97.49	4.79	138.200	#####
0A10109D	69.20 W		0.000151	0.000514	0.000004	0.098344	1.971127	317.76	± 3.25	97.78	4.80	82.295	#####
0A10110D	69.60 W		0.000045	0.000345	0.000000	0.039239	0.786479	317.76	± 5.05	98.32	1.92	48.842	#####
0A10111D	69.60 W		0.000116	0.001166	0.000000	0.076988	1.536783	316.56	± 3.32	97.81	3.76	28.392	± 35.929
0A10112D	71.50 W		0.000156	0.000000	0.000000	0.073503	1.465946	316.31	± 3.03	96.94	3.59	#####	#####
0A10114D	72.50 W		0.000096	0.000000	0.000000	0.051066	1.022864	317.57	± 3.26	97.29	2.49	#####	#####
0A10127D	80.00 W		0.000075	0.000000	0.000004	0.029547	0.594154	318.71	± 4.29	96.40	1.44	#####	#####
0A10128D	81.00 W		0.000160	0.000514	0.000000	0.095943	1.923064	317.76	± 2.36	97.59	4.69	80.201	#####
0A10129D	83.00 W		0.000075	0.000092	0.000000	0.036574	0.735180	318.60	± 3.87	97.06	1.79	170.959	#####
		Σ	0.005247	0.016363	0.000116	2.047238	40.509111						

Information on Analysis

VP09-23
Kfeld
Laser
FJ

Project = Arkaroola
Irradiation = I6t25h
J = 0.0096090 ± 0.0000183
GA1550 = 98.790 ± 0.533 Ma

Results	40(r)/39(k)	± 2σ	Age (Ma)	± 2σ	MSWD	39Ar(k) (%,n)	K/Ca	± 2σ
Weighted Plateau	19.7006	± 0.0532 ± 0.27%	312.77	± 1.34 ± 0.43%	1.02	75.52 18	2.487	± 2.733
			External Error	± 1.75	2.11	Statistical T Ratio		
MSWD = 1.02, probability = 0.44			Analytical Error	± 0.78	1.0084	Error Magnification		
Total Fusion Age	19.7872	± 0.0597 ± 0.30%	314.03	± 1.40 ± 0.45%		26	53.799	± 22.324
			External Error	± 1.80				
			Analytical Error	± 0.87				

Table 8: ^{40}Ar/^{39}Ar data acquisition for sample VP09024

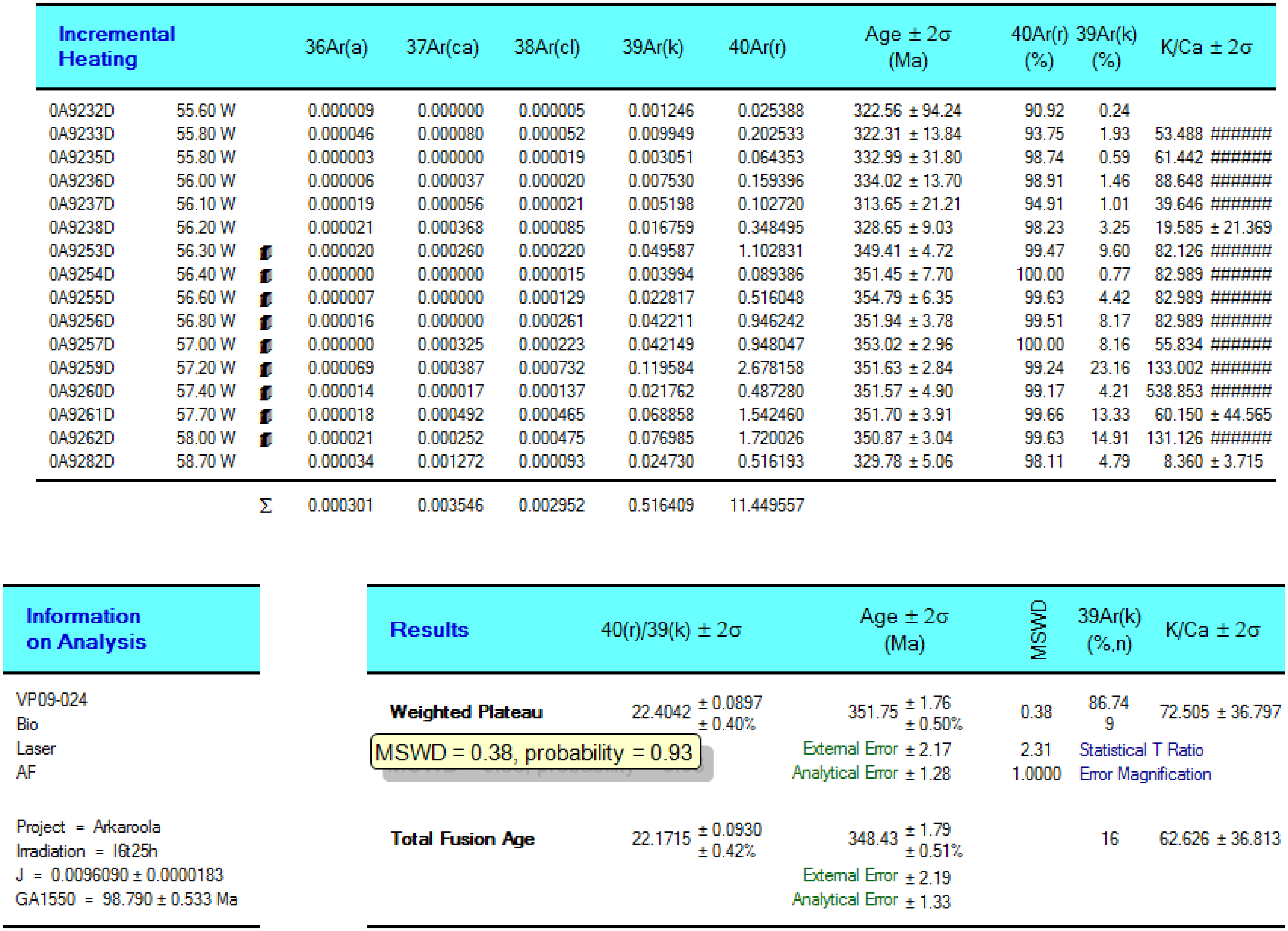

Incremental Heating			36Ar(a)	37Ar(ca)	38Ar(cl)	39Ar(k)	40Ar(r)	Age ± 2σ (Ma)	40Ar(r) (%)	39Ar(k) (%)	K/Ca ± 2σ
0A9232D	55.60 W		0.000009	0.000000	0.000005	0.001246	0.025388	322.56 ± 94.24	90.92	0.24	
0A9233D	55.80 W		0.000046	0.000080	0.000052	0.009949	0.202533	322.31 ± 13.84	93.75	1.93	53.488 ######
0A9235D	55.80 W		0.000003	0.000000	0.000019	0.003051	0.064353	332.99 ± 31.80	98.74	0.59	61.442 ######
0A9236D	56.00 W		0.000006	0.000037	0.000020	0.007530	0.159396	334.02 ± 13.70	98.91	1.46	88.648 ######
0A9237D	56.10 W		0.000019	0.000056	0.000021	0.005198	0.102720	313.65 ± 21.21	94.91	1.01	39.646 ######
0A9238D	56.20 W		0.000021	0.000368	0.000085	0.016759	0.348495	328.65 ± 9.03	98.23	3.25	19.585 ± 21.369
0A9253D	56.30 W	■	0.000020	0.000260	0.000220	0.049587	1.102831	349.41 ± 4.72	99.47	9.60	82.126 ######
0A9254D	56.40 W	■	0.000000	0.000000	0.000015	0.003994	0.089386	351.45 ± 7.70	100.00	0.77	82.989 ######
0A9255D	56.60 W	■	0.000007	0.000000	0.000129	0.022817	0.516048	354.79 ± 6.35	99.63	4.42	82.989 ######
0A9256D	56.80 W	■	0.000016	0.000000	0.000261	0.042211	0.946242	351.94 ± 3.78	99.51	8.17	82.989 ######
0A9257D	57.00 W	■	0.000000	0.000325	0.000223	0.042149	0.948047	353.02 ± 2.96	100.00	8.16	55.834 ######
0A9259D	57.20 W	■	0.000069	0.000387	0.000732	0.119584	2.678158	351.63 ± 2.84	99.24	23.16	133.002 ######
0A9260D	57.40 W	■	0.000014	0.000017	0.000137	0.021762	0.487280	351.57 ± 4.90	99.17	4.21	538.853 ######
0A9261D	57.70 W	■	0.000018	0.000492	0.000465	0.068858	1.542460	351.70 ± 3.91	99.66	13.33	60.150 ± 44.565
0A9262D	58.00 W	■	0.000021	0.000252	0.000475	0.076985	1.720026	350.87 ± 3.04	99.63	14.91	131.126 ######
0A9282D	58.70 W		0.000034	0.001272	0.000093	0.024730	0.516193	329.78 ± 5.06	98.11	4.79	8.360 ± 3.715
		Σ	0.000301	0.003546	0.002952	0.516409	11.449557				

Information on Analysis

VP09-024
Bio
Laser
AF

Project = Arkaroola
Irradiation = I6t25h
J = 0.0096090 ± 0.0000183
GA1550 = 98.790 ± 0.533 Ma

Results	40(r)/39(k) ± 2σ	Age ± 2σ (Ma)	MSWD	39Ar(k) (%,n)	K/Ca ± 2σ
Weighted Plateau	22.4042 ± 0.0897 ± 0.40%	351.75 ± 1.76 ± 0.50%	0.38	86.74 9	72.505 ± 36.797
MSWD = 0.38, probability = 0.93		External Error ± 2.17	2.31	Statistical T Ratio	
		Analytical Error ± 1.28	1.0000	Error Magnification	
Total Fusion Age	22.1715 ± 0.0930 ± 0.42%	348.43 ± 1.79 ± 0.51%		16	62.626 ± 36.813
		External Error ± 2.19			
		Analytical Error ± 1.33			

Table 9: McLaren *et al.* (2002) ^{39}Ar/^{40}Ar cooling age data for hornblende, muscovite, biotite and k-feldspar

	Cooling Ages (Ma)		
Mineral	**Basement**	**Metasedimentary and Basement Contact**	**Metasedimentary Rocks**
Distance	distance from contact is 2 m	0.5 m either side of the contact	distance from contact is 1.75 to 3 m
Hornblende	422.5 ±6.1	395.3 ± 4.2	N/A
		435.5 ± 5.1	
Muscovite	395.1 ± 3.1	396.1 ± 3.2	407.3 ± 3.2
	383.6 ± 3	395.7 ± 3.1	
	376.5 ± 3.2	390.9 ± 3	
		363 ± 2.9	
		361.6 ± 2.8	
Biotite	365.8 ± 3	383.3 ± 3.2	386.3 ± 3.1
	343.9 ±2.7	370.5 ± 2.9	
		398.7 ± 3.2	
		378.6 ± 3	
K-Feldpar	349.2 ± 2.8	341.3 ± 2.6	367.2 ± 2.9
	323.7 ±2.5	327 ± 3.9	388.3 ±3.1
		323.9 ± 2.6	573.3 ± 6.1
		323.4 ± 2.5	360.1 ±3
		334.6 ± 2.8	

12. FIGURES

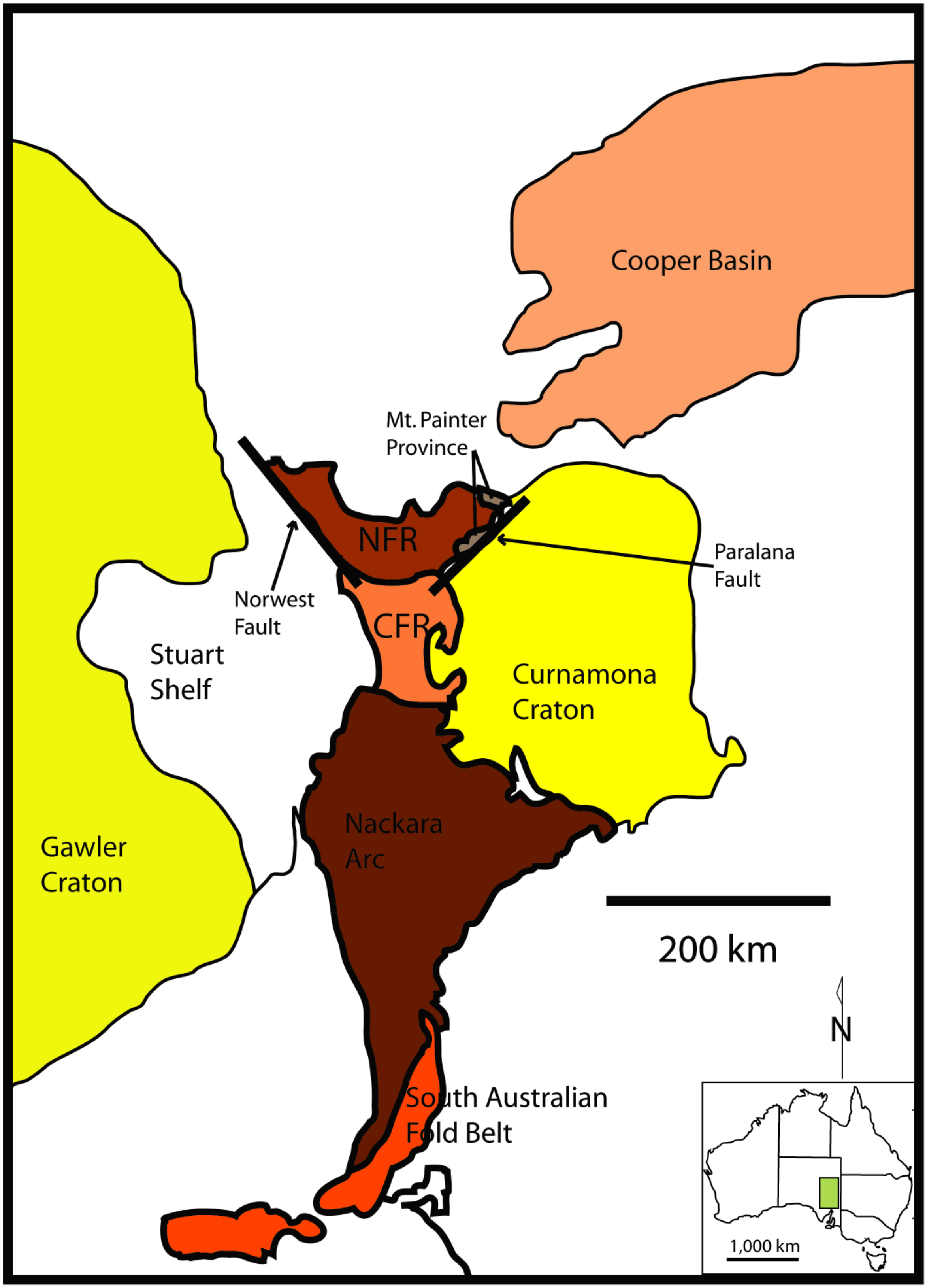

Figure 1

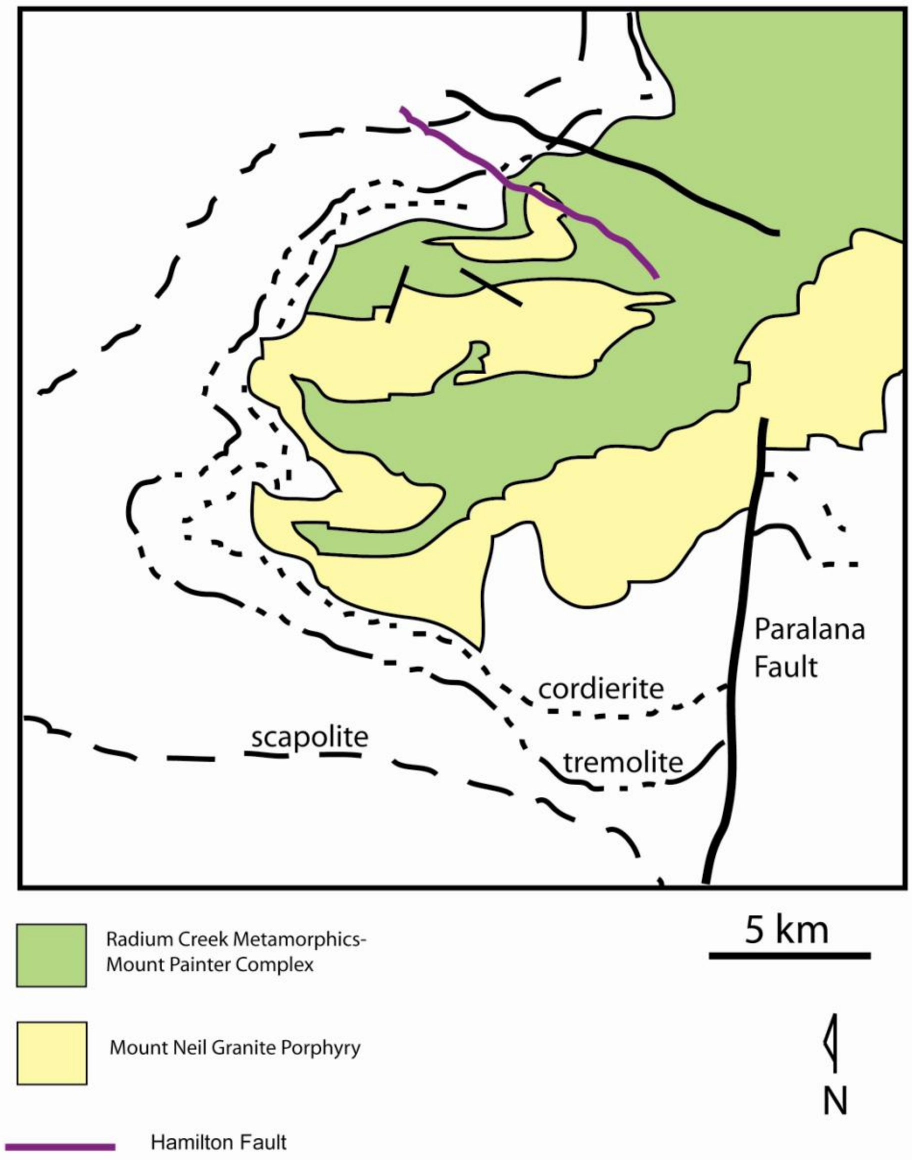
Paralana Fault
cordierite
scapolite
tremolite
5 km
N
Radium Creek Metamorphics-Mount Painter Complex
Mount Neil Granite Porphyry
Hamilton Fault

Figure 2

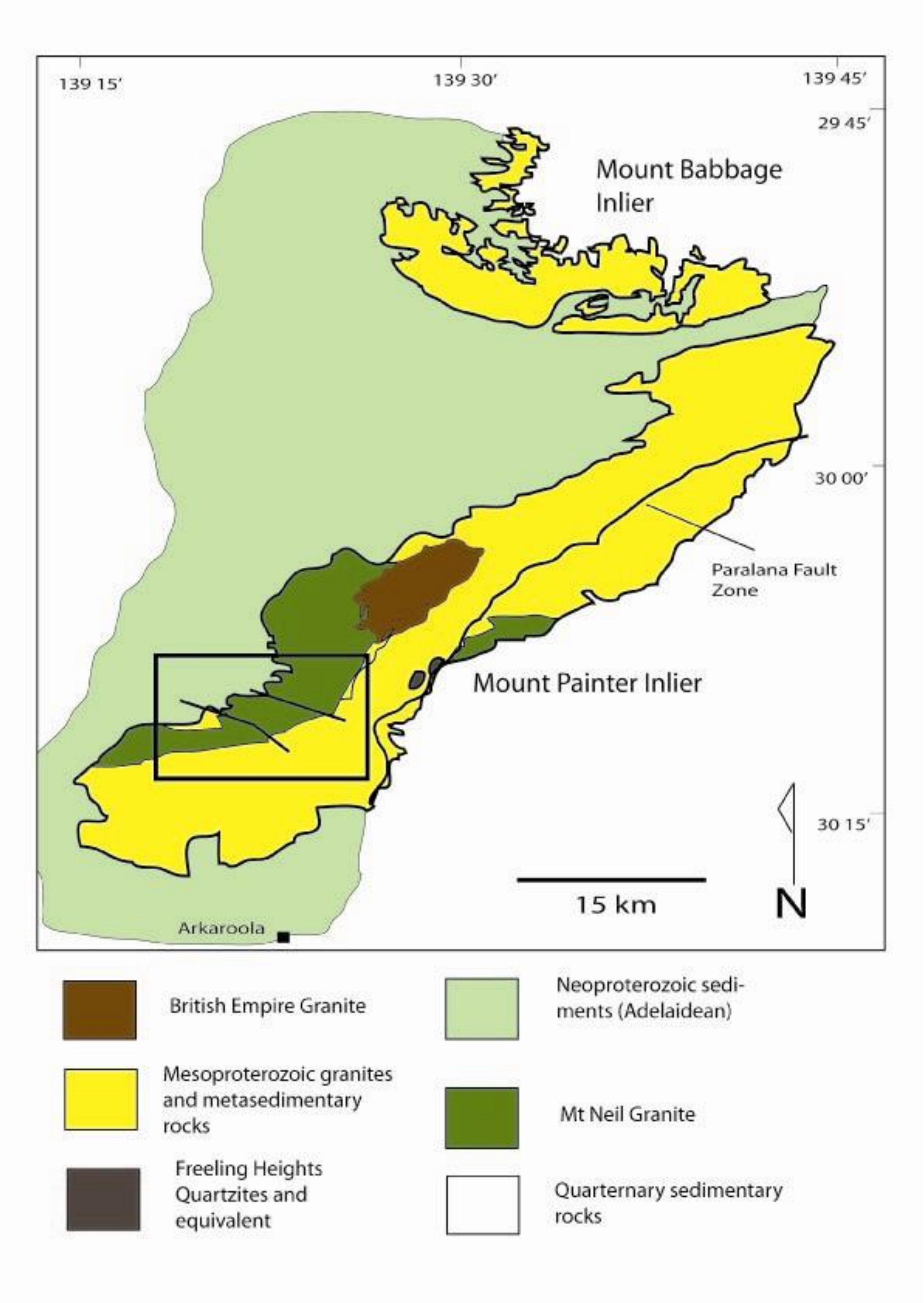
139 15′
139 30′
139 45′
29 45′
30 00′
30 15′
Mount Babbage Inlier
Paralana Fault Zone
Mount Painter Inlier
15 km
N
Arkaroola
British Empire Granite
Mesoproterozoic granites and metasedimentary rocks
Freeling Heights Quartzites and equivalent
Neoproterozoic sediments (Adelaidean)
Mt Neil Granite
Quarternary sedimentary rocks

Figure 3

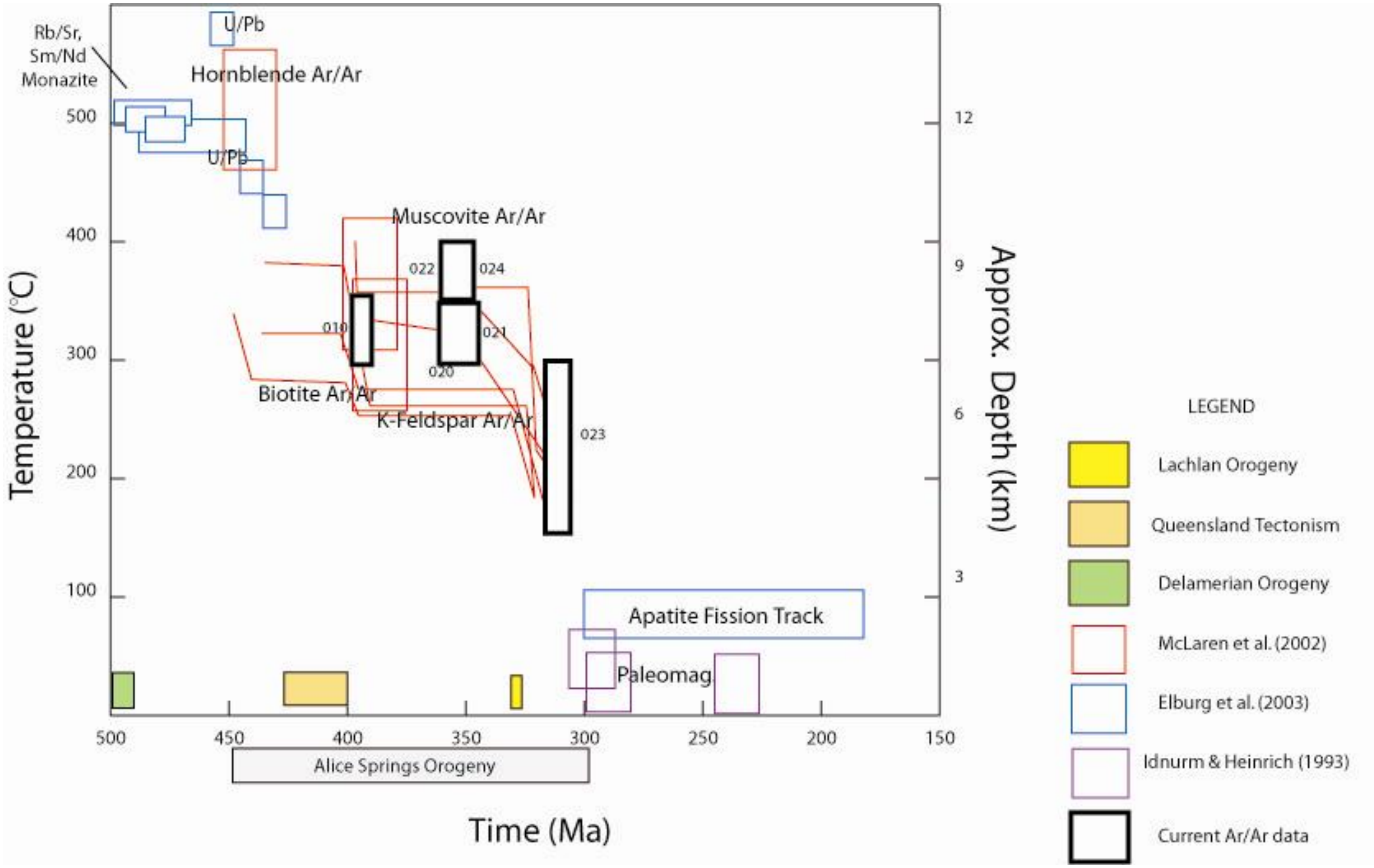
Rb/Sr,
Sm/Nd
Monazite
U/Pb
Hornblende Ar/Ar
U/Pb
Muscovite Ar/Ar
022
024
010
021
020
Biotite Ar/Ar
K-Feldspar Ar/Ar
023
Apatite Fission Track
Paleomag
Temperature (°C)
500
400
300
200
100
Approx. Depth (km)
12
9
6
3
500
450
400
350
300
250
200
150
Alice Springs Orogeny
Time (Ma)
LEGEND
Lachlan Orogeny
Queensland Tectonism
Delamerian Orogeny
McLaren et al. (2002)
Elburg et al. (2003)
Idnurm & Heinrich (1993)
Current Ar/Ar data

Figure 4

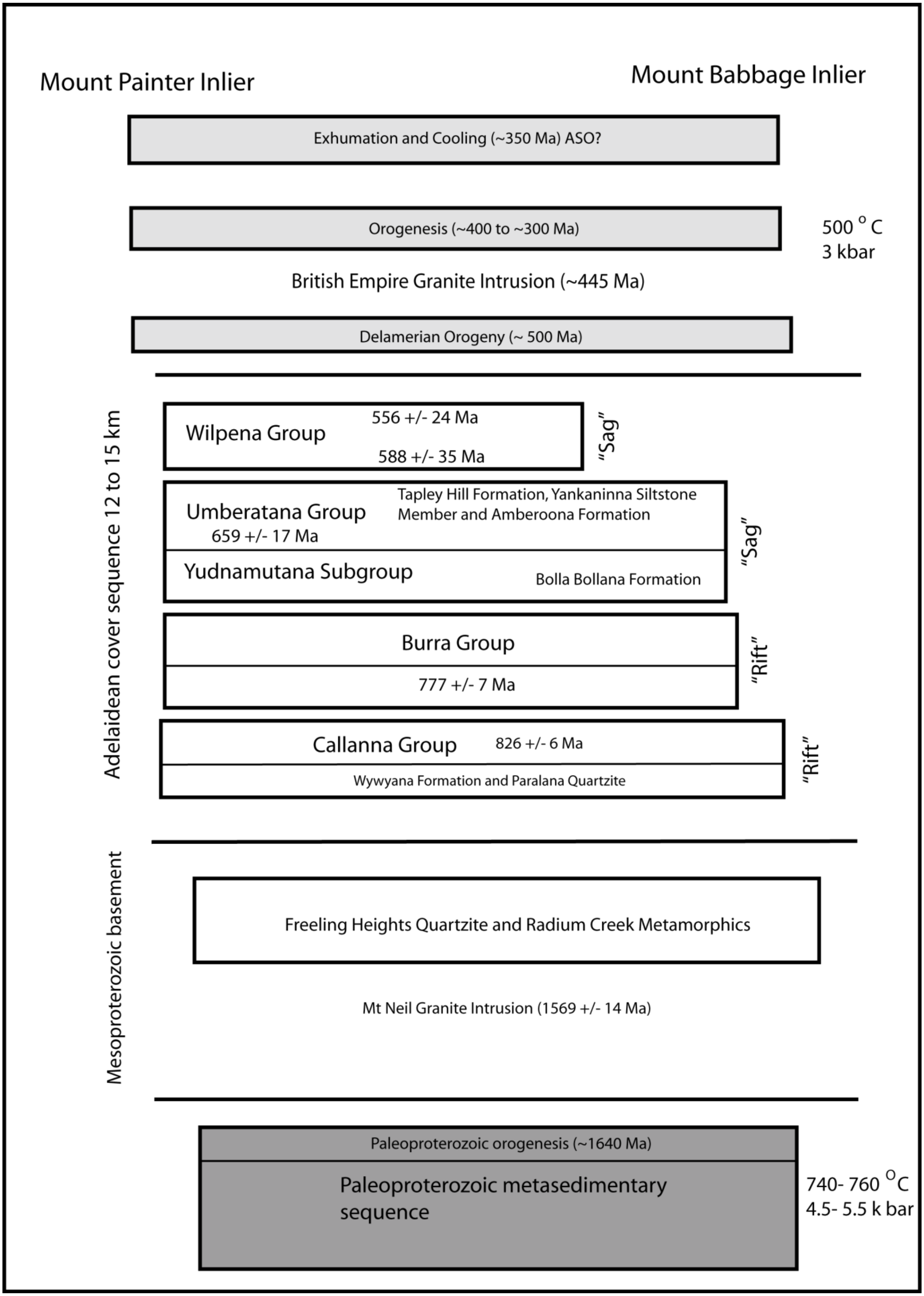

Mount Painter Inlier
Mount Babbage Inlier
Exhumation and Cooling (~350 Ma) ASO?
Orogenesis (~400 to ~300 Ma)
500 °C
3 kbar
British Empire Granite Intrusion (~445 Ma)
Delamerian Orogeny (~ 500 Ma)
Adelaidean cover sequence 12 to 15 km
Wilpena Group
556 +/- 24 Ma
588 +/- 35 Ma
"Sag"
Umberatana Group
659 +/- 17 Ma
Tapley Hill Formation, Yankaninna Siltstone Member and Amberoona Formation
Yudnamutana Subgroup
Bolla Bollana Formation
"Sag"
Burra Group
777 +/- 7 Ma
"Rift"
Callanna Group
826 +/- 6 Ma
Wywyana Formation and Paralana Quartzite
"Rift"
Mesoproterozoic basement
Freeling Heights Quartzite and Radium Creek Metamorphics
Mt Neil Granite Intrusion (1569 +/- 14 Ma)
Paleoproterozoic orogenesis (~1640 Ma)
Paleoproterozoic metasedimentary sequence
740- 760 °C
4.5- 5.5 k bar

Figure 5

The Hamilton Fault Schematic Cross Sections

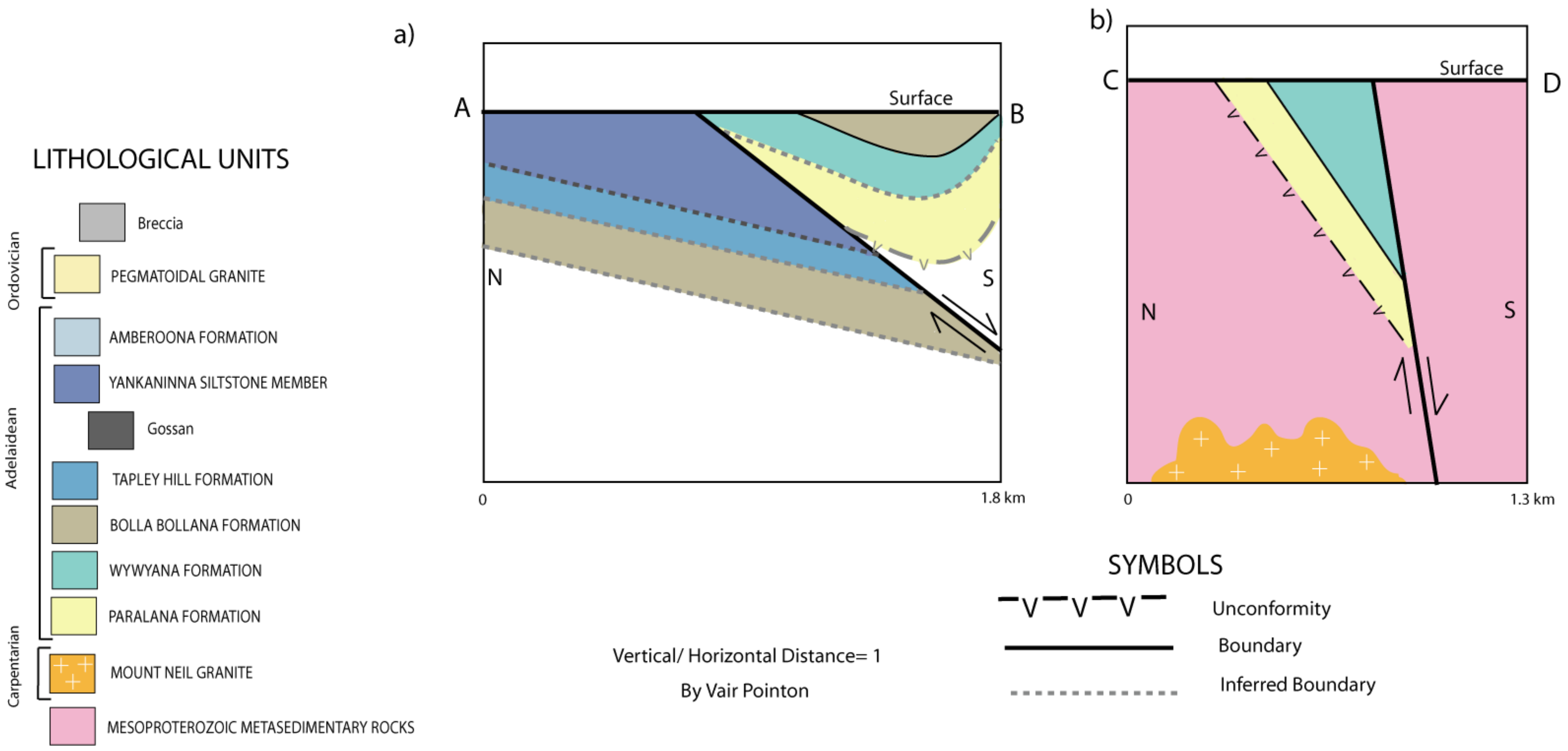

Figure 7

Figure 8

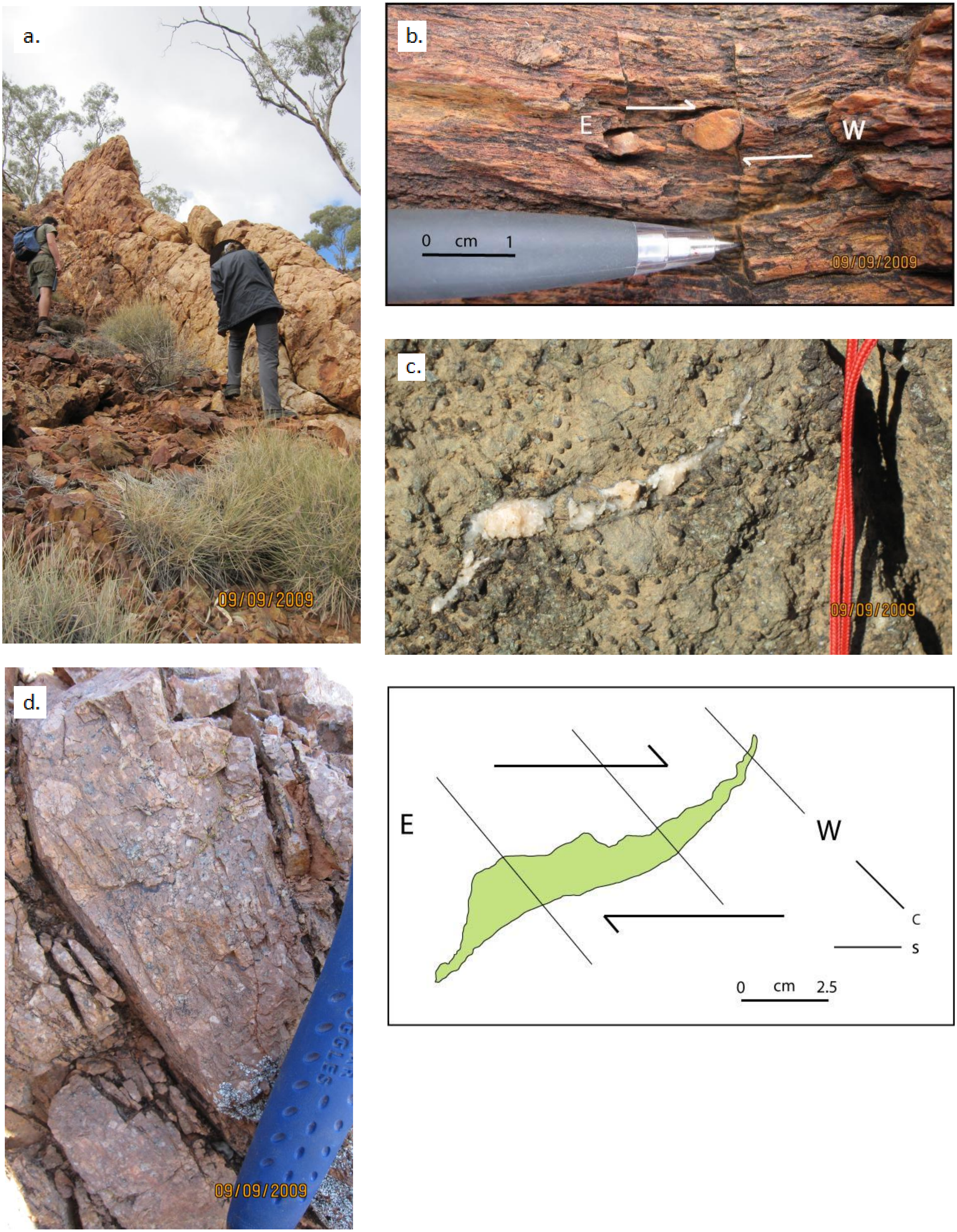
a.
09/09/2009
b.
E
W
0 cm 1
09/09/2009
c.
09/09/2009
d.
09/09/2009
E
W
c
s
0 cm 2.5


e.
CODES
www.codes.utas.edu.au
22/11/2009


f.
CODES
www.codes.utas.edu.au
22/11/2009


g.
08/09/2009


h.
10/09/2009


i.
E
W
09/09/2009


j.
09/09/2009

Figure 9

a. All Adelaidean, dip to dip direction data. No. of points: 39

Calculated gridle: 38/088

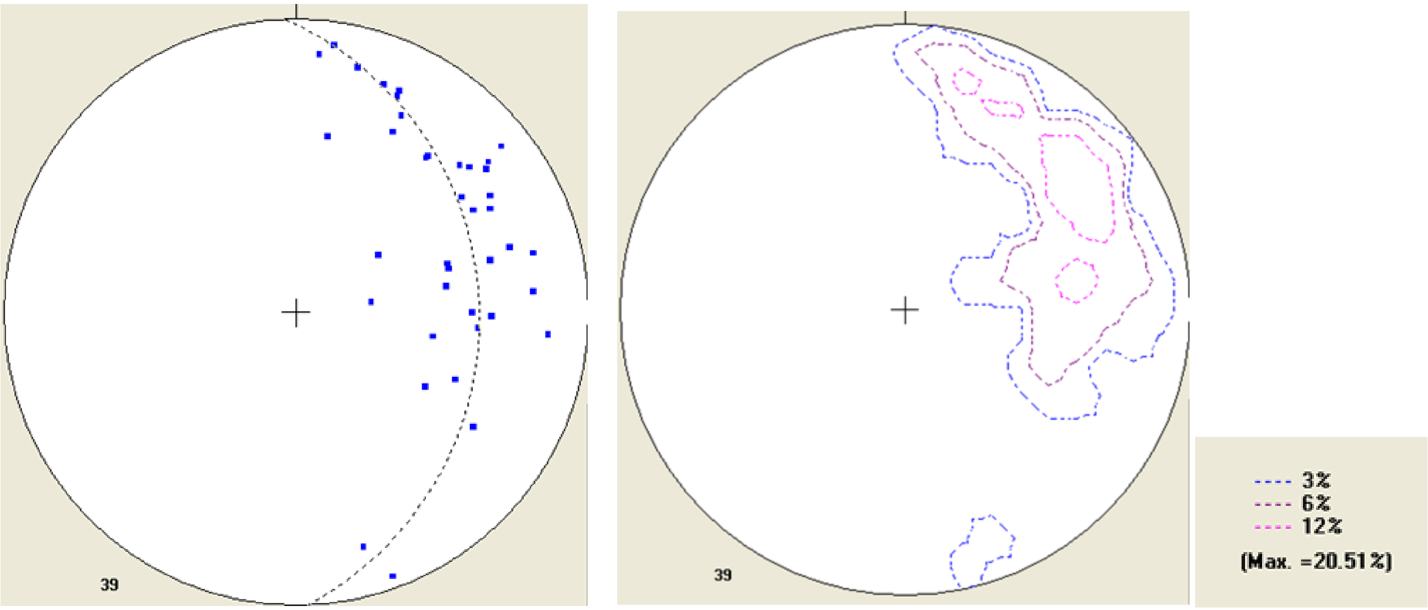

b. All basement, foliation data. No. of points: 8

Calculated gridle: 39/098

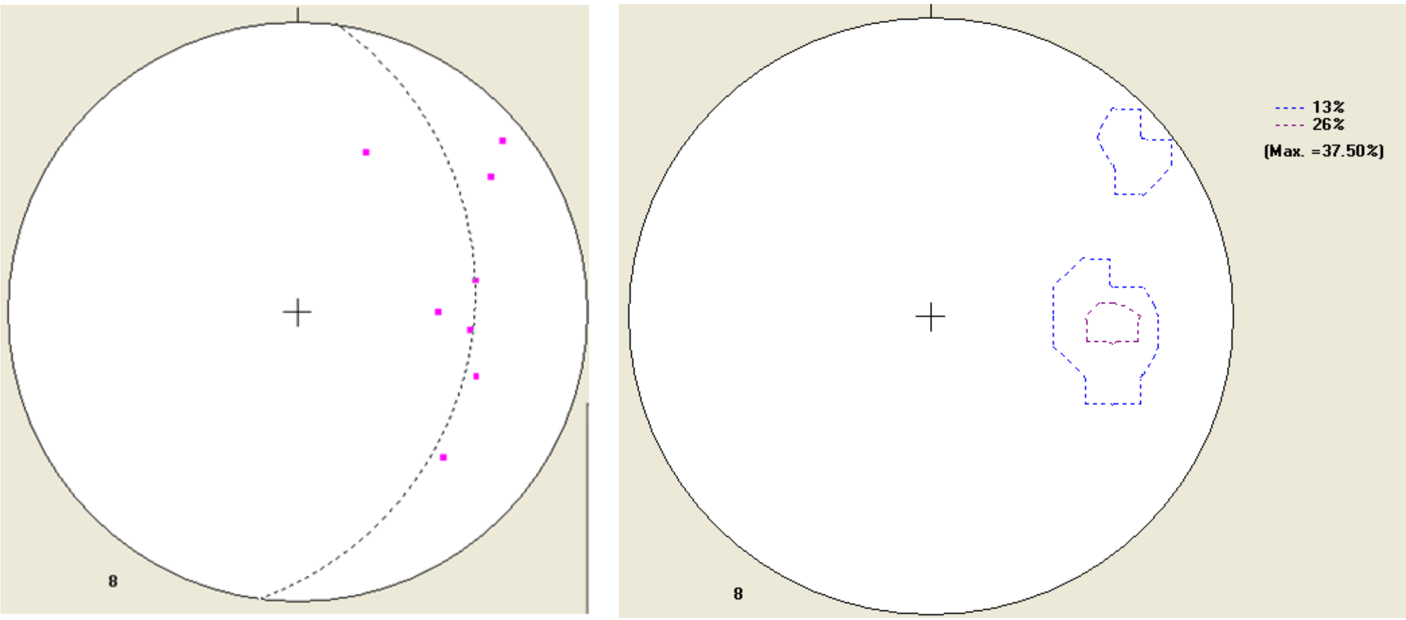

c. All lineation readings from the Hamilton Fault. No. of points: 25

Calculated gridle: 67/205

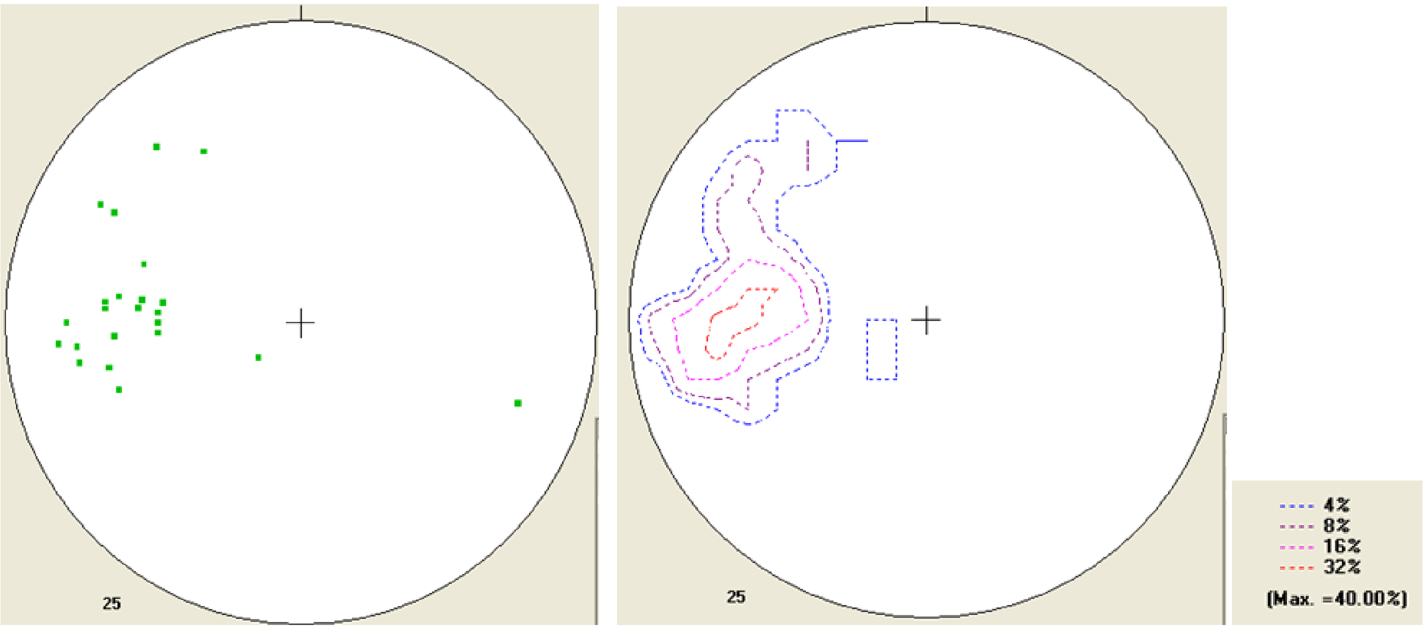

Figure 10 a.

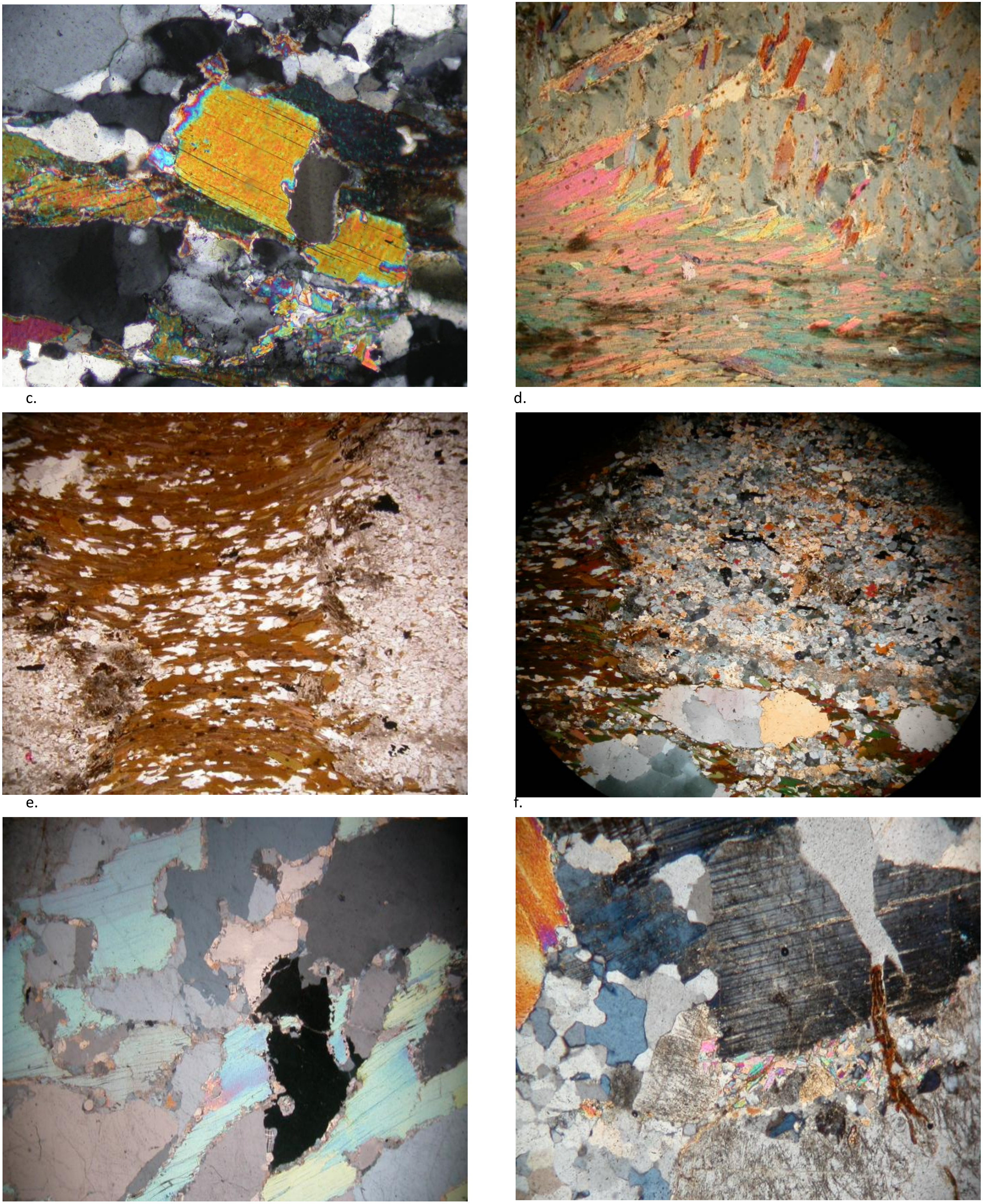

b.

c.

d.

e.

f.

g.

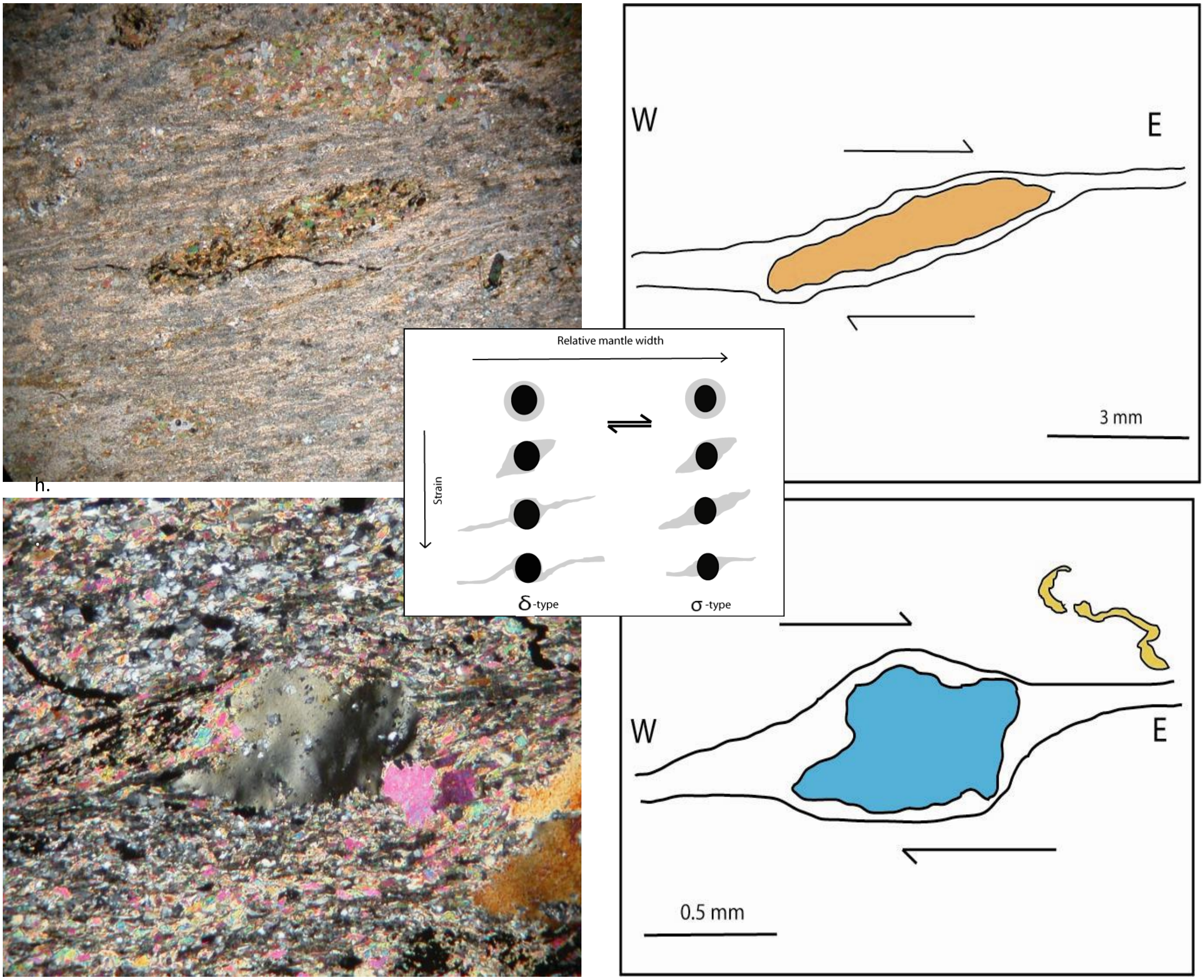
W
E
3 mm
Relative mantle width
Strain
δ-type
σ-type
W
E
0.5 mm

h.

i.

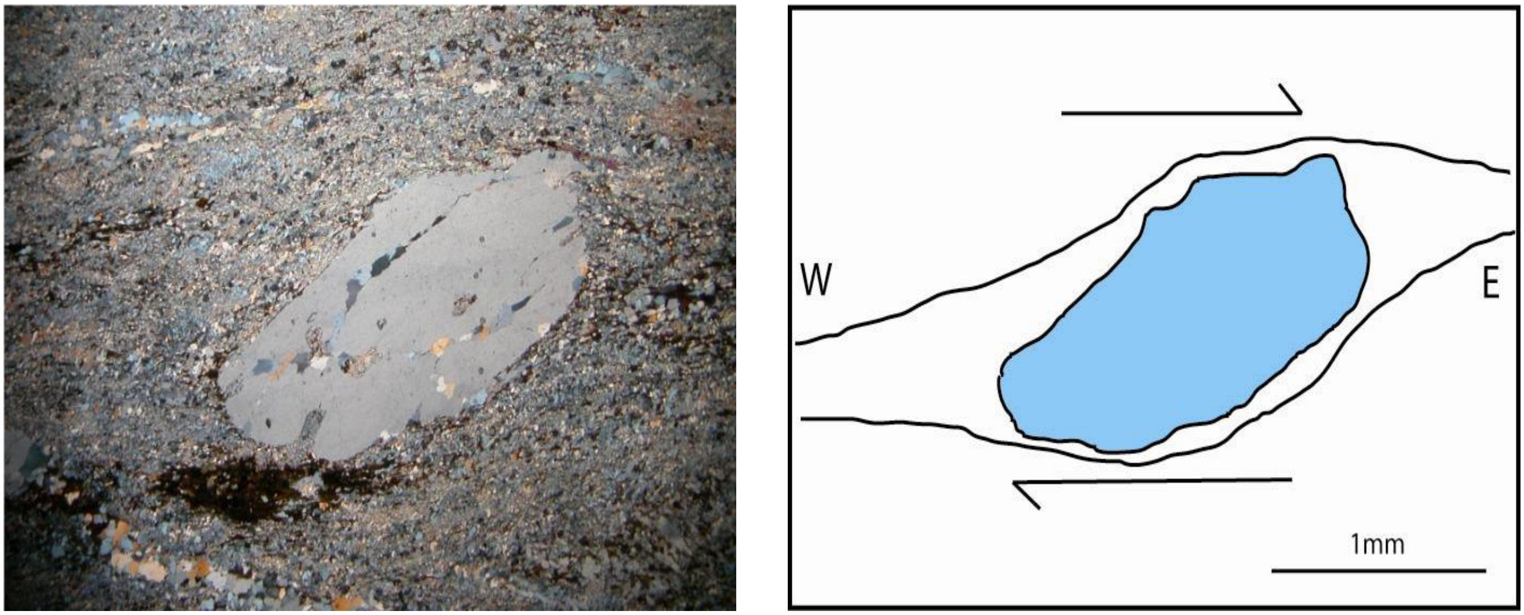
W
E
1mm

j.

k.

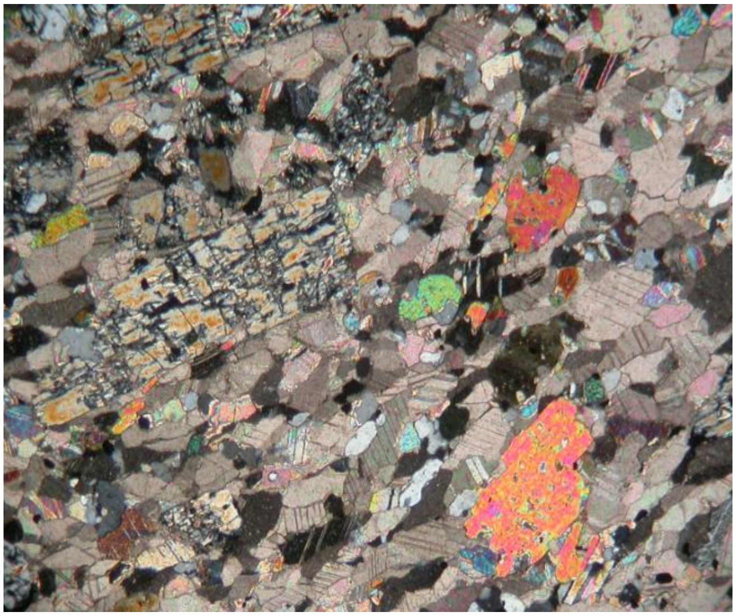

l.

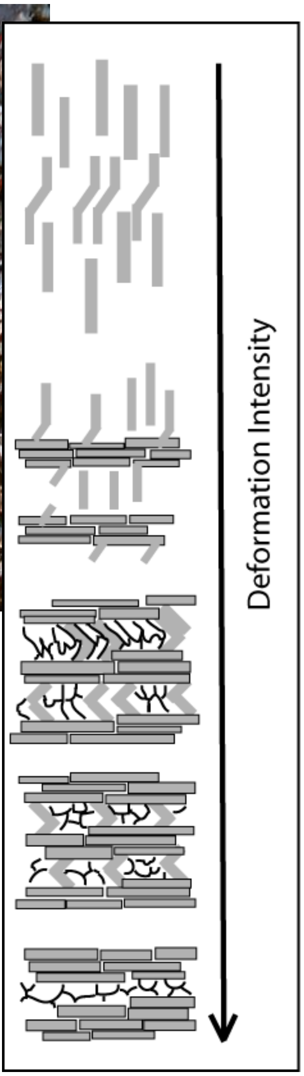

The Hamilton Fault 1:25 000: Location of Samples

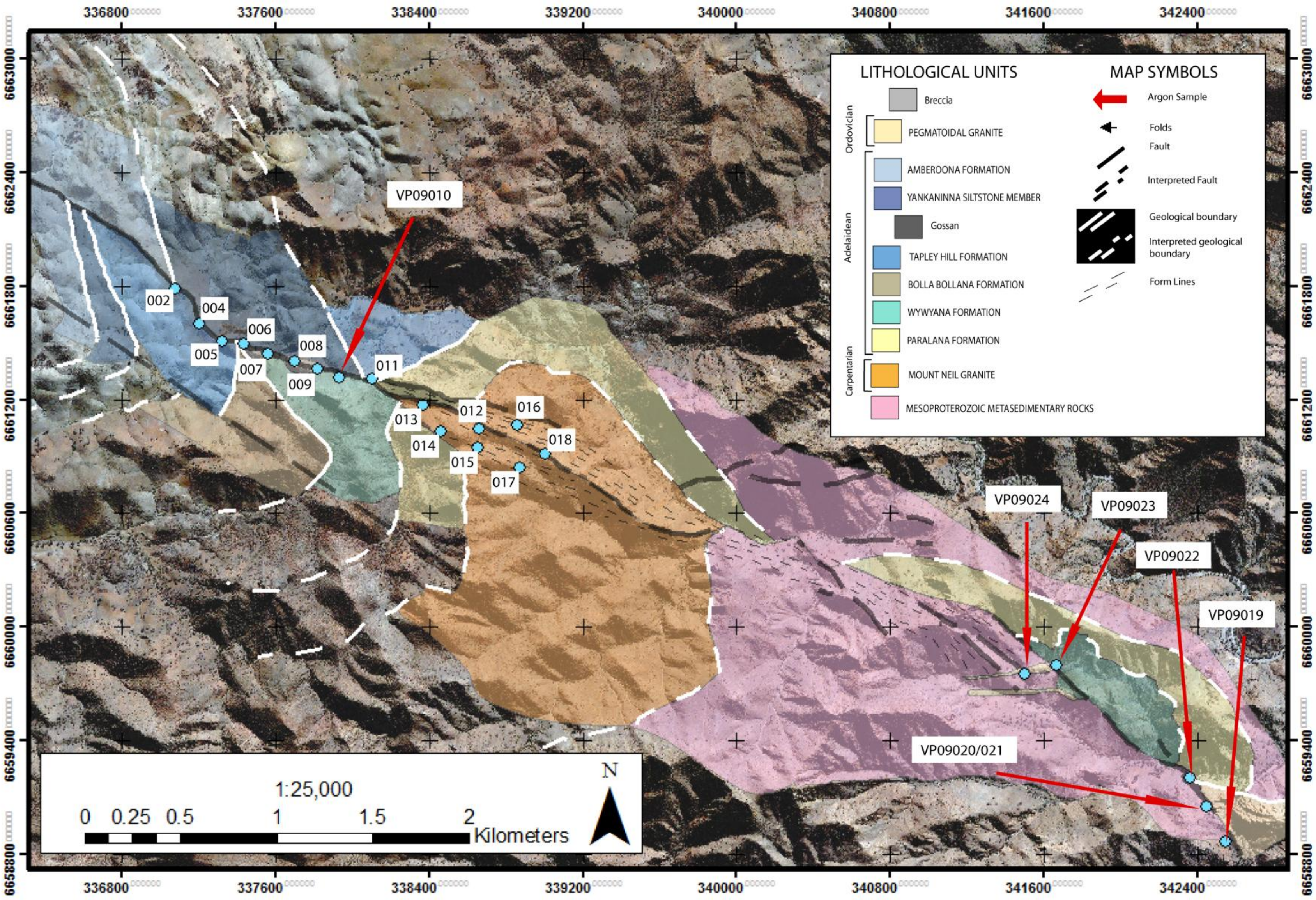

Figure 11

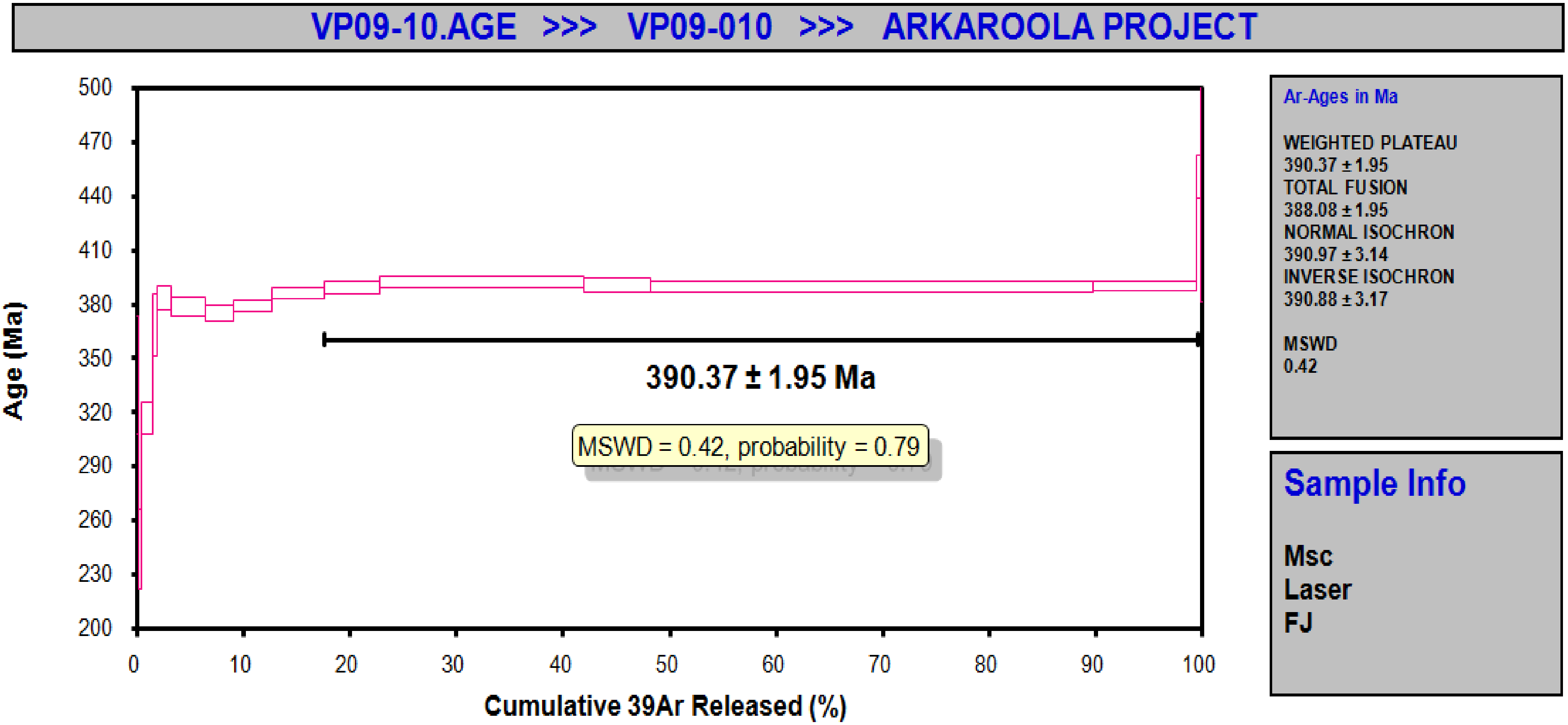
VP09-10.AGE >>> VP09-010 >>> ARKAROOLA PROJECT
Age (Ma)
500
470
440
410
380
350
320
290
260
230
200
0
10
20
30
40
50
60
70
80
90
100
Cumulative 39Ar Released (%)
390.37 ± 1.95 Ma
MSWD = 0.42, probability = 0.79
Ar-Ages in Ma
WEIGHTED PLATEAU
390.37 ± 1.95
TOTAL FUSION
388.08 ± 1.95
NORMAL ISOCHRON
390.97 ± 3.14
INVERSE ISOCHRON
390.88 ± 3.17
MSWD
0.42
Sample Info
Msc
Laser
FJ

Figure 12

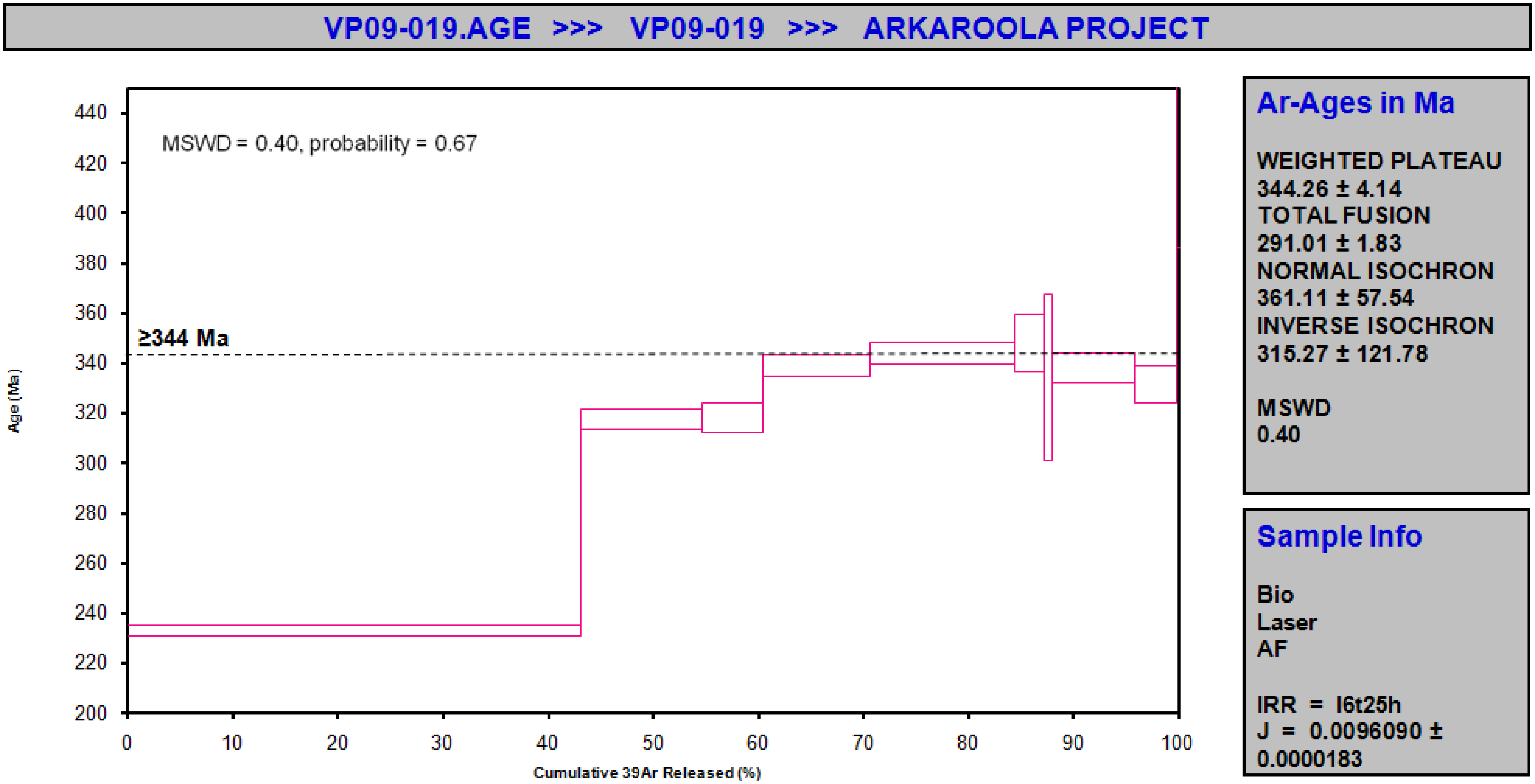
VP09-019.AGE >>> VP09-019 >>> ARKAROOLA PROJECT

Ar-Ages in Ma

WEIGHTED PLATEAU
344.26 ± 4.14
TOTAL FUSION
291.01 ± 1.83
NORMAL ISOCHRON
361.11 ± 57.54
INVERSE ISOCHRON
315.27 ± 121.78

MSWD
0.40

Sample Info

Bio
Laser
AF

IRR = I6t25h
J = 0.0096090 ± 0.0000183

Figure 13

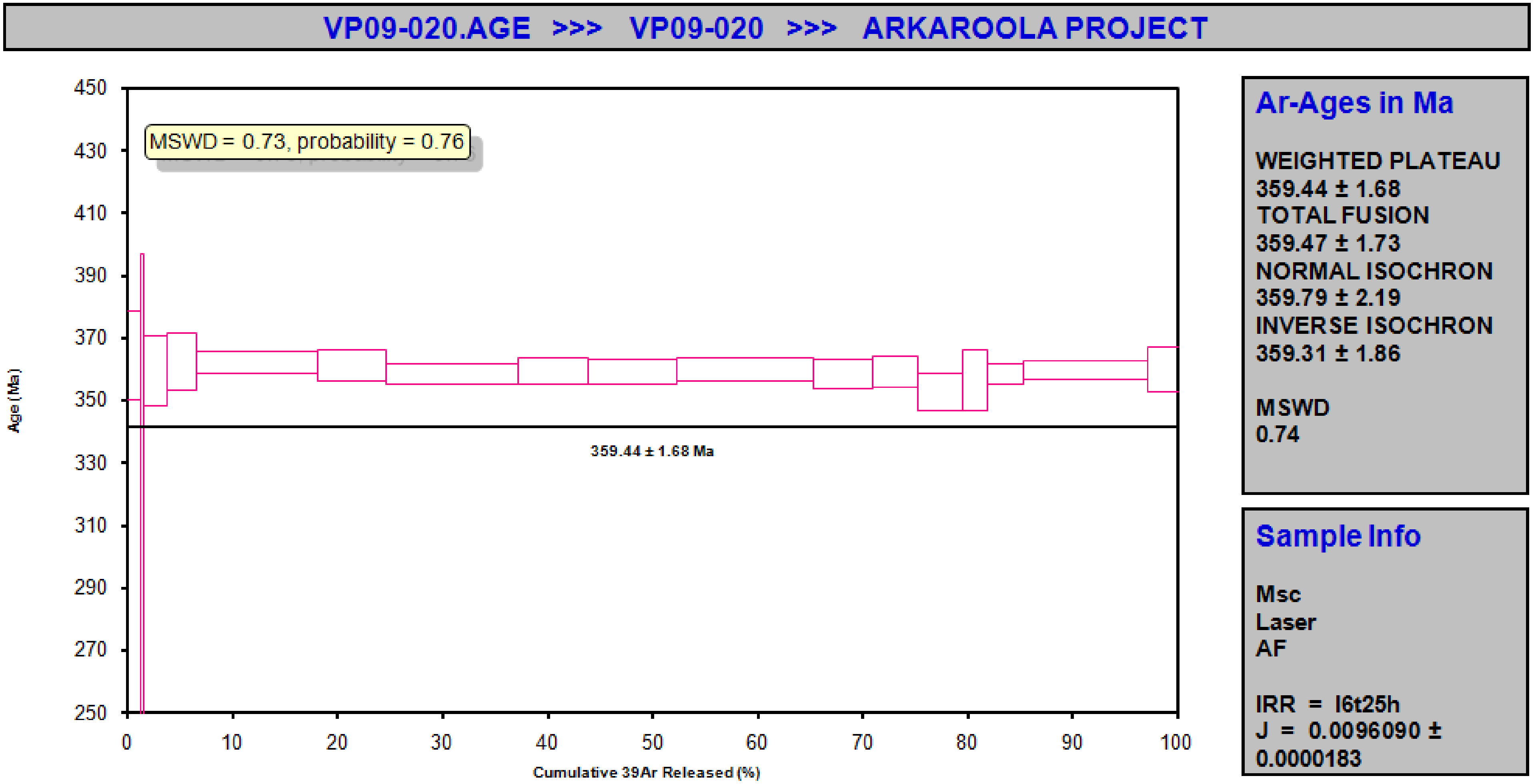
VP09-020.AGE >>> VP09-020 >>> ARKAROOLA PROJECT
MSWD = 0.73, probability = 0.76
359.44 ± 1.68 Ma
Age (Ma)
450
430
410
390
370
350
330
310
290
270
250
0
10
20
30
40
50
60
70
80
90
100
Cumulative 39Ar Released (%)
Ar-Ages in Ma
WEIGHTED PLATEAU
359.44 ± 1.68
TOTAL FUSION
359.47 ± 1.73
NORMAL ISOCHRON
359.79 ± 2.19
INVERSE ISOCHRON
359.31 ± 1.86
MSWD
0.74
Sample Info
Msc
Laser
AF
IRR = I6t25h
J = 0.0096090 ±
0.0000183

Figure 14

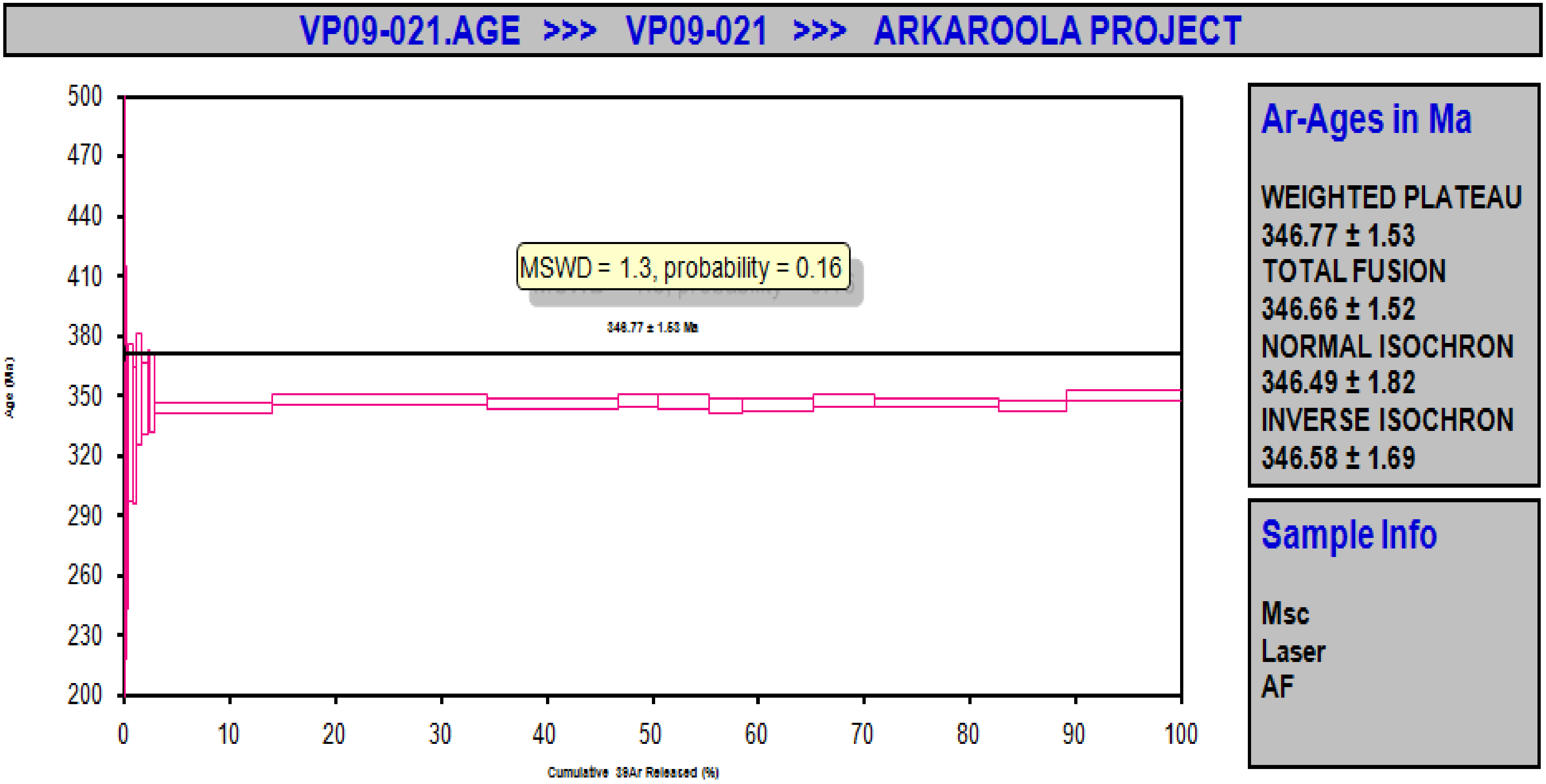
VP09-021.AGE >>> VP09-021 >>> ARKAROOLA PROJECT
MSWD = 1.3, probability = 0.16
346.77 ± 1.53 Ma
Age (Ma)
500
470
440
410
380
350
320
290
260
230
200
0
10
20
30
40
50
60
70
80
90
100
Cumulative 39Ar Released (%)
Ar-Ages in Ma
WEIGHTED PLATEAU
346.77 ± 1.53
TOTAL FUSION
346.66 ± 1.52
NORMAL ISOCHRON
346.49 ± 1.82
INVERSE ISOCHRON
346.58 ± 1.69
Sample Info
Msc
Laser
AF

Figure 15

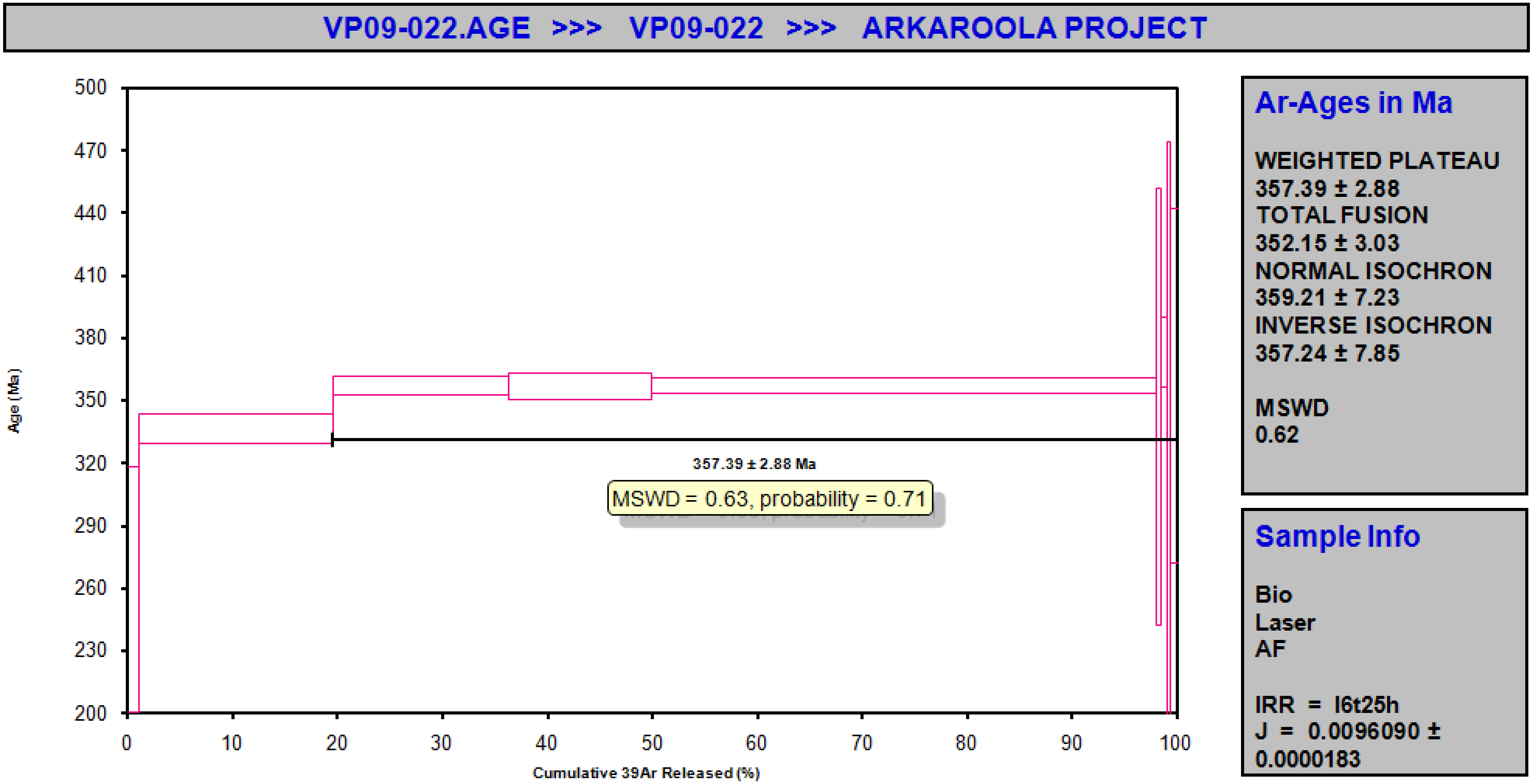
VP09-022.AGE >>> VP09-022 >>> ARKAROOLA PROJECT
Age (Ma)
500
470
440
410
380
350
320
290
260
230
200
0
10
20
30
40
50
60
70
80
90
100
Cumulative 39Ar Released (%)
357.39 ± 2.88 Ma
MSWD = 0.63, probability = 0.71
Ar-Ages in Ma
WEIGHTED PLATEAU
357.39 ± 2.88
TOTAL FUSION
352.15 ± 3.03
NORMAL ISOCHRON
359.21 ± 7.23
INVERSE ISOCHRON
357.24 ± 7.85
MSWD
0.62
Sample Info
Bio
Laser
AF
IRR = l6t25h
J = 0.0096090 ± 0.0000183

Figure 16

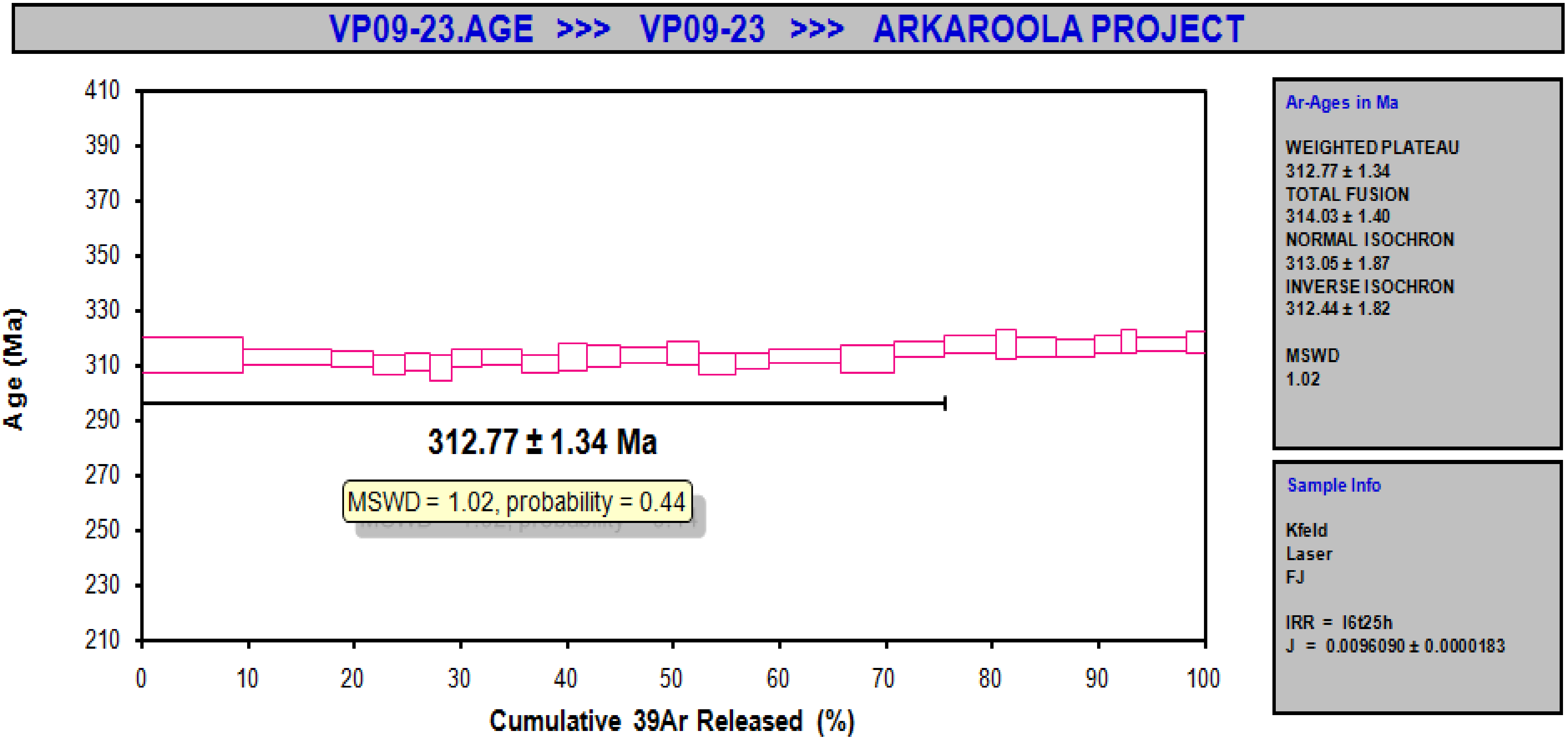
VP09-23.AGE >>> VP09-23 >>> ARKAROOLA PROJECT
Age (Ma)
410
390
370
350
330
310
290
270
250
230
210
0
10
20
30
40
50
60
70
80
90
100
Cumulative 39Ar Released (%)
312.77 ± 1.34 Ma
MSWD = 1.02, probability = 0.44
Ar-Ages in Ma
WEIGHTED PLATEAU
312.77 ± 1.34
TOTAL FUSION
314.03 ± 1.40
NORMAL ISOCHRON
313.05 ± 1.87
INVERSE ISOCHRON
312.44 ± 1.82
MSWD
1.02
Sample Info
Kfeld
Laser
FJ
IRR = I6t25h
J = 0.0096090 ± 0.0000183

Figure 17

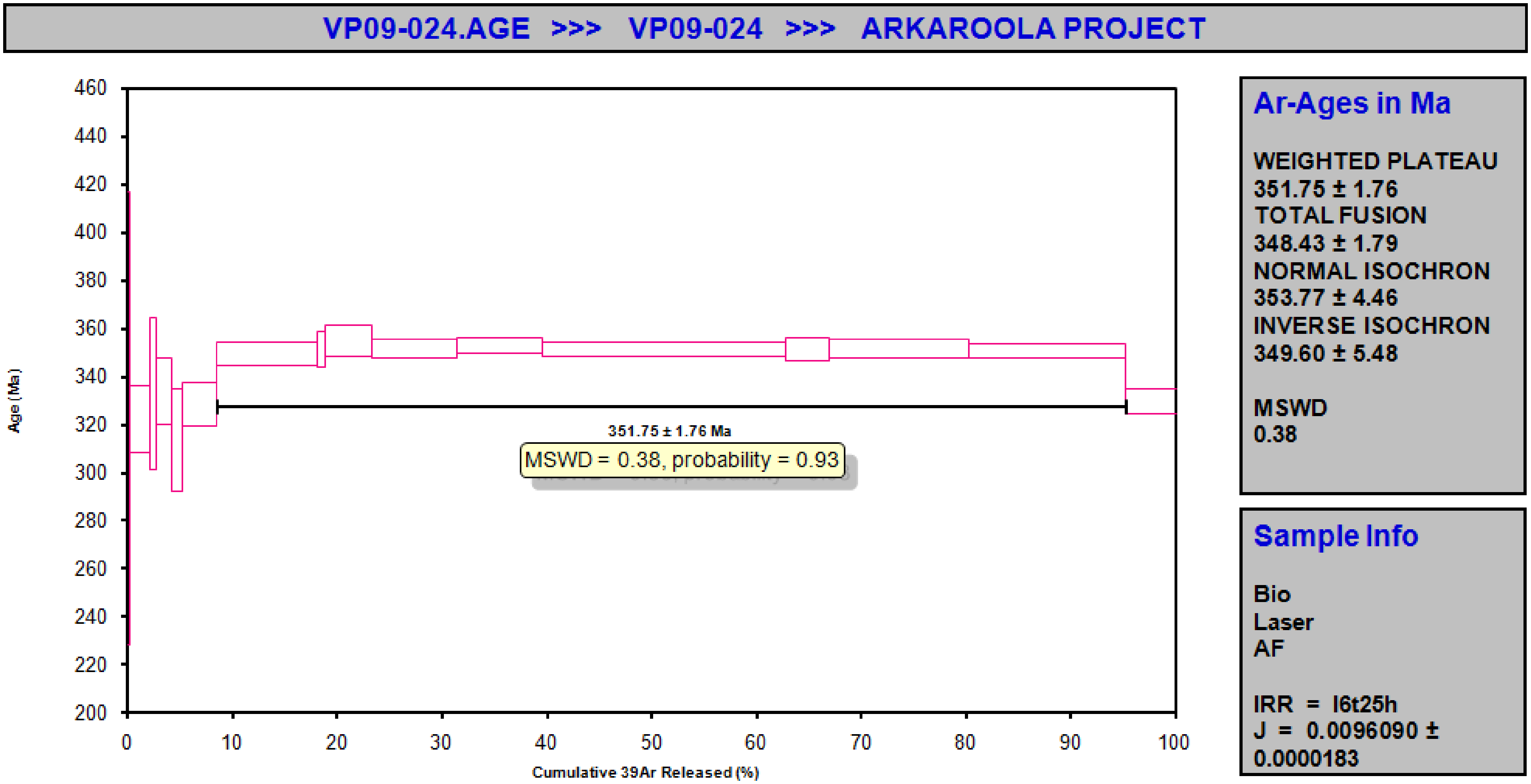
VP09-024.AGE >>> VP09-024 >>> ARKAROOLA PROJECT
460
440
420
400
380
360
340
320
300
280
260
240
220
200
Age (Ma)
0
10
20
30
40
50
60
70
80
90
100
Cumulative 39Ar Released (%)
351.75 ± 1.76 Ma
MSWD = 0.38, probability = 0.93
Ar-Ages in Ma
WEIGHTED PLATEAU
351.75 ± 1.76
TOTAL FUSION
348.43 ± 1.79
NORMAL ISOCHRON
353.77 ± 4.46
INVERSE ISOCHRON
349.60 ± 5.48
MSWD
0.38
Sample Info
Bio
Laser
AF
IRR = I6t25h
J = 0.0096090 ± 0.0000183

Figure 18

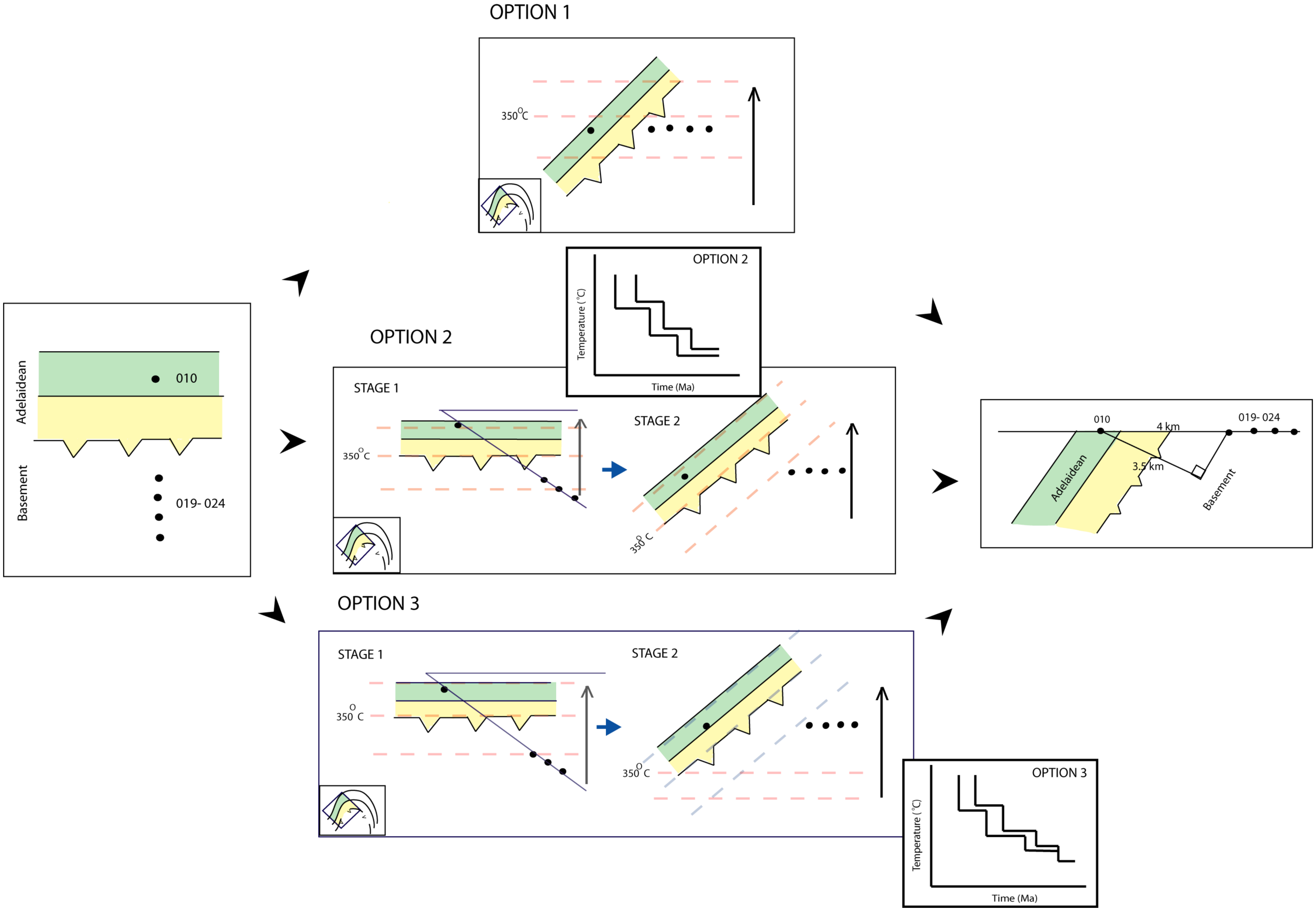
OPTION 1
350°C
Adelaidean
010
Basement
019- 024
OPTION 2
Temperature (°C)
Time (Ma)
OPTION 2
STAGE 1
350°C
STAGE 2
350°C
010
4 km
019- 024
3.5 km
Adelaidean
Basement
OPTION 3
STAGE 1
350°C
STAGE 2
350°C
OPTION 3
Temperature (°C)
Time (Ma)

Figure 19

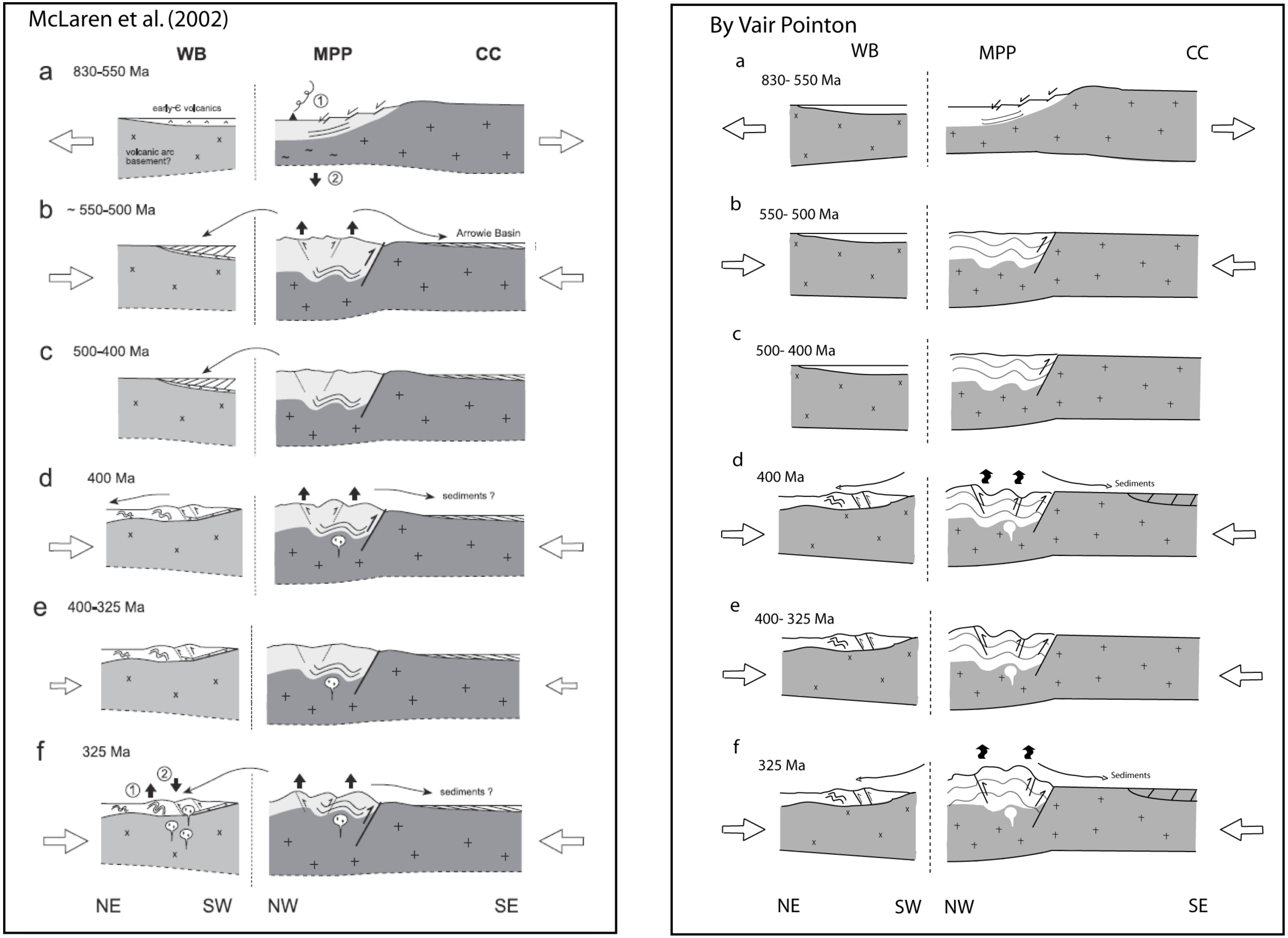
McLaren et al. (2002)
WB
MPP
CC
a
830-550 Ma
early-Є volcanics
volcanic arc basement?
①
②
b
~ 550-500 Ma
Arrowie Basin
c
500-400 Ma
d
400 Ma
sediments ?
e
400-325 Ma
f
325 Ma
①
②
sediments ?
NE
SW
NW
SE
By Vair Pointon
WB
MPP
CC
a
830- 550 Ma
b
550- 500 Ma
c
500- 400 Ma
d
400 Ma
Sediments
e
400- 325 Ma
f
325 Ma
Sediments
NE
SW
NW
SE

Figure 20

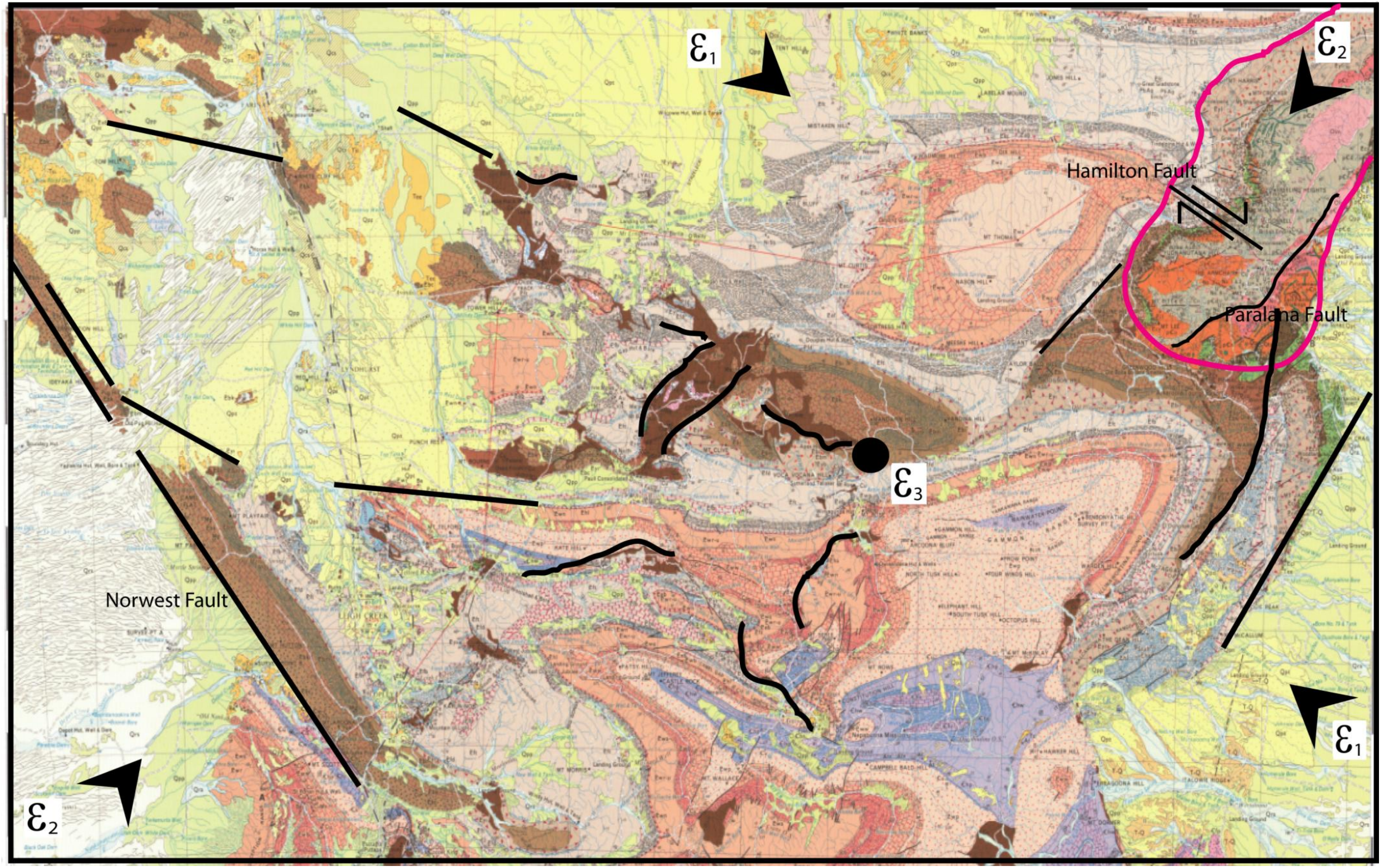

Figure 21

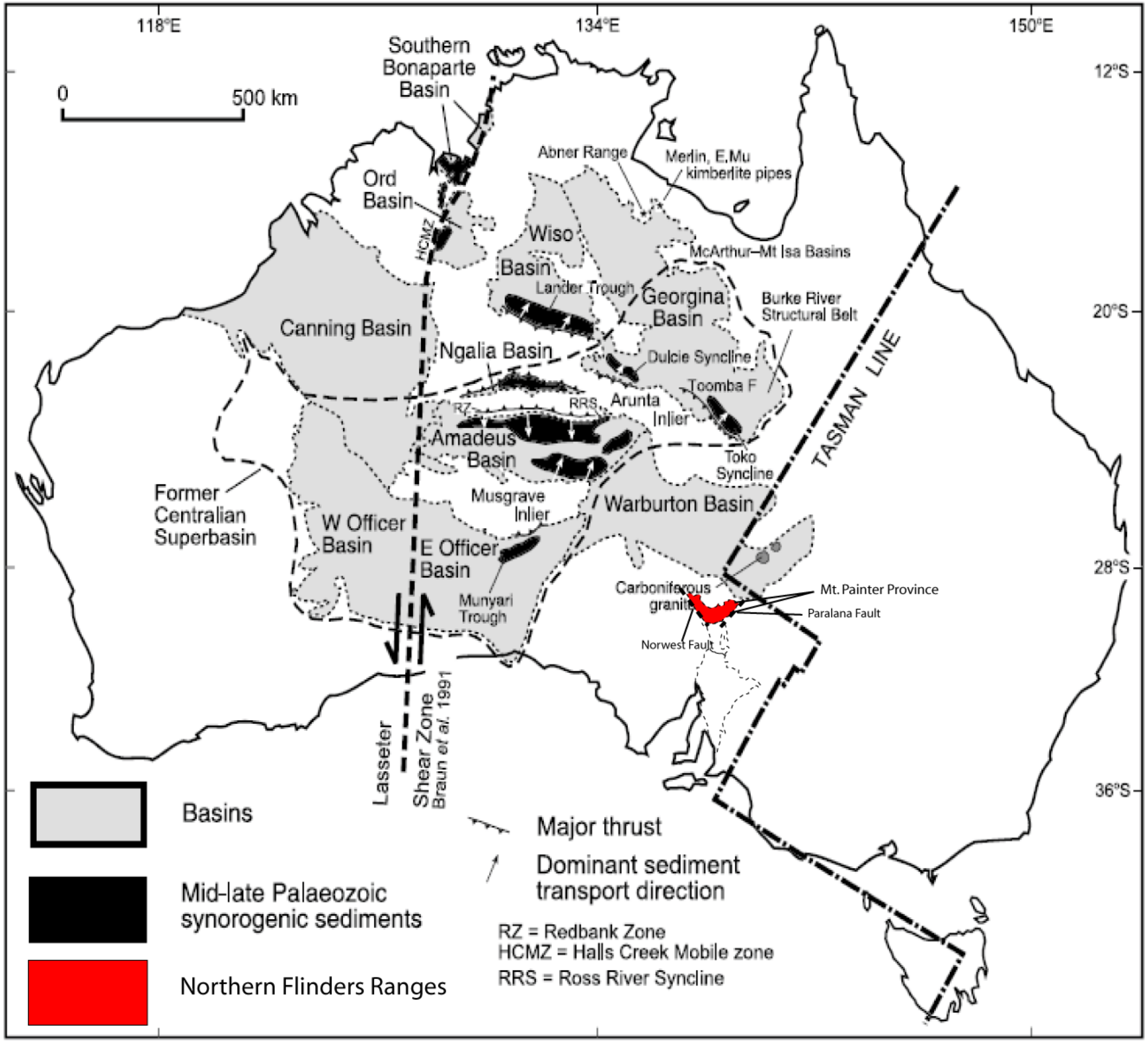
118°E
134°E
150°E
12°S
20°S
28°S
36°S
0
500 km
Southern Bonaparte Basin
Ord Basin
HCMZ
Abner Range
Merlin, E.Mu kimberlite pipes
Wiso Basin
McArthur–Mt Isa Basins
Lander Trough
Georgina Basin
Burke River Structural Belt
Canning Basin
Ngalia Basin
Dulcie Syncline
Toomba F
RZ
RRS
Arunta Inlier
Amadeus Basin
Toko Syncline
TASMAN LINE
Former Centralian Superbasin
Musgrave Inlier
Warburton Basin
W Officer Basin
E Officer Basin
Munyari Trough
Carboniferous granite
Mt. Painter Province
Paralana Fault
Norwest Fault
Lasseter Shear Zone
Braun et al. 1991
Basins
Mid-late Palaeozoic synorogenic sediments
Northern Flinders Ranges
Major thrust
Dominant sediment transport direction
RZ = Redbank Zone
HCMZ = Halls Creek Mobile zone
RRS = Ross River Syncline

Figure 22